Observational Constraints on the Nature of Dark Energy: First Cosmological Results from the ESSENCE Supernova Survey

W. M. Wood-Vasey[1], G. Miknaitis[2], C. W. Stubbs[1,3], S. Jha[4,5], A. G. Riess[6,7],
P. M. Garnavich[8], R. P. Kirshner[1], C. Aguilera[9], A. C. Becker[10], J. W. Blackman[11],
S. Blondin[1], P. Challis[1], A. Clocchiatti[12], A. Conley[13], R. Covarrubias[10], T. M. Davis[14],
A. V. Filippenko[4], R. J. Foley[4], A. Garg[1,3], M. Hicken[1,3], K. Krisciunas[8,16],
B. Leibundgut[17], W. Li[4], T. Matheson[18], A. Miceli[10], G. Narayan[1,3], G. Pignata[12],
J. L. Prieto[19], A. Rest[9], M. E. Salvo[11], B. P. Schmidt[11], R. C. Smith[9], J. Sollerman[14,15],
J. Spyromilio[17], J. L. Tonry[20], N. B. Suntzeff[9,16], and A. Zenteno[9]

wmwood-vasey@cfa.harvard.edu

arXiv:astro-ph/0701041v1 2 Jan 2007

ABSTRACT

We present constraints on the dark energy equation-of-state parameter, $w = P/(\rho c^2)$, using 60 Type Ia supernovae (SNe Ia) from the ESSENCE supernova survey. We derive a set of constraints on the nature of the dark energy assuming a flat Universe. By including constraints on (Ω_{M}, w) from baryon acoustic oscillations, we obtain a value for a static equation-of-state parameter

[1]Harvard-Smithsonian Center for Astrophysics, 60 Garden Street, Cambridge, MA 02138

[2]Fermilab, P.O. Box 500, Batavia, IL 60510-0500

[3]Department of Physics, Harvard University, 17 Oxford Street, Cambridge, MA 02138

[4]Department of Astronomy, 601 Campbell Hall, University of California, Berkeley, CA 94720-3411

[5]Kavli Institute for Particle Astrophysics and Cosmology, Stanford Linear Accelerator Center, 2575 Sand Hill Road, MS 29, Menlo Park, CA 94025

[6]Space Telescope Science Institute, 3700 San Martin Drive, Baltimore, MD 21218

[7]Johns Hopkins University, 3400 North Charles Street, Baltimore, MD 21218

[8]Department of Physics, University of Notre Dame, 225 Nieuwland Science Hall, Notre Dame, IN 46556-5670

[9]Cerro Tololo Inter-American Observatory, Casilla 603, La Serena, Chile

[10]Department of Astronomy, University of Washington, Box 351580, Seattle, WA 98195-1580

[11]The Research School of Astronomy and Astrophysics, The Australian National University, Mount Stromlo and Siding Spring Observatories, via Cotter Road, Weston Creek, PO 2611, Australia

[12]Pontificia Universidad Católica de Chile, Departamento de Astronomía y Astrofísica, Casilla 306, Santiago 22, Chile

[13]Department of Astronomy and Astrophysics, University of Toronto, 50 Saint George Street, Toronto, ON M5S 3H4, Canada

[14]Dark Cosmology Centre, Niels Bohr Institute, University of Copenhagen, Juliane Maries Vej 30, DK-2100 Copenhagen Ø, Denmark

[15]Department of Astronomy, Stockholm University, AlbaNova, 10691 Stockholm, Sweden

[16]Department of Physics, Texas A&M University, College Station, TX 77843-4242

[17]European Southern Observatory, Karl-Schwarzschild-Strasse 2, D-85748 Garching, Germany

[18]National Optical Astronomy Observatory, 950 North Cherry Avenue, Tucson, AZ 85719-4933

[19]Department of Astronomy, Ohio State University, 4055 McPherson Laboratory, 140 West 18th Avenue, Columbus, OH 43210

[20]Institute for Astronomy, University of Hawaii, 2680 Woodlawn Drive, Honolulu, HI 96822

$w = -1.05^{+0.13}_{-0.12}$ (stat 1σ) ± 0.13 (sys) and $\Omega_{\mathrm{M}} = 0.274^{+0.033}_{-0.020}$ (stat 1σ) with a best-fit χ^2/DoF of 0.96. These results are consistent with those reported by the Super-Nova Legacy Survey in a similar program measuring supernova distances and redshifts. We evaluate sources of systematic error that afflict supernova observations and present Monte Carlo simulations that explore these effects. Currently, the largest systematic currently with the potential to affect our measurements is the treatment of extinction due to dust in the supernova host galaxies. Combining our set of ESSENCE SNe Ia with the SuperNova Legacy Survey SNe Ia, we obtain a joint constraint of $w = -1.07^{+0.09}_{-0.09}$ (stat 1σ) ± 0.13 (sys), $\Omega_{\mathrm{M}} = 0.267^{+0.028}_{-0.018}$ (stat 1σ) with a best-fit χ^2/DoF of 0.91. The current SNe Ia data are fully consistent with a cosmological constant.

Subject headings: cosmological parameters — supernovae — cosmology: observations

1. Introduction: Supernovae and Cosmology

We report the analysis of 60 Type Ia supernovae (SNe Ia) discovered in the course of the ESSENCE program (Equation of State: Supernovae trace Cosmic Expansion—an NOAO Survey Program) from 2002 to 2005. The aim of ESSENCE is to measure the history of cosmic expansion over the past 5 billion years with sufficient precision to distinguish whether the dark energy is different from a cosmological constant at the $\sigma_w = \pm 0.1$ level. Here we present our first results and show that we are well on our way towards that goal. Our present data are fully consistent with a $w = -1$, flat Universe, and our uncertainty in w, the parameter that describes the cosmic equation of state, analyzed in the way we outline here, will shrink below 0.1 for models of constant w as the ESSENCE program is completed. Other approaches to using the luminosity distances have been suggested to constrain possible cosmological models. We here provide the ESSENCE observations in a convenient form suitable for a testing a variety of models.[1]

As reported in a companion paper (Miknaitis et al. 2007), ESSENCE is based on a supernova search carried out with the 4-m Blanco Telescope at the Cerro Tololo Inter-American Observatory (CTIO) with the prime-focus MOSAIC II 64 Megapixel CCD camera. Our search produces densely sampled R-band and I-band light curves for supernovae in our fields. As described in that paper, we optimized the search to provide the best constraints

---

[1] http://www.ctio.noao.edu/essence/

on w, given fixed observing time and the properties of the MOSAICII camera and CTIO 4-m telescope. Spectra from a variety of large telescopes, including Keck, VLT, Gemini, and Magellan, allow us to determine supernova types and redshifts. We have paid particular attention to the central problems of calibration and systematic errors that, when the survey is complete in 2008, will be more important to the final precision of our cosmological inferences than statistical sampling errors for about 200 objects.

This first cosmological report from the ESSENCE survey derives some properties of dark energy from the sample presently in hand, which is still small enough that the statistics of the sample size make a noticeable contribution to the uncertainty in dark-energy properties. But our goal is to set out the systematic uncertainties in a clear way so that these are exposed to view and so that we can concentrate our efforts where they will have the most significant effect. To infer luminosity distances to the ESSENCE supernovae over the redshift interval 0.15–0.70, we employ the relations developed for SNe Ia at low redshift (Jha et al. 2007) among their light-curve shapes, colors, and intrinsic luminosities. The expansion history from $z \approx 0.7$ to the present provides leverage to constrain the equation-of-state parameter for the dark energy as described below. In §1 we sketch the context of the ESSENCE program. In §2 we show from a set of simulated light curves that this particular implementation of light-curve analysis is consistent, with the same cosmology emerging from the analysis as was used to construct the samples, and that the statistical uncertainty we ascribe to the inference of the dark-energy properties is also correctly measured. This modeling of our analysis chain gives us confidence that the analysis of the actual data set is reliable and its uncertainty is correctly estimated. Section 3 delineates the systematic errors we confront, estimates their present size, and indicates some areas where improvement can be achieved. Section 4 describes the sample and provides the estimates of dark energy properties using the ESSENCE sample. The conclusions of this work are given in §5.

1.1. Context

Supernovae have been central to cosmological measurements from the very beginning of observational cosmology. Shapley (1919) employed supernovae against the "island universe" hypothesis arguing that objects such as SN 1885A in Andromeda would have $M = -16$ which was "out of the question." Edwin Hubble (Hubble 1929) noted "a mysterious class of exceptional novae which attain luminosities that are respectable fractions of the total luminosities of the systems in which they appear." These extra-bright novae were dubbed "supernovae" by Baade & Zwicky (1934) and divided into two classes, based on their spectra, by Minkowski (1941). Type I supernovae (SNe I) have no hydrogen lines while Type II

supernovae (SNe II) show Hα and other hydrogen lines.

The high luminosity and observed homogeneity of the first handful of SN I light curves prompted Wilson (1939) to suggest that they be employed for fundamental cosmological measurements, starting with time dilation of their characteristic rise and fall to distinguish true cosmic expansion from "tired light." After the SN Ib subclass was separated from the SNe Ia (see Filippenko 1997, for a review) this line of investigation has grown more fruitful as techniques of photometry have improved and as the redshift range over which supernovae have been well observed and confirmed to have standard light-curve shapes and luminosities has increased (Rust 1974; Leibundgut et al. 1996; Riess et al. 1997; Goldhaber et al. 2001; Riess et al. 2004; Foley et al. 2005; Hook et al. 2005; Conley et al. 2006; Blondin et al. 2006). Within the uncertainties, the results agree with the predictions of cosmic expansion and provide a fundamental test that the underlying assumption of an expanding universe is correct.

Evidence for the homogeneity of SNe Ia comes from their small scatter in the Hubble diagram. Kowal (1968) compiled data for the first well-populated Hubble diagram of SNe I. The 1σ scatter about the Hubble line was 0.6 mag, but Kowal presciently speculated that supernova distances to individual objects might eventually be known to 5-10% and suggested that "[i]t may even be possible to determine the second-order term in the redshift-magnitude relation when light curves become available for very distant supernovae." Precise distances to SNe Ia enable tests for the linearity of the Hubble law and provide evidence for local deviations from the local Hubble flow, attributed to density inhomogeneities in the local universe (Riess et al. 1995, 1997; Zehavi et al. 1998; Bonacic et al. 2000; Radburn-Smith et al. 2004; Jha et al. 2007). While SN Ia cosmology is not dependent on the value of H_0, it is sensitive to deviations from a homogeneous Hubble flow and these regional velocity fields may limit our ability to estimate properties of dark energy, as emphasized by Hui & Greene (2006) and by Cooray & Caldwell (2006). Whether the best strategy is to map the velocity inhomogeneities thoroughly or to skip over them by using a more distant low-redshift sample remains to be demonstrated. We have used a lower limit of redshift $z > 0.015$ in constructing our sample of SNe Ia.

The utility of SNe Ia as distance indicators results from the demonstration that the intrinsic brightness of each SN Ia is closely connected to the shape of its light curve. As the sample of well-observed SNe Ia grew, some distinctly bright and faint objects were found. For example, SN 1991T (Filippenko et al. 1992b; Phillips et al. 1992) and SN 1991bg (Filippenko et al. 1992a; Leibundgut et al. 1993) were of different luminosity, and their light curves were not the same, either. The possible correlation of the shapes of supernova light curves with their luminosities had been explored by Pskovskii (1977). More homogeneous

photometry from CCD detectors, more extreme examples from larger samples, and more reliable distance estimators enabled Phillips (1993) to establish the empirical relation between light-curve shapes and supernova luminosities. The Calán-Tololo sample (Hamuy et al. 1996) and the CfA sample (Riess et al. 1999; Jha et al. 2006b), have been used to improve the methods for using supernova light curves to measure supernova distances. Many variations on Phillips' idea have been developed, including Δm_{15} (Phillips et al. 1999), MLCS (Riess et al. 1996; Jha et al. 2007), DM15 (Prieto et al. 2006), stretch (Goldhaber et al. 2001), CMAGIC (Wang et al. 2003), and SALT (Guy et al. 2005).

These methods are capable of achieving the 10% precision for supernova distances that Kowal (1968) foresaw 40 years ago. In the ESSENCE analysis, we have used a version of the Jha et al. (2007) method called MLCS2k2. We have compared it with the results of the SALT (Guy et al. 2005) light-curve fitter used by the SuperNova Legacy Survey (SNLS; Astier et al. 2006). This comparison provides a test: if the two approaches do not agree when applied to the same data they cannot both be correct. As shown in §2, SALT and this version of MLCS2K2, with our preferred extinction prior, are in excellent accord when applied to the same data. While gratifying, this agreement does not prove they are both correct. Moreover, as described in §4, the cosmological results depend somewhat on the assumptions about SN host-galaxy extinction that are employed. This has been an ongoing problem in supernova cosmology. The work of Lira (1995) demonstrated the empirical fact that although SN Ia have a range of colors at maximum light, they appear to reach the same intrinsic color about 30–90 days past maximum light, independent of light curve shape.

Riess et al. (1996) used de-reddened SN Ia data to show that near maximum light intrinsic color differences existed with fainter SNe Ia appearing redder than brighter objects and then used this information to construct an absorption-free Hubble diagram. Given a good set of observations in several bands, the reddening for individual supernovae can then be determined and the general relations between supernova luminosity and the light curve shapes in many bands can be established (Hamuy et al. 1996; Riess et al. 1999; Phillips et al. 1999). The initial detections of cosmic acceleration employed either these individual absorption corrections (Riess et al. 1998) or a full-sample statistical absorption correction (Perlmutter et al. 1999). Finding the best approach to this problem, whether by shifting observations to the infrared, limiting the sample to low-extinction cases, or making other restrictive cuts on the data, is an important area for future work. Some ways to explore this issue are sketched in §4.

Kowal (1968) recognized that second-order terms in cosmic expansion might be measured with supernovae once the precision and redshift range grew sufficiently large. More direct approaches with the *Hubble Space Telescope (HST)* were imagined by Colgate (1979)

and with special clarity by Tammann (1979). Tammann anticipated that *HST* photometry of SNe Ia at $z \approx 0.5$ would lead to a direct determination of cosmic deceleration and that the time dilation of SN Ia light curves would be a fundamental test of the expansion hypothesis. While *HST* languished on the ground after the Challenger disaster, this line of research was attempted from the ground at the European Southern Observatory (ESO) by a Danish group in 1986–1988. Their cyclic CCD imaging of the search fields used image registration, convolution and subtraction, and real-time data analysis (Hansen et al. 1987). Alas, the rate of SNe Ia in their fields was lower than they had anticipated, and only one SN Ia, SN 1988U was discovered and monitored in two years of effort (Hansen et al. 1987; Norgaard-Nielsen et al. 1989). More effective searches by the Lawrence Berkeley Lab (LBL) group exploiting larger CCD detectors and sophisticated detection software showed that this approach could be made practical and used to find significant numbers of high-redshift SNe Ia (Perlmutter et al. 1995).

By 1995, two groups, the LBL-based Supernova Cosmology Project (SCP) and the High-Z Supernova Search Team (HZT; Schmidt et al. 1998)) were working in this field. The first SN Ia cosmology results using 7 high-redshift SNe Ia(Perlmutter et al. 1997) found a Universe consistent with $\Omega_{\mathrm{M}} = 1$ but subsequent work by the SCP (Perlmutter et al. 1998) and by the HZT (Garnavich et al. 1998) revised this initial finding to favor a lower value of Ω_{M}. At the January 1998 meeting of the American Astronomical Society both teams reported that the SN Ia results favored a universe that would expand without limit, but at that time neither team claimed the Universe was accelerating. The subsequent publication of stronger results based on larger samples by the HZT (Riess et al. 1998) and by the SCP (Perlmutter et al. 1999) provided a big surprise. The supernova data showed that SNe Ia at $z \approx 0.5$ were about 0.2 mag dimmer than expected in an open universe and pointed firmly at an accelerating universe (for first-hand accounts, see Overbye 1999; Riess 2000; Filippenko 2001; Kirshner 2002; Perlmutter 2003); reviews are given by Leibundgut (2001), Filippenko (2005b) and others.

The supernova route to cosmological understanding continues to improve. One source of uncertainty has been the small sample of very well observed low-redshift supernovae (Hamuy et al. 1996; Riess et al. 1999). The most recent contribution is the summary of CfA data obtained in 1997–2001 (Jha et al. 2006b), but significantly enhanced samples from the CfA (Hicken et al. 2006) together with new data from the Katzman Automatic Imaging Telescope (KAIT; Li et al. 2000; Filippenko et al. 2001; Filippenko 2005a), from the Carnegie SN Program (Hamuy et al. 2006), from the Supernova Factory (Wood-Vasey et al. 2004; Copin et al. 2006), and from the Sloan Digital Sky Survey II Supernova Survey (SDSS II; Frieman et al. 2004; Dilday et al. 2005) are in prospect. As the low-z sample approaches 200 objects, the size of the sample will cease to be a source of statistical uncertainty for the determination

of cosmological parameters. As described in §3, systematic errors of calibration and K-correction will ultimately impose the limits to understanding dark energy's properties, and we are actively working to improve these areas (Stubbs & Tonry 2006).

Some of the potential sources of systematic error in the high-z sample have been examined. The fundamental assumption is that distant SNe Ia can be analyzed using the methods developed for the low-z sample. Since nearby samples show that the SNe Ia in elliptical galaxies have a different distribution in luminosity than the SNe Ia in spirals (Hamuy et al. 2000; Gallagher et al. 2005; Neill et al. 2006; Sullivan et al. 2006b), morphological classification of the distant sample may provide some useful clues to help improve the cosmological inferences (Williams et al. 2003). For example, Sullivan et al. (2003) showed that restricting the SCP sample to SNe Ia in elliptical galaxies gave identical cosmological results to the complete sample, which is principally in spiral galaxies. The possibility of grey dust raised by Aguirre (1999a,b) was examined by Riess et al. (2000) and and by Nobili et al. (2005) through infrared observations of high-z supernovae and was put to rest by the very high-redshift observations of Riess et al. (2004). Improved methods for handling the vexing problems of absorption by dust have been developed by Knop et al. (2003) and by Jha et al. (2007). These questions are described in more detail in §3.3.

The question of whether distant supernovae have spectra that are the same as nearby supernovae has been investigated by Coil et al. (2000), Lidman et al. (2005), Matheson et al. (2005), Hook et al. (2005), Howell et al. (2005), and Blondin et al. (2006). The more telling question of whether these spectra evolve in the same way as those of nearby objects was approached by Foley et al. (2005). In all cases, the evidence points toward nearby supernovae behaving in the same way as distant ones, bolstering confidence in the initial results. This observed consistency does not mean that the samples are identical, only that the variations between the nearby and distant samples are successfully accounted for by the methods currently in hand. We do not know whether this will continue to be the case as future investigations press for more stringent limits on cosmological parameters (Albrecht et al. 2006).

The highest redshift SN Ia data (Riess et al. 2004) show the qualitative signature expected from a mixed dark-energy/dark-matter cosmology. That is, they show cosmic deceleration due to dark matter preceded the current era of cosmic acceleration due to dark energy. The sign of the observed effect on supernova apparent magnitudes reverses—SNe Ia at $z \sim 0.5$ appear 0.2 mag dimmer than expected in a coasting cosmology but the very distant supernovae whose light comes from $z > 1$ appear brighter than they would in that cosmology. By itself, this turnover is a very encouraging sign that supernova cosmology does not founder on grey dust or even on a simple evolution of supernova properties with cosmic

epoch. As part of this analysis, Riess et al. (2004) constructed the "gold" sample of high-z and low-z supernovae whose observations met reasonable criteria for inclusion in an analysis of all of the published light curves and spectra using a uniform method of deriving distances from the light curves.

The analysis of the gold sample provided an estimate of the time derivative of the equation-of-state parameter, w, for dark energy. These observations are very important conceptually because the simplest fact about the cosmological constant as a candidate for dark energy is that it should be constant (i.e., $w' = dw/dz = 0$). The observations are consistent with a constant dark energy over the redshift range out to $z \approx 1.6$. Other forms of dark energy could satisfy the observed constraints, but this observational test is one that the cosmological constant could have failed. In the analysis of the ESSENCE data presented in §4, we use the supernova data to constrain the properties of w, as first carried out by White (1998) and by Garnavich et al. (1998). This parameterization of dark energy by w is not the only possible approach. A more detailed approach is to compare the observational data to a specific model and, for example, try to reconstruct the dark energy scalar-field potential (see, for example, Li et al. 2006). A more agnostic view is that we are simply measuring the expansion history of the universe, and a kinematic description of that history in terms of expansion rate, acceleration, and jerk (Riess et al. 2004; Rapetti et al. 2006) covers the facts without assuming the nature of dark energy.

The ESSENCE project was conceived to tighten the constraints on dark energy at $z \approx 0.5$ to reveal any discrepancy between the observations and the leading candidate for dark energy, the cosmological constant. A simple way to express this is that we aim for a 10% uncertainty in the value of w. This program is similar to the approach of the SuperNova Legacy Survey (SNLS) being carried out at the Canada-France-Hawaii Telescope, and we compare our methods and results to theirs (Guy et al. 2005; Astier et al. 2006) at several points in the analysis below.

The SNLS has taken the admirable step of publishing their light curves online and making the code of their light-curve fitting program, SALT, available for public inspection and use[2]. Making the light curves public, as was done for the results of the HZT and its successors Riess et al. (1998); Tonry et al. (2003); Barris et al. (2004); Krisciunas et al. (2005); Clocchiatti et al. (2006), by Knop et al. (2003), by Riess et al. (2004) for the very high redshift *HST* supernova program, and for the low-z data of Hamuy et al. (1996), Riess et al. (1999), and Jha et al. (2006b), provides the opportunity for others to perform their own analysis of the results. In addition to exploring a variety of approaches to analyzing our own

---

[2]http://snls.in2p3.fr/conf/release/

SN Ia observations, we show the first joint constraints from ESSENCE and SNLS, and some joint constraints derived from combining these with the Riess et al. (2004) gold sample in §4.

2. Luminosity Distance Determination

The physical quantities of interest in our cosmological measurements are the redshifts and distances to a set of space-time points in the Universe. The redshifts come from spectra and the luminosity distances, D_L, come from the observed flux of the supernova combined with our understanding of SN Ia light curves from nearby objects.

Extracting a luminosity distance to a supernova from observations of its light curve necessitates a number of assumptions. We use the observations of nearby supernovae to establish the relations between color, light-curve shape in multiple bands, and peak luminosity. These nearby observations attain high signal-to-noise ratios, and the nearby objects can be observed in more passbands (including infrared) than faint distant objects. We assume that the resulting method of converting light curves to luminosity distances applies at all redshifts. The observed spectral uniformity of supernovae over a range of redshift (Lidman et al. 2005; Hook et al. 2005; Blondin et al. 2006) supports this approach. We assume that R_V, the ratio of selective to absolute extinction, is independent of redshift. Below in §3.3, we test the potential systematic effect of departures from this assumption. We adopt an astrophysically sensible prior distribution of host-galaxy extinction properties, with a redshift dependence that is derived from the simulations we present below.

Our approach is to conduct comprehensive simulations of the ESSENCE data and analysis. As described by Miknaitis et al. (2007), we use this same approach to explore our photometric performance. For the aspects of our analysis that are "downstream" of the light-curve generation, we generate sets of synthetic light curves and subject them to our analysis pipeline. In this way we can test the performance of our distance-fitting tools, and by exaggerating various systematic errors (zeropoint offsets, etc.) we can assess the impact of these effects on our determination of w.

We must recognize and emphasize that in the era of precision SN Ia cosmology (constraining dark energy properties, rather than just detecting its existence), careful attention to systematic errors is of paramount importance: shifts of a few hundredths of a magnitude can lead to constraints on w that change by 0.1. Different, yet defensible, choices in the analysis chain may show such effects.

2.1. Extracting Luminosity Distances from Light Curves: Distance Fitters

We use the MLCS2k2 method of Jha et al. (2007) as the primary tool to derive relative luminosity distances to our SNe Ia. For comparison, we also provide the results obtained using the Spectral Adaptive Lightcurve Template (SALT) fitter of Guy et al. (2005) on the

ESSENCE light curves. SALT was used in the recent cosmological results paper from the SNLS (Astier et al. 2006, , hereafter A06). We provide a consistent and comprehensive set of distances obtained to nearby, ESSENCE, and SNLS supernovae for each luminosity-distance fitting technique. The ESSENCE light curves used in this analysis were presented by Miknaitis et al. (2007) and we provide them online, together with our set of previously published light curves for nearby SNe Ia, for the convenience of those interested.[3] Additional SN Ia light-curve fitting methods will be further explored in future ESSENCE analyses. Understanding the behavior of our distance determination method is critical to our goal of quantifying the uncertainties of our analysis chain.

MLCS2k2 and SALT, as well as the light-curve "stretch" approach used by Perlmutter et al. (1997, 1999), Goldhaber et al. (2001) and Knop et al. (2003), exploit the fact that the rate of decline, the color, and the intrinsic luminosity of SNe Iaare correlated. At present we treat SNe Ia as a single-parameter family, and the distance fitting techniques use multi-color light curves to deduce a luminosity distance and host-galaxy reddening for each supernova. Previous papers have shown that the different techniques produce relative luminosity distances that scatter by ~ 0.10 mag for an individual SN Ia (e.g., Tonry et al. 2003), but this scatter is uncorrelated with redshift. As a consequence, the cosmology results are insensitive to the distance fitting technique. However, as described by Miknaitis et al. (2007), the measurement of the equation-of-state parameter hinges on subtle distortions in the Hubble diagram, so we have undertaken a comprehensive set of simulations to understand potential biases introduced by MLCS2k2.

The MLCS2k2 approach (Riess et al. 1996, 1998; Jha et al. 2007) to determining luminosity distances uses well-observed nearby SNe Ia to establish a set of light-curve templates in multiple passbands. The parameters Δ (roughly equivalent to the variation in peak visual luminosity, this parameter characterizes intrinsic color, rate of decline, and peak brightness), A_V (the V-band extinction of the supernova light in its host galaxy), and μ (the distance modulus) are then determined by fitting each multi-band set of distant supernova light curves to redshifted versions of these templates. Jha et al. (2006c) present results from MLCS2k2 based on nearby SN Ia. Here we have modified MLCS2k2 for application to both high and low-redshift SNe Ia. We begin with a rest-frame model of the SN Ia in its host galaxy, and then propagate the model light curves through the host-galaxy extinction, K-correction, Milky Way extinction to the detector, incorporating the measured passband response (including the atmosphere for ground-based observations). We then fit this model directly to the natural-system observations. This forward-modeling approach has particular advantages

---

[3]http://www.ctio.noao.edu/essence/

in application to the more sparsely sampled (in color and time) data typical of high-redshift SN searches.

The SALT method of Guy et al. (2005), which was used for the SNLS first-results analysis of A06, constructs a fiducial SN Ia template using combined spectral and photometric information, then transforms this template into the rest frame of the SN Ia, and finally calculates a flux, stretch, and generalized color. The color parameter in SALT is notable in that it includes both the intrinsic variation in SN Ia color and the extinction from dust in the host galaxy within a single parameter (in contrast, MLCS2k2 attempts to separate these components of the observed colors for each supernova). While the reddening vector (attenuation vs. color excess) is similar to the SN Ia color vs. absolute magnitude relation, the two sources of correlated color and luminosity variation are not identical.

The stretch and color parameters of SALT were used by A06 to estimate luminosity distances by fitting for the stretch-luminosity and color-luminosity relationships in the nearby sample and applying those to the full SNe Ia sample. Given that the SALT color parameter conflates the two physically distinct phenomena of host-galaxy extinction and SN Ia color variation, it is remarkable and perhaps a source of deep insight that this treatment works as well as it does. Because of both survey selection effects and possible demographic shifts in the host environments of SNe Iawe would not expect that the proportion of reddening from dust and from intrinsic variation would remain constant with redshift as this approach assumes. However, the SALT/A06 method does seem to work quite well in practice.

2.2. Sensitivity to Assumptions about the Host-Galaxy Extinction Distribution: Extinction Priors

The best way to treat host-galaxy extinction is a serious question for this work and for the field of supernova cosmology. The Bayesian approach we use is detailed in §3.4. Here we describe simulations that are designed to evaluate the effects of those methods.

There have been four basic approaches to combining reddening measurements with astrophysical knowledge to determine the host galaxy extinction along the line-of sight: (1) assume that linear A_V is the natural space for extinction and assume a flat prior (Perlmutter et al. 1999; Knop et al. 2003); (2) use models of the dust distribution in galaxies (Hatano et al. 1998; Commins 2004; Riello & Patat 2005) to model line-of-sight extinction values (Riess et al. 1998; Tonry et al. 2003; Riess et al. 2004); (3) assume that the distribution of host-galaxy A_V follows an exponential form (Jha et al. 2007), based on observed distributions of A_V in nearby SNe Ia; and (4) self-calibrate within a set of low-z SNe Ia to obtain a consistent

color$+A_V$ relationship and assume that relation for the full set (Astier et al. 2006).

Approach (1) assumes the least prior knowledge about the distribution of A_V and produces a Gaussian probability distribution for the fitted luminosity distance. However, this approach weakens the ability to separate intrinsic SN Iacolor from A_V and results in a fit parameter A_V that is a mixture of the two. An A_V that is truly related to the dust extinction should never be negative. The probability prior with $-\infty < A_V < +\infty$ is not the natural range over which to assume a flat distribution. The physically reasonable prior on A_V should be strictly positive. One approach is to base the prior for absorption on the distribution of dust in galaxies. Theoretical modeling of dust distributions in galaxies, such as that of Hatano et al. (1998), Commins (2004), and Riello & Patat (2005), provides a physically motivated dust distribution. This method represents approach (2) above and is the method we adopt here. In contrast, Jha et al. (2007) empirically derived an exponential A_V distribution from MLCS2k2 fits to nearby SNe Ia by assuming a particular color distribution of SNe Ia. This distribution was derived using the empirical fact that SNe Ia reach a common color about 40 days past maximum light (Lira 1995). They found an exponential distribution of A_V,

$$p(A_V) \propto \exp\left(\frac{-A_V}{\tau}\right), \tag{1}$$

where $\tau = 0.46$ mag. Unfortunately, the highest-extinction objects drive the tail of this exponential and significantly affect the fit, resulting in a prior sensitive to sample selection, which differs significantly in high-redshift searches compared to the nearby objects studied by Jha et al. (2007).

A06 analyzed the results of the SALT SN Ia light-curve fitter with approach (4) and have systematic sensitivities that are similar to those of approach (1).

We use MLCS2k2 as our main analysis tool. We designate approach (1) the "flatnegav" prior and approach (3) the "default" prior and discuss both of these further in §3.4. Approach (2) is based on a galactic line-of-sight or "glos" prior on A_V:

$$\hat{p}(A_V) \propto \frac{A}{\tau}\exp\left(\frac{-A_V}{\tau}\right) + \frac{2B}{\sqrt{2\pi}\sigma}\exp\left(\frac{-A_V^2}{2\sigma^2}\right), \tag{2}$$

where $A = 1$, $B = 0.5$, $\tau = 0.4$, $\sigma = 0.1$, and $\hat{p}(A_V) \equiv 0$ for $A_V < 0$. This exponential plus one-sided narrow Gaussian "glos" prior is based on the host-galaxy dust models of Hatano et al. (1998), Commins (2004), and Riello & Patat (2005). As described below, we have modeled our selection effects with redshift to adapt the "glos" prior into the "glosz" prior that is the basis for our analysis. We feel this approach leverages our best understanding of the effects of extinction and selection.

Figs. 1 and 2 show the distribution of the fit parameters and overlay the prior distribution assumed for each of these approaches. Fig. 7 compares the fit distances and extinction/color parameters of the MLCS2k2 "glosz" and SALT fit results for the ESSENCE, SNLS, and nearby samples. The distribution of recovered Δ and A_V match their imposed priors for MLCS2k2 "glosz" while the stretch and color fit parameters from SALT show a consistent distribution for the three different sets of SNe Ia.

2.3. ESSENCE Selection Effects and the Motivation for a Redshift-Dependent Extinction Prior

We examined the effect of the survey selection function on the expected demographics of the ESSENCE SNe Ia and explored the interplay between extinction, Malmquist bias, and our observed light curves. To determine the impact of the selection bias, we developed a Monte Carlo simulation of the ESSENCE search. We created a range of supernova light curves that match the properties of the nearby sample, added noise based on statistics from actual ESSENCE photometry, and then fit the resulting light curves in the same way the real events are analyzed. In this way we estimated the impact of subtle biases, although this simulation cannot test for errors in our light-curve model or population drift with redshift.

Based on its low-redshift training set, MLCS2K2 is able to output a finely sampled light curve given a redshift (z), distance modulus (μ), light-curve shape parameter (Δ), host extinction (A_V), host extinction law (R_V), date of rest-frame B-band maximum light (t_0), Milky Way reddening ($E(B - V)_{\mathrm{MW}}$), and the bandpasses of the observations. At a given redshift we calculated a distance modulus, μ_{true}, from the luminosity distance for the standard cosmology ($\Omega_m = 0.3$, $\Omega_\Lambda = 0.7$) and that distance modulus plus an assumed $M_B = -19.5$ for SNe Ia set the brightness for our simulated supernovae. Varying the assumed cosmology does not significantly impact the simulation results since we are comparing the input distance modulus with the recovered distance modulus, μ_{obs}, which is independent of the cosmology.

At each of a series of fixed redshifts, we created ~ 1000 simulated light curves with parameters chosen from random distributions. The light-curve width, Δ, was selected from the Jha et al. (2007) distribution measured from the low-z sample. The Δ distribution is approximately a Gaussian peaking at $\Delta = -0.15$ with an extended tail out to $\Delta = 1.5$. The host extinction for each simulated event, A_V, was selected from either the Jha et al. (2007) distribution ("default") estimated from the local sample or from a "galaxy line-of-sight" estimation ("glos"). The "default" distribution was an exponential decay with index 0.46 mag and set to zero for $A_V < 0.0$ mag. The "glos" distribution is also set to zero for

$A_V < 0.0$ mag and combines a narrow Gaussian with a exponential tail for $A_V > 0.0$ mag (see Eq. 2). The extinction law is assumed to be $R_V = 3.1$. The Milky Way reddening $[E(B-V)_{MW}]$ distribution was constructed from the Schlegel et al. (1998) (hereafter SFD) reddening maps that cover the ESSENCE fields. The $E(B-V)_{MW}$ was measured for 10,000 random locations in each ESSENCE field and the reddening was selected from the sum of the histograms (see Figure 2). The dates of observation for a simulated SN Ia were based on the actual dates of ESSENCE 4-m observations. An ESSENCE field was chosen at random from the list of monitored fields and a date of maximum, t_0, selected to fall randomly between the Modified Julian Date (MJD) of the first and last observation of an observing season. The simulated light curve was then interpolated for only those dates that ESSENCE took images. With each ESSENCE field observation, we estimated the magnitude in R and I that provided a 10σ photometric detection based on the seeing and sky brightness. The signal-to-noise ratio (SNR) for each simulated light-curve point was then scaled from the 10σ detection magnitude, assuming the noise was dominated by the sky background.

For each date of ESSENCE observation, we have a simulated noiseless magnitude and an estimate of the SNR of the observation. To each simulated observation we added an appropriate random value in flux space selected from a normal distribution with a width corresponding to the predicted SNR.

MLCS2k2 was then used to fit the simulated light curves and provide estimates of μ, Δ, A_V, and t_0, assuming a fixed $R_V = 3.1$. MLCS2k2 required an initial guess of the date of maximum, an estimate achieved by selecting from a normal distribution about the true date with a 1σ width of 2 days. The SFD Milky Way reddening was also required in MLCS2k2 and was provided from the true reddening after adding an uncertainty of 10%. Finally, in the real ESSENCE data we discarded supernovae when the MLCS2k2 reduced χ^2 indicated a very poor fit. For the simulated light curves, we dropped events from the sample if the reduced χ^2 exceeded 2.

2.3.1. Deriving an Extinction Prior from the Simulation Results

Simulated ESSENCE samples were created at a range of redshifts out to $z = 0.70$ and the light curves that passed the detection criteria from the actual ESSENCE search were fit with MLCS2k2. The fitting was done with the "default" prior and the "glos" prior (with corresponding A_V distributions). The difference between the "true" (input) distance modulus and recovered (fit) distance modulus, $\Delta\mu$, was calculated for each event and the mean, median, and dispersion for the ensemble were calculated at each redshift. The median $\Delta\mu$ of the simulations was within 0.03 mag for $z < 0.45$, but at higher redshift the simulated

supernovae were estimated to be brighter than the input supernovae by more than 0.2 mag. This bias results from the loss of faint events (large A_V and large Δ) from the sample as the distance increases. In a sense, this is a classic Malmquist bias, but here it is caused by an uninformed prior. These results are shown in Fig. 3.

The decreasing ability to observe large A_V events as the redshift increases (see Fig. 4) makes it clear that a using single A_V prior for all redshifts is not correct. Because events with large A_V and large Δ are lost at large redshift due to the magnitude limits of the search, we should adjust the prior as a function of z to account for these predictable losses. Applying redshift-dependent window functions to the basic "glos" prior provides a much better prior as a function of redshift.

We fit the recovered A_V distributions derived from the simulations, which start with a uniform A_V, to a window function based on the error function (integral of a Gaussian), and two parameters describe where that function drops to half its peak value ($A_{1/2}$) and the width of the transition (σ_A). The window function W has the form

$$W(A_V, A_{1/2}, \sigma_A) = 1 - \frac{1}{\sqrt{\pi}} \int_{-\infty}^{(A_V - A_{1/2})\sigma_A} e^{-x^2} \, dx \tag{3}$$

where $A_{1/2}$ and σ_A are functions of z and estimated from the simulations. A similar process was applied to the Δ distribution and a table providing the parameters is given in Table 2. We embody this prescription in the "glosz" prior we use for our main MLCS2k2 light-curve fitting. The "glosz" prior is the "glos" prior modified by the window functions in A_V and Δ. The simulations using the "glosz" prior provide a median $\Delta\mu$ within 0.03 mag for $z < 0.7$, which we judge to be satisfactory performance.

2.4.   Comparison of MLCS2k2 and SALT Luminosity Distance Fitters

The release of the source code to the SALT fitter (Guy et al. 2005) makes a modern SN Ia light-curve fitter fully accessible and available to the community. This public release of SALT allows us to compare the results of our MLCS2k2 distance fitter with the SALT fitter used in the SNLS first results paper (Astier et al. 2006). We present the results of SALT fits to our nearby and ESSENCE samples in Table 10. To compute the distance moduli we quote in that table, we assume the $\alpha = 1.52$, $\beta = 1.57$ values from A06. To calibrate the additional dispersion to add to the distance moduli of MLCS2k2 and SALT, we fit a ΛCDM model to the nearby sample alone and derived the additional σ_{add} to added in quadrature to recover $\chi^2/\mathrm{DoF} = 1$ for the nearby sample. This σ_{add} is related to the intrinsic dispersion of the absolute luminosity of SNe Ia, but is not precisely the same both because the light-curve fitters include varying degrees of model uncertainty and because the light curves of the

SNe Ia are subject to photometric uncertainty. We find $\sigma_{\mathrm{add}} = 0.10$ for MLCS2k2 with the "glosz" prior and $\sigma_{\mathrm{add}} = 0.13$ for SALT. These values should be added to the σ_{μ} uncertainties given Tables 9 and 10 Fig. 7 visually demonstrates that the relative luminosity distances using the SALT light-curve fitter agree, within uncertainties, with the MLCS2k2 distances when the latter are fit using the "glosz" A_V prior.

2.5. Testing the Recovery of Cosmological Models Using Simulations of the ESSENCE Dataset

In order to assess the reliability with which we recover cosmological parameters, we have simulated 100 sets of 100 light curves representing both the nearby and the ESSENCE light curves. Table 1 presents the quality cuts for MLCS2k2 we derived from these simulated light-curve sets. Our light-curve goodness-of-fit cuts, when applied to these simulated light curves (see Table 1) and combined with the same external constraints of baryon acoustic oscillations (BAO; Eisenstein et al. 2005) and flatness, allow us to recover our input cosmology of ($\Omega_M = 0.3, \Omega_\Lambda = 0.7, w = -1$) to within ± 0.11 in w. This ± 0.11 uncertainty on an individual measurement of w is matched by the $\sigma = 0.11$ distribution of recovered w values from the 100 sets of simulated light curves. This confirms our statistical error estimate on w; the estimated uncertainty matches the distribution, and within the self-consistent realm of synthetic and analyzed light curves based on MLCS2k2 our estimates of luminosity distance are not biased.

3. Potential Sources of Systematic Error

Here we identify and assess sources of systematic error that could afflict our measurements. These can be divided into two groups. Certain sources of systematic error may introduce perturbations either to individual photometric data points or to the distances or redshifts estimated to the SNe Ia. Others affect the data in a more or less random fashion and produce excess *scatter* in the Hubble diagram. Errors that are uncorrelated with either distance or redshift will not bias the cosmological result. These sources of photometric error are detailed by Miknaitis et al. (2007); we summarize those results here in Table 4. We add these effects in quadrature to the statistical uncertainties given by the luminosity distance fitting codes for each SN Ia distance measurement: $\sigma_\mu^{\mathrm{photscatter}} = 0.026$ mag.

In §2 we discussed our testing of the MLCS2k2 fitter on simulated data sets that replicate the data quality of the ESSENCE and nearby SNe Ia. We explore the issue of host-galaxy extinction further in §3.3 & 3.4. The interaction of Malmquist bias and selection effects with the extinction and color distribution of SNe Iais discussed in §3.5.

Any non-cosmological difference in measurements of nearby and distant SNe Ia has the potential to perturb our measurement of w. Table 5 lists potential systematic effects of this sort. We present both our estimate of the sensitivity dw/dx of the equation-of-state parameter to each potential systematic effect and our best estimate of the potential size of the perturbation, Δx. The upper bound on the bias introduced in w is then $\Delta w = dw/dx \times \Delta x$. Miknaitis et al. (2007) discusses the systematic uncertainties on μ, which we convert here to systematic uncertainties on w, due to photometric errors from astrometric uncertainty on faint objects ($\Delta w = 0.005$), potential biases from the difference imaging ($\Delta w = 0.001$), and linearity of the MOSAIC II CCD ($\Delta w = 0.005$). None of these contributed noticeably to the systematic uncertainty in our measurement of w. The rest of this section describes how we appraised our additional potential sources of systematic uncertainty.

The conclusion of this section is that our current overall estimate for the 1σ equivalent systematic uncertainty in a static equation-of-state parameter is $\Delta w = 0.13$ for our "glosz" analysis.

3.1. Photometric Zeropoints

Supernova cosmology fundamentally depends on the ability to accurately measure fluxes of objects over a range in redshift. Errors in photometric calibration translate to errors in cosmology in two basic ways.

Nearby objects at redshifts < 0.1 play a crucial role in establishing a comparison reference for cosmological measurements. ESSENCE is inefficient at finding and observing low-redshift objects with the same telescope and detector system, so we use photometry of low-redshift SNe Ia in the literature from our own work and that of others (for the full list see Jha et al. 2007). Using these external SNe Ia requires understanding the photometric calibration of our high-redshift sample relative to this low-redshift sample. Every supernova cosmology result to date has made use of more or less the same low-redshift photometry, so any inaccuracies in the nearby sample are a source of common systematic error for all SN Ia cosmology experiments. Calibration of photometry at the $\sim 1\%$ level required to make precise inferences about the nature of dark energy is notoriously difficult (Stubbs & Tonry 2006).

Photometric miscalibration can result in a second, more insidious systematic error if there is an error in the relative flux scaling between the broad-band passbands. This offset would distort the observed colors for the entire sample. Since these colors are used to infer the extinction, even small color errors result in significant biases in the measured distances. After all, the inferred host galaxy extinction, A_V, is related to the measured color excess, $E(B-V)$, by $A_V \approx 3.1 E(B-V)$ (for Milky Way-like dust). A color error in rest-frame $B-V$ (observer-frame R, I for ESSENCE) of 0.01 mag can result in 0.03 mag error in extinction, an inaccuracy that would lead directly to a 3% error in the distance modulus, or a 1.5% error in the distance. We currently estimate our color zeropoint uncertainty at 0.02 mag and our absolute zeropoint (relative to the nearby SNe Ia) uncertainty to be 0.02 mag. These respectively translate to 0.04 and 0.02 shifts in w (see Table 5).

Miknaitis et al. (2007) describe the calibration program we undertook to measure the transmission of the CTIO 4-m MOSAIC II system with the R and I filters of the ESSENCE survey. The calibration of the ESSENCE survey fields will be further improved by an intensive calibration program we are undertaking on the CTIO 4-m in 2006. Together with the improved calibration of the SDSS Southern Stripe by the SDSSII project, which overlaps 25% of our ESSENCE fields, we aim to achieve 1% photometric calibration of our CTIO 4-m MOSAIC II BVRI natural system.

We here use MLCS2k2 v004 with the Bohlin & Gilliland (2004) values for the magnitudes of Vega: i.e., `alpha_lyr_stis_002.fits` with $R_{\mathrm{Vega}} = 0.033$ mag. This value for R_{Vega} comes from Bessell et al. (1998) but has been shifted down by 0.004 mag as Bohlin & Gilliland (2004) suggest (from their $V_{\mathrm{Vega}} = 0.026$ mag compared to Bessell et al. (1998) $V_{\mathrm{Vega}} = 0.030$ mag).

3.2. K-Corrections and Bandpass Uncertainty

Uncertainty in the transmission function, typically called the bandpass, of the optical path of the telescope+detector is an important and potentially systematic effect. In this context, bandpass refers to the wavelength-dependent throughput of the entire optical path, including atmospheric transmission, mirror reflectivity, filter function, and CCD response. Since an error in the assumed bandpasses translates into a redshift-dependent error in the supernova flux, it is important to account for possible errors in the bandpass estimates.

The *relative* error due to bandpass miscalibration is small for objects with similar spectra, such as SNe Ia. Bandpass shape errors are largely accounted for by the filter zeropoint calibration, with residual errors corresponding to the difference between the spectral energy distribution of the objects of interest and those of the calibration sources. In the case of SN Ia observations, any residual zeropoint error is absorbed when we marginalize over the "nuisance parameter," $\mathcal{M} = M_B - 5\log_{10}(H_0) + 25$ (Kim et al. 2004). This relative comparison results in a very small systematic error in the cosmological parameters from a global calibration error across bandpasses. Moreover, variations in atmospheric transmission are expected to contribute only random uncertainty.

However, the bandpass uncertainty becomes important when we compare SNe Ia at different redshifts for which the bandpass samples different spectral regions. In order to compare SNe Ia at multiple redshifts, we need to perform a K-correction (Leibundgut 1990; Hamuy et al. 1993; Kim et al. 1996; Nugent et al. 2002). That is, we assume a spectral distribution for the supernova and convert the observed magnitude to what it would have been had the supernova been at another redshift. This process involves performing synthetic photometry of the assumed spectral distribution over the assumed bandpass. We address the issue of systematics arising from errors in the assumed spectral distribution in the supernova evolution section, §3.6. Here we address systematics arising from errors in our determination of the CTIO 4-m MOSAIC II R and I bandpass functions. Systematic effects on supernova cosmology that result from bandpass uncertainties are discussed more thoroughly by Davis et al. (2006).

Calculating the effect of bandpass uncertainty is fairly difficult because of the arbitrary nature of the shape changes that might affect the bandpass. However, we can make several general calculations. As a first step, we take standard bandpasses and add white noise to represent a miscalibrated filter. White noise contributes power on all scales, so this approach adds small-scale discrepancies as well as large-scale warps or shifts in the filter. By averaging over many such miscalibrated filters, we can estimate the effect of filter miscalibration. Fig. 16 of Davis et al. (2006) shows photometric error as a function of noise amplitude. A noise amplitude of 0.02 produces a typical deviation of 2% from the nominal filter shape

at any wavelength. Calibrating the bandpass to better than 3% allows us to keep the K-correction error introduced from a mismeasurement of our effective bandpass to less than 0.005 mag (0.5% in flux) and a systematic uncertainty of $\Delta w = 0.005$.

3.3. Extinction

The most significant cause of variation in luminosity of SNe Ia is the extinction experienced by the light from the SN Iadue to scattering and absorption from dust in the host galaxy.

Dust introduces a wavelength-depended diminution of a supernova's light. In the case of Milky Way dust, we correct for its effects by using tabulated values as a function of Galactic longitude and latitude measured by other means (SFD Schlegel et al. 1998), being sure in our MLCS2k2 fits to properly account for its uncertainty and correlation across all observations. For dust in the supernova's host galaxy, we infer the extinction from the reddening of each supernova's light curve.

However, the slope of differential reddening, characterized in the Cardelli et al. (1989) extinction model by the parameter R_V, may vary. The nominal value of R_V for the Milky Way is 3.1, but different lines of sight within our galaxy have values of R_V that vary from 2.1 to 5.1. Studies of R_V in other galaxies have been more limited because we lack sources of known color and luminosity with which to probe the dust.

Because we use the supernova rest-frame $B - V$ color to determine the reddening of each SN Ia, and the distance modulus to a supernova is corrected by a value approximately three times the inferred reddening, extinction correction magnifies any source of systematic error in a supernova's observed effective color. Systematic color errors can result from photometry errors, redshift-dependent K-correction errors, and evolution in the colors of supernovae.

Using the IR-emission maps of the Galaxy from the all-sky COBE/DIRBE and IRAS/ISSA maps, SFD have estimated the dust column density around the sky, which can then be translated to a color excess. This analysis has largely superseded the work of Burstein & Heiles (1978), who used radio HI measurements and a relationship between gas and extinction to estimate the color excess across the sky. Burstein (2003) has reanalyzed the IR and HI measurements and finds that Milky Way extinctions are more precisely derived using the IR method. However, Burstein (2003) still finds a discrepant value for extinction at the poles, with SFD providing extinctions that are $E(B - V) = 0.02$ mag higher than what the HI measurements indicate. Burstein (2003) suggests as a possible explanation for the discrepancy that SFD may predict too large an extinction in areas with high gas-to-dust ratios.

Finkbeiner et al. (1999) precisely estimated their sensitivities to these systematics and concluded they had controlled them to 0.01 mag. The ESSENCE program targets fields at high Galactic latitude to minimize Galactic extinction. Although nearby and distant SNe Iaare both affected by the assumed Milky Way extinction, the nearby objects are observed in $B - V$, whereas the $z \approx 0.5$ objects are observed in $R - I$. An $E(B - V) = 0.02$ difference in extinction at the pole leads to approximately a 0.02 mag difference in the relative distances between $z = 0$ and $z = 0.5$ objects, assuming a Galactic reddening law, host-galaxy corrections based on rest-frame $B - V$ color, and distances based on V. For this analysis, we use the SFD extinction map values with an uncertainty of 16% for each individual SN Ia but assume an additional 0.01 mag of systematic uncertainty in our distance moduli to account for the known source of uncertainty of extinction at the pole.

In most supernova work we assume the Galactic reddening law (Cardelli et al. 1989) applies to external galaxies ($R_V = 3.1$), but studies of individual SNe Ia have found a range of values extending to much smaller values of R_V (Riess et al. 1996; Tripp 1998; Phillips et al. 1999; Krisciunas et al. 2000; Wang et al. 2003; Altavilla et al. 2004; Reindl et al. 2005; Elias-Rosa & The E: 2005). These measurements are dominated by objects with large extinction values, where a significant measurement can be made can be made of the extinction law (lessening the effects of intrinsic color scatter and systematic color variations with luminosity), and it is possible that R_V is correlated with total extinction (Jha et al. 2007). In principle, with photometry in three or more passbands, it is possible to fit for R_V, but in practice, at $z > 0.2$, there are only a few SNe Ia in the literature with the requisite high-precision photometry extending from the rest-frame UV to the near-IR. The systematic error on our measurement of D_L caused by assuming a particular value of R_V depends on the average extinction as a function redshift, assuming R_V is constant with z, except for a small correction caused by the rest-frame effective bandpass of our filters drifting away from the low-z values, depending on the precise redshift of each object. To quantify this effect, we fit our complete distance set with three different values of R_V: 2.1, 3.1, and 4.1.

3.4. Color and Extinction Distributions and Priors

To evaluate the systematic effects produced by various prior assumptions about extinction, we have fit the entire data set with a variety of plausible priors: the "exponential" prior of Jha et al. (2007), a flat prior from $-\infty$ to $+\infty$ (the "flatnegav" prior), and an exponential prior with an added Gaussian around zero that is based on models of the dust distribution in galaxies ("glos" and the redshift-dependent "glosz"). These results are presented in §4 and form the basis for Table 6.

To separate the effects of color and extinction, Jha et al. (2007) noted that the distribution of color excess in their nearby sample was consistent with a Gaussian distribution of $\sigma = 0.2$ convolved with a one-sided exponential, $\exp(-A_V/\tau)$, where $\tau = 0.46$ mag. As discussed in §2.2, the "glosz" prior we adopt here is derived from models of line-of-sight dust distributions in galaxies. It has more parameters than the simple exponential model of Jha et al. (2007), but we believe these additional parameters are well motivated.

The power of MLCS2k2 to distinguish between color and extinction lies in the ability to treat the two phenomena independently. A06 uses SALT and makes the assumption that the color+extinction distribution is the same in the nearby and in the high-redshift samples; the separation of the A_V component in the MLCS2k2 model allows us to model our expected distribution of A_V based on both models of dust in galaxies and selection effects of the ESSENCE survey. This separation allows us to take the nominal "glos" model and create the "glosz" prior that combines the distribution of dust in galaxies with the redshift-dependent selection effects.

The difference in the mean estimated parameter for a constant w is given in Table 6 for the different MLCS2k2 A_V priors discussed above. For the main MLCS2k2 "glosz" analysis we present here, we find a slope of $\Delta w/\Delta R_V = 0.02$ in the dependence of w on the assumed R_V. The effect on w of varying R_V is substantially greater for the less restrictive A_V priors because the covariance between A_V and μ is substantially greater for these priors. A reasonable variation of 0.5 in the value for R_V contributes a systematic uncertainty of $\Delta w = 0.01$

Differences in the inferred value of w for various assumed absorption priors shows that this is a significant systematic effect. The maximum difference between two priors, "exponential" and "glosz," for the nominal $R_V = 3.1$ case is $\Delta w = 0.165$. While we have conducted careful simulations to determine the most appropriate prior for our sample (see §2.3) and it is clear that the "exponential" is not appropriate for this analysis, we nonetheless take half of the difference between the two as representative of our systematic uncertainty, $\Delta_w^{\mathrm{prior}} = 0.08$, due to the choice of prior. The residual 0.02 mag shift of the simulations with the "glosz" prior shown in Fig. 4 for $z \approx 0.65$ results in a very small shift in Δw of only 0.001. Since we use an A_V, that obviously interacts strongly with our understanding of the intrinsic color distribution of SNe Ia. We estimate this contribution to our systematic error budget at $\Delta w = 0.06$ We have not undertaken a similar analysis with the SALT fitter, but the underlying assumption that the color, extinction, luminosity relationship for SNe Ia is constant with redshift is subject to uncertainties analogous to those considered here in the context of the MLCS2k2 A_V prior. The issue of color and extinction distributions clearly needs to be addressed for substantial further progress to be made in the field of supernova

cosmology.

3.5. Malmquist Bias and Other Selection Effects

As with all magnitude-limited surveys, at the faint limits of the survey we are more likely to observe objects drawn from the bright end of the SN Ia luminosity distribution. This Malmquist bias is particularly dangerous for inferences about cosmology based on supernova observations. However, it is not necessarily troubling that we may observe more luminous, broad events at high redshift, as long as the known empirical luminosity-width relation is valid at those redshifts. Rather, the concern for cosmological measurements is that at high redshift, we may preferentially find SNe Ia which are bright *for their light curve shape.* A second and more subtle concern is that at higher redshifts we are also less likely to detect SNe Ia whose light suffers significant absorption due to dust in their host galaxies.

We have modeled both of these effects (see §2.3 & 3.3) and have controlled for their impact. Our current limits on systematics due to uncontrolled selection effects is $\Delta_w^{\text{selection}} = 0.02$. A thorough study of the efficiency of the ESSENCE survey will be presented by Pignata et al. (2007). We aim for this future work to allow us to reduce this contribution to our systematic error to no more than 1%.

3.6. Type Ia Supernova Evolution

A persistent concern for any standard-candle cosmology is the possibility that the distant candles may differ slightly from their low-redshift counterparts. In a recent paper (Blondin et al. 2006) we compare the spectra of the high-redshift SNe Ia in this sample with low-redshift SNe Ia and demonstrate that there is no evidence for any systematic difference in their properties. This conclusion is based on line-profile morphology and measurements of the phase-evolution of the velocity location of maximum absorption and peak emission.

These results confirm a number of other studies of distant SNe Ia(e.g., Coil et al. 2000; Sullivan et al. 2003; Lidman 2004) that all confirm that, to the accuracy of current observations, the high and low redshift supernova populations are indistinguishable. Recently Hook et al. (2005) used spectral dating, spectral time sequences, and measurements of expansion velocities to compare distant and nearby SNe Ia; they also find no evidence for evolution in SN Ia properties up to $z \approx 0.8$.

Although we are confident that the subtypes of distant SNe Ia are well represented by the subtypes seen nearby, we cannot rule out a subtle shift in the population demographics that

may yet bias the estimates of cosmological parameters. This potential bias is of particular concern for future experiments that plan to measure the equation-of-state parameter, w, with an accuracy of a few percent. There is now evidence that SN Ia properties are correlated with host-galaxy morphology. Hamuy et al. (1996) and Riess et al. (1999) show that the brightest SNe Ia occur only in galaxies with on-going star formation. However, they observe no residual correlation after light-curve shape correction. Because the galactic demographics over the redshift range of interest change less than current variations in stellar population of SN Iahost galaxies, we remain confident that our one-parameter correction for supernova luminosity adequately corrects any shift in the average luminosity of SNe Ia to the same precision as in the nearby Universe, $\sigma_\mu < 0.02$ mag. We thus estimate a systematic uncertainty from possible SN Iaevolution on our measurement of w of $\Delta w = 0.02$.

One way to verify this confidence is to search for additional parameters that allow tighter luminosity groupings of the low-redshift population. In a first, reassuring step, Hubble diagrams for subsets of SNe Ia based on host-galaxy type separately confirm the accelerated expansion of the Universe (Sullivan et al. 2003).

3.7.   Hubble Bubble and Local Large-Scale Structure

The local large-scale structure and associated correlated flows of the Universe should not yet present a significant contribution to the systematic error budget of the current survey (Hui & Greene 2006; Cooray & Caldwell 2006). However, at the lowest multipoles we are sensitive to local correlated flows, and, at the most extreme, our cosmological results would be sensitive to a local velocity monopole or "Hubble bubble." Jha et al. (2007) see such an effect in their analysis of nearby SNe Ia. We use only the subset of SNe Ia from Jha et al. (2007) with $z > 0.015$ and find that this effect could contribute as much as 0.065 to our systematic error budget in w. We will rely on future sets of nearby SNe Ia ($0.01 < z < 0.05$) that are now being acquired at the CfA, by the Carnegie Supernova program, by the Lick Observatory Supernova Search, and by the SNfactory to reduce this uncertainty below 2% to help achieve the desired systematic uncertainty required for the final ESSENCE analysis.

3.8.   Gravitational Lensing

Gravitational lensing can increase or decrease the observed flux from a distant object. The expected distribution is asymmetric about the average flux multiplier of unity. Holz & Linder (2005) calculate the effect for SN Iasurveys and determine that any sys-

tematic effect from neglecting the asymmetry of the probability distribution function for magnification (as we do here) decreases quickly with the number of SNe Ia per effective bin. Roughly speaking, at a $z \approx 0.5$, in a redshift bin width of $\Delta z \sim 0.1$, ten SNe Ia per bin are sufficient to reduce any systematic effect in luminosity distance to less than 0.3%, which makes no noticeable contribution to our systematic error budget. For the redshifts of interest in the ESSENCE survey, lensing has a more significant effect in the scatter it adds to the observed brightness of SNe Ia. Holz & Linder (2005) calculate a 3% increase in the dispersion in distance modulus at $z \approx 0.5$. We include the effect of lensing in our analysis by adding a statistical dispersion of $\sigma_\mu^{\mathrm{lensing}} = 0.03$ to our luminosity distance uncertainty for the ESSENCE and SNLS SNe Ia.

3.9.   Grey Dust

When the first cosmological results with SNe Ia were announced, that distant SNe Ia were dimmer than they would be in a decelerating Universe, Aguirre (1999a,b) suggested various models for intergalactic grey dust that could explain this dimming without producing observable reddening. To explain SNe Iabecoming consistently dimmer with distance, this dust would need to be distributed throughout intergalactic space beginning at least at $z = 2$ (Goobar et al. 2002). The most naive model of such dust distribution and creation would predict that SNe Ia should continue to get dimmer relative to a flat, $\Omega_{\mathrm{M}} = 1$, cosmology all the way up to at least a redshift of 2. The high-redshift SN Ia work of Riess et al. (2004) demonstrated that this continued dimming is not what is observed: the apparent magnitudes of SNe Ia become first a little dimmer and then a little brighter with redshift than they would in an empty Universe. This is exactly what we expect from an early phase of deceleration followed by a recent phase of acceleration in a mixed, dark-matter/dark-energy cosmology.

A more complicated model of dust was contrived by Goobar et al. (2002). It involves the creation of intergalactic dust at just the right rate to match the decrease in opacity due to expansion of the Universe. This carefully constructed model mimics the signal of an accelerating universe and is difficult to distinguish from a universe that is presently dominated by dark energy. This model does not have a strong underpinning in the behavior of known dust and represents a form of fine-tuning. In the larger context of converging cosmological evidence, this particular scheme for matching the data seems less plausible than a universe with dark energy.

Recent observational constraints from non-SN Ia sources have independently placed significant constraints on the amount of intergalactic dust (Petric et al. 2006; Östman et al. 2006). In particular, the observations of Petric et al. (2006) limit intergalactic dust to con-

tributing no more than one percent to potential dimming of light out to a redshift of 0.5, based on upper limits to X-ray scattering by dust along the line of sight to a quasar at $z = 4.3$.

4. Cosmological Results from the ESSENCE Four-Year Data

The ESSENCE SNe Ia allow us test the hypothesis of a ΛCDM concordance model and constrain flat, constant-w models of the Universe. We use our MLCS2k2 light-curve fitting technique to measure luminosity distances to nearby and ESSENCE SNe Ia (Table 9). When then fit cosmological models to constrain the properties of the dark energy. We compare the results we obtain using MLCS2k2 with those obtained using the SALT light-curve fitter (Guy et al. 2005). The SALT fitter was used to fit the nearby light curves, our ESSENCE light curves, and the SNLS light curves.[4] To verify that we were making appropriate use of the fitter, we fit the nearby and SNLS light curves with SALT, taking the same $\alpha = 1.52$ and $\beta = 1.57$ width and color parameters used in A06. We recovered the w result of A06 to within 0.01 in best-fit constant w in a model with a flat Universe using the cosmology fitter that we employ here[5]. We have compiled our light curves of nearby SNe Ia from the literature independently of the SNLS analysis and used slightly different quality cuts, so it is quite encouraging that we can replicate these results. Table 10 gives the SALT fit parameters for the nearby, ESSENCE, and SNLS SNe Ia discussed here.

4.1. ESSENCE SN Ia Sample

For the ESSENCE project we find that using photometric selection criteria based on the color and rise time of the candidate object, similar to those used by the SNLS (Howell et al. 2005; Sullivan et al. 2006a), and in good weather and seeing conditions, 80% of the candidates we take spectra of are SNe Ia. We use a deterministic analysis (Blondin 2007), as described in Miknaitis et al. (2007), to determine final types and redshifts for our SNe and to cull objects that are not SNe Ia from our sample. All of the ESSENCE supernovae used in this analysis were spectroscopically confirmed as SNe Ia.

From 2002–2005 the ESSENCE project discovered and spectroscopically confirmed 113 SNe Ia. As discussed by Miknaitis et al. (2007), which gives full details of these SNe Ia including their RA and Dec, only 4 of the 15 SNe Ia from 2002 have been fully analyzed so that leaves us with 102 SNe Ia. Although we kept 91T-like SNe Ia such as d083, d085, and d093, we rejected the peculiar SN Ia d100 (Matheson et al. 2005). Three SNe Ia were rejected from the nearby+ESSENCE only fits because they were at redshifts greater than 0.67 (see below). After we applied the cuts in Tables 1 and Tables 3, we were left with 57 and 60 SNe Ia for

---

[4]http://snls.in2p3.fr/conf/release/

[5]http://qold.astro.utoronto.ca/conley/simple_cosfitter/

MLCS2k2 and SALT respectively.

With the MLCS2k2 fitter, the largest cut was the 32 SNe Ia rejected because they had fewer than 8 data points with an SNR > 5, no such points after $+9$ days, or no such points before $+4$ days. Two of the 102 SNe Ia were located near edges of the detector field-of-view that we later determined were photometrically less reliable. Due to high χ^2/DoF or related poor light-curve goodness-of-fit values, we eliminated an additional 6 SNe Ia. This left us with a total of 57 SNe Ia for our main MLCS2k2 nearby+ESSENCE analysis. The SALT fitter successfully fit three more SNe Ia than MLCS2k2, but, in general, our SALT quality cuts accepted the same SNe Ia as our MLCS2k2 quality cuts. The requirements we imposed here on the light curves were stringent cuts to ensure reliable fit parameters. We are currently engaged in an active program to improve the sensitivity of SN Ia light-curve fitters and we anticipate recovering 50% of the SNe Ia rejected here in the final ESSENCE analysis.

4.2. Nearby SN Ia Sample

The SN Ia cosmological measurement is fundamentally a comparison of the luminosity distance vs. redshift relation at low redshift and high redshift. The ESSENCE SNe Ia alone provide a homogeneous set of luminosity distance vs. redshift measurements covering the redshift range $0.15 < z < 0.7$. We selected our nearby SNe Ia from the set compiled by Jha et al. (2007). We applied the light-curve criteria from Tables 1 and 3 and also rejected known peculiar SNe Ia such as SN 2000cx (Li et al. 2001) and SN 2002cx (Li et al. 2003; Jha et al. 2006a). Our list of nearby SNe Ia has 41 SNe Ia in common with the set used by A06. To minimize complications from loosely constrained local peculiar and coordinated flows, we only considered SNe Ia with CMB-frame redshifts of $z > 0.015$. Our final sample consists of 45 nearby SNe Ia as listed in the fit parameter tables (Tables 9 and 10). We used the re-derived Landolt/Vega calibration of A06 to determine the passbands for this set of nearby SNe Ia. The light curves we used for these SNe Ia are also included with the ESSENCE light curves available on our website.[6]

---

[6]http://www.ctio.noao.edu/essence/

4.3. External Constraints

To provide complementary cosmological constraints on our SN Ia observations, we include external information from baryon acoustic oscillations (BAO; Eisenstein et al. 2005). The BAO constraints on (Ω_M, w) from Eisenstein et al. (2005) are the most complementary measurement in the (Ω_M, w) plane to our SN Ia measurements, relying only on the observed redshift and angular size of the first doppler peak in the CMB and not on H_0. In addition, because the BAO constraints on Ω_M are similar in precision (and value) to those derived from large scale structure (Percival et al. 2001, 2002), WMAP directly (Spergel et al. 2006), and from the study of X-ray clusters (for a review see Voit 2005), we choose to combine our results only with the BAO results.

We compare the specific model of a flat Universe with either $w = -1$ or constant w of any value to our data. SNe Ia have very little leverage on the global flatness of the Universe because they effectively measure the difference between Ω_M and Ω_Λ, and flatness depends on the sum. Eisenstein et al. (2005) have constrained curvature to be within $\Omega_K = \pm 0.01$ of flat. The results presented here (from the SNe Ia) on w are not significantly affected by variation of Ω_K by this amount, because the effects of curvature are not noticeable until looking back to much higher redshift. However, non-flat models will significant alter the BAO results on (Ω_M, w) and therefore our joint constraints.

For our analysis of the ESSENCE and nearby SNe Ia, we have chosen to additionally limit our redshift range to $z < 0.670$ to avoid using the rest-frame U band. Since this remove just three ESSENCE SNe Ia from our sample, the tradeoff is worthwhile to minimize this source of uncertainty (see §2). When we add in the SNLS or Riess gold samples, we relax this constraint to incorporate those higher-redshift SNe Ia.

In Figs. 8 and 9 we show Hubble diagrams of the nearby, ESSENCE, and SNLS samples for the two different fitters we consider in this paper. We overplot an empty Universe $(\Omega_M, \Omega_\Lambda, w) = (0, 0, -1)$, a matter-only open Universe $(0.3, 0, -1)$, and a ΛCDM concordance cosmology $(0.27, 0.73, -1)$. The residuals in luminosity distance are then shown with respect to the ΛCDM model. MLCS2k2 appears to be more suited for the ESSENCE data sample than SALT, although the latter benefits from its flux-based fitting by being able to extract useful luminosity distances from a few more SNe Ia. One SN Ia, "d083," is a particular outlier in both fitters at ~ 0.5 mag brighter than expected in the best-fit or ΛCDM cosmologies. Matheson et al. (2005) found the spectrum of this object to be like that of SN 1991T, which is the archetype of over-luminous SNe Ia. This SN Ia is likely an interesting object worthy of further study and is potentially similar to a similarly super-luminous object, SN 2003fg, found in the SNLS survey (Howell et al. 2006). However, given that our sample comprises 60 objects, we certainly allow for the reasonable statistical possibility of a 3σ outlier such as

"d083" and thus retain it in our sample.

In Fig. 10 we show the 1σ, 2σ, and 3σ probability contours for our measurement of w vs. Ω_M for ESSENCE+nearby alone, the BAO constraints from Eisenstein et al. (2005), and the combination of the SN Ia and BAO constraints.

Table 7 shows the cosmological parameters w and Ω_M for each of these sets for flat models of the Universe with a constant w as well as the χ^2/DoF for a concordance cosmology and the 1-D marginalized values. A ΛCDM model of the Universe fits the MLCS2k2-analyzed ESSENCE+nearby sample with a χ^2/DoF of 0.96and a residual standard deviation of 0.20 mag. Thus, while the estimated w parameter in the constant-w models is $w = -1.05^{+0.13}_{-0.12}$ (stat 1σ) ± 0.13 (sys), a flat, $w = -1$ model of the Universe is consistent with our data.

Our results from these 60 SNe Ia from the ESSENCE survey are consistent with the results of A06. It is reassuring that two independent teams using different telescopes and studying different regions of the sky find that SNe Ia at high redshift exhibit the same luminosity distance vs. redshift relationship. These samples strengthen and extend the evidence from SNe Ia for dark energy and, together with complementary constraints on Ω_M, point toward simple ΛCDM models for our Universe.

4.4. Joint ESSENCE+SNLS Cosmological Constraints

A new opportunity presents itself with the release of the SNLS light curves from A06 and the light curves presented in this paper. For the first time it is possible to do a proper, self-consistent joint fit of two large, independent sets of distant SNe Ia.

When fitting the SNLS SNe Ia with MLCS2k2 and the "glosz" prior we shift the assumed A_V and Δ prior selection window functions by $\Delta z = +0.20$ to represent the greater depth of the SNLS survey. The proper way to derive this prior for SNLS would be to model the SNLS survey efficiency and and fit simulated SNe Ia with MLCS2k2 as we presented in §2.3 for the ESSENCE survey. Similar concerns apply for possible selection effects in the heterogeneously nearby sample. Nevertheless, we believe our use of the "glosz" prior is appropriate for the low-redshift sample (where it is just the "glos" prior) and the simple extension in redshift to be a reasonable approach for the SNLS sample. The additional systematic errors introduced by this joint comparison center on the photometric calibration of the distant sample relative to the nearby SNe Ia. We estimate that uncertainty to be the same as the calibration uncertainty to the nominal Vega system used by each project: $\Delta\text{zpt} = 0.02$ mag. We have not modeled different offsets between the two data sets, but merely express the uncertainty

as an additional uncertainty in our inferred cosmological parameters. This relative zeropoint uncertainty adds an additional $\Delta w = 0.02$ to our overall systematic uncertainty on w.

With our combined analysis, we start with the traditional Ω_M-$\Omega_\Lambda$contour plot that was the first clear evidence for dark energy.

Table 8 shows the cosmological parameters w_0 and Ω_M for each of these sets for flat models of the Universe with a constant w as well as the χ^2/DoF for a concordance cosmology. A ΛCDM model of the Universe fits the SNLS+ESSENCE+nearby sample analyzed using MLCS2k2 "glosz" with a χ^2/DoF of 0.90 from 162 SNe Iaand a residual standard deviation of 0.23 mag. A joint analysis of the luminosity distances from the SALT fitter results in a χ^2/DoF of 2.76 from 178 SNe Iaand a residual standard deviation of 0.28 mag.. Fig. 11 show the joint MLCS2k2 and SALT results for this joint sample. The estimated w parameter in the constant-w models is $w = -1.07^{+0.09}_{-0.09}$ (stat 1σ) ± 0.13 (sys), and a flat, $w = -1$ model of the Universe remains consistent with the current generation of SN Ia data.

4.5. Joint ESSENCE+SNLS+Riess Gold Sample Cosmological Constraints

In order to explore models with varying w, we now include the gold sample from Riess et al. (2004) to extend our reach out to $z \approx 1.5$. The high-quality intermediate-redshift samples of the ESSENCE and SNLS surveys provide an excellent complement to the high-redshift SNe Iain this set. The heterogeneous nature of the collection of SNe Ia in the gold sample makes it beyond the scope of this paper to produce definite estimates of the systematic errors that result from including this additional set, but it is tempting to add these SNe Ia and examine the new constraints on cosmological parameters.

We used the 39 nearby SNe Ia in common between the nearby SN Ia sample we discuss here and the gold sample to normalize the luminosity distances between the two sets. To avoid double-counting of SNe Ia in this joint analysis, we then drop the nearby SNe Ia from the gold sample and use only the nearby SNe Ia fit in this paper.

We first compute the Ω_M-Ω_Λ contours to update the case for dark energy from SNe Ia. Fig. 12 represents the most stringent demonstration to date of the existence of dark energy. The SNe Ia data alone rule out an empty Universe at 4.5 σ, an $(\Omega_M, \Omega_\Lambda) = (0.3, 0)$ Universe at 10 σ, and an $(\Omega_M, \Omega_\Lambda) = (1, 0)$ σ Universe at > 20 σ. The joint constraints on constant-w models from this full set are $w = -1.09^{+0.09}_{-0.10}$. The highest-redshift data do not noticeably improve constraints for these models over the set of intermediate-redshift SNe Ia from ESSENCE+SNLS. It is for models with variable w that the high-redshift data summarized by Riess et al. (2004) provide the most utility. We here provide the global constraints

on models characterized by $w = w_0 + w_a(1-a)$ (Linder 2003; Albrecht et al. 2006). Using the BAO constraints on variable w models would require integration from $z = 0.35$ to $z \sim 1089$ and the corresponding assumption that $w = w_0 + w_a(1-a)$ is the proper parameterization over this stretch. If one is willing to make this assumption, then BAO+CMB already places significant constraints on the allowed (w_0, w_a) parameter space. However, given that our multi-variable parameterizations of w are arbitrary models with no clear theoretical motivation, we instead choose to regard $w = w_0 + w_a(1-a)$ as a local expansion valid out to a redshift of ~ 2 but not necessarily to $z \sim 1089$. We then explicitly assume $\Omega_M = 0.27 \pm 0.03$. Fig. 13 shows the (w_0, w_a) contours for this combined analysis. These constraints represent the advances of our understanding of dark energy. It is clear that work remains to constrain models of variable w.

5. Conclusions

The ESSENCE survey has successfully discovered, confirmed, and followed 119 SNe Ia in our first four years of operation. We presented results from an analysis of 60 of those SNe Ia here, chosen so as to maximize insight while minimizing susceptibility to systematic errors. We have expended considerable effort to make quantitative estimates of various sources of systematic uncertainty that may afflict the ESSENCE results; of these, host-galaxy extinction and a potential local velocity monopole are currently the predominant concerns. We are working to devise ways to better estimate extinction, using both spectroscopic and photometric observations. Ideally, we would use all available information to arrive at an extinction prior customized for each supernova (e.g., different priors for elliptical and spiral host galaxies), rather than applying a single prior to the collection of all light curves.

The ESSENCE photometric calibration uncertainties will be reduced by an intensive calibration campaign this fall on the CTIO 4-m telescope in conjunction with the improved calibration of the SDSS southern stripe from the SDSS II project (Frieman et al. 2004; Dilday et al. 2005). We hope to reduce our overall systematic uncertainty to the 5% level through this improved photometric calibration and an improved external nearby SN Ia sample from KAIT, the Nearby Supernova Factory, CfA, SDSS II, and the Carnegie SN Program to reduce our systematic sensitivity to a potential velocity monopole in the local SN Ia sample.

Combining our SN Ia observations with the BAO results of Eisenstein et al. (2005) we find that a fit to a constant-w, flat-Universe model to our data finds an estimated parameter value of $w = -1.05^{+0.13}_{-0.12}$ (stat 1σ) ± 0.13 (sys) with a $\chi^2/\mathrm{DoF}=0.96$ using our full set analyzed with the MLCS2k2 fitter of Jha et al. (2007). A $w = -1$, flat-Universe model is consistent with our data. A combined analysis of ESSENCE+SNLS+nearby results in a estimated mean parameter of $w = -1.07^{+0.09}_{-0.09}$ (stat 1σ) ± 0.13 (sys). We have no reliable estimate of the systematic effects involving the SALT fitter but take our general systematic uncertainty of 0.13 as representative of the issues currently confronting supernova cosmology.

The statistical increase from the SNe Ia from the entire 6-year ESSENCE data set plus improved photometric calibration of our detector and photometric measurements will reduce our statistical uncertainty to 7% and, together with an improvement in our systematic uncertainties to the level 5%, allow us to surpass our goal of a 10% measurement of a constant w in a flat Universe.

Establishing the nature of dark energy is among the most pressing issues in the physical sciences today. The emerging impression that the equation-of-state parameter is close to $w = -1$ makes it difficult to determine whether the underlying physics arises in the particle

physics sector or from the classical cosmological constant of general relativity. A value of $w = -1$ is perhaps the least informative possible outcome. In our view, this state of affairs motivates a vigorous effort to push the observational constraints to improve our sensitivity to the value and derivative of w and strongly encourages searching for other indications of new physics, as we well may need another piece to solve the puzzle handed us by Nature.

6. Acknowledgments

REFERENCES

Aguirre, A. N. 1999a, ApJ, 512, L19

—. 1999b, ApJ, 525, 583

Albrecht, A., Bernstein, G., Cahn, R., Freedman, W. L., Hewitt, J., Hu, W., Huth, J., Kamionkowski, M., Kolb, E. W., Knox, L., Mather, J. C., Staggs, S., & Suntzeff, N. B. 2006, ArXiv Astrophysics e-prints

Altavilla, G., Fiorentino, G., Marconi, M., Musella, I., Cappellaro, E., Barbon, R., Benetti, S., Pastorello, A., Riello, M., Turatto, M., & Zampieri, L. 2004, MNRAS, 349, 1344

Astier, P., Guy, J., Regnault, N., Pain, R., Aubourg, E., Balam, D., Basa, S., Carlberg, R. G., Fabbro, S., Fouchez, D., Hook, I. M., Howell, D. A., Lafoux, H., Neill, J. D., Palanque-Delabrouille, N., Perrett, K., Pritchet, C. J., Rich, J., Sullivan, M., Taillet, R., Aldering, G., Antilogus, P., Arsenijevic, V., Balland, C., Baumont, S., Bronder, J., Courtois, H., Ellis, R. S., Filiol, M., Gonçalves, A. C., Goobar, A., Guide, D., Hardin, D., Lusset, V., Lidman, C., McMahon, R., Mouchet, M., Mourao, A., Perlmutter, S., Ripoche, P., Tao, C., & Walton, N. 2006, A&A, 447, 31

Baade, W. & Zwicky, F. 1934, Proceedings of the National Academy of Science, 20, 254

Barris, B. J., Tonry, J. L., Blondin, S., Challis, P., Chornock, R., Clocchiatti, A., Filippenko, A. V., Garnavich, P., Holland, S. T., Jha, S., Kirshner, R. P., Krisciunas, K.,

Leibundgut, B., Li, W., Matheson, T., Miknaitis, G., Riess, A. G., Schmidt, B. P., Smith, R. C., Sollerman, J., Spyromilio, J., Stubbs, C. W., Suntzeff, N. B., Aussel, H., Chambers, K. C., Connelley, M. S., Donovan, D., Henry, J. P., Kaiser, N., Liu, M. C., Martín, E. L., & Wainscoat, R. J. 2004, ApJ, 602, 571

Bessell, M. S., Castelli, F., & Plez, B. 1998, A&A, 333, 231

Blondin, S., Dessart, L., Leibundgut, B., Branch, D., Höflich, P., Tonry, J. L., Matheson, T., Foley, R. J., Chornock, R., Filippenko, A. V., Sollerman, J., Spyromilio, J., Kirshner, R. P., Wood-Vasey, W. M., Clocchiatti, A., Aguilera, C., Barris, B., Becker, A. C., Challis, P., Covarrubias, R., Davis, T. M., Garnavich, P., Hicken, M., Jha, S., Krisciunas, K., Li, W., Miceli, A., Miknaitis, G., Pignata, G., Prieto, J. L., Rest, A., Riess, A. G., Salvo, M. E., Schmidt, B. P., Smith, R. C., Stubbs, C. W., & Suntzeff, N. B. 2006, AJ, 131, 1648

Blondin, S. *et al.* 2007

Bohlin, R. C. & Gilliland, R. L. 2004, AJ, 127, 3508

Bonacic, A., Schommer, R. A., Suntzeff, N. B., & Phillips, M. M. 2000, in Bulletin of the American Astronomical Society, 1285

Burstein, D. 2003, AJ, 126, 1849

Burstein, D. & Heiles, C. 1978, ApJ, 225, 40

Cardelli, J. A., Clayton, G. C., & Mathis, J. S. 1989, ApJ, 345, 245

Clocchiatti, A., Schmidt, B. P., Filippenko, A. V., Challis, P., Coil, A. L., Covarrubias, R., Diercks, A., Garnavich, P., Germany, L., Gilliland, R., Hogan, C., Jha, S., Kirshner, R. P., Leibundgut, B., Leonard, D., Li, W., Matheson, T., Phillips, M. M., Prieto, J. L., Reiss, D., Riess, A. G., Schommer, R., Smith, R. C., Soderberg, A., Spyromilio, J., Stubbs, C., Suntzeff, N. B., Tonry, J. L., & Woudt, P. 2006, ApJ, 642, 1

Coil, A. L., Matheson, T., Filippenko, A. V., Leonard, D. C., Tonry, J., Riess, A. G., Challis, P., Clocchiatti, A., Garnavich, P. M., Hogan, C. J., Jha, S., Kirshner, R. P., Leibundgut, B., Phillips, M. M., Schmidt, B. P., Schommer, R. A., Smith, R. C., Soderberg, A. M., Spyromilio, J., Stubbs, C., Suntzeff, N. B., & Woudt, P. 2000, ApJ, 544, L111

Colgate, S. A. 1979, ApJ, 232, 404

Commins, E. D. 2004, New Astronomy Review, 48, 567

Conley, A., Howell, D. A., Howes, A., Sullivan, M., Astier, P., Balam, D., Basa, S., Carlberg, R. G., Fouchez, D., Guy, J., Hook, I., Neill, J. D., Pain, R., Perrett, K., Pritchet, C. J., Regnault, N., Rich, J., Taillet, R., Aubourg, E., Bronder, J., Ellis, R. S., Fabbro, S., Filiol, M., Le Borgne, D., Palanque-Delabrouille, N., Perlmutter, S., & Ripoche, P. 2006, AJ, 132, 1707

Cooray, A. & Caldwell, R. R. 2006, Phys. Rev. D, 73, 103002

Copin, Y., Blanc, N., Bongard, S., Gangler, E., Saugé, L., Smadja, G., Antilogus, P., Garavini, G., Gilles, S., Pain, R., Aldering, G., Bailey, S., Lee, B. C., Loken, S., Nugent, P., Perlmutter, S., Scalzo, R., Thomas, R. C., Wang, L., Weaver, B. A., Pécontal, E., Kessler, R., Baltay, C., Rabinowitz, D., & Bauer, A. 2006, New Astronomy Review, 50, 436

Davis, T. M., Schmidt, B. P., & Kim, A. G. 2006, PASP, 118, 205

Dilday, B., Barentine, J., Bassett, B., Becker, A., Bendar, R., Bremer, M., Brewington, H., DeJongh, F., Dembicky, J., DePoy, D. L., Doi, M., Edge, A., Elson, E., Frieman, J., Garnavich, P., Goobar, A., Gueth, T., Harvanek, M., Holtzman, J., Hopp, U., Kollatschny, W., Krzesinski, J., Lamenti, D., Lampeitl, H., Kessler, R., Ketzeback, B., Konishi, K., Long, D., Marriner, J., Marshall, J. L., McMillan, R., Mendez, J., Miknaitis, G., Nichol, R., Pan, K., Prieto, J. L., Richmond, M., Riess, A., Romani, R., Romer, K., Ruiz-Lapuente, P., Sako, M., Schneider, D., Smith, M., Snedden, S., Subbarao, M., Takanashi, N., van der Heyden, K., Wheeler, C., & Yasuda, N. 2005, in Bulletin of the American Astronomical Society, 1459–+

Eisenstein, D. J., Zehavi, I., Hogg, D. W., Scoccimarro, R., Blanton, M. R., Nichol, R. C., Scranton, R., Seo, H.-J., Tegmark, M., Zheng, Z., Anderson, S. F., Annis, J., Bahcall, N., Brinkmann, J., Burles, S., Castander, F. J., Connolly, A., Csabai, I., Doi, M., Fukugita, M., Frieman, J. A., Glazebrook, K., Gunn, J. E., Hendry, J. S., Hennessy, G., Ivezić, Z., Kent, S., Knapp, G. R., Lin, H., Loh, Y.-S., Lupton, R. H., Margon, B., McKay, T. A., Meiksin, A., Munn, J. A., Pope, A., Richmond, M. W., Schlegel, D., Schneider, D. P., Shimasaku, K., Stoughton, C., Strauss, M. A., SubbaRao, M., Szalay, A. S., Szapudi, I., Tucker, D. L., Yanny, B., & York, D. G. 2005, ApJ, 633, 560

Elias-Rosa, N. & The Esc Collaboration. 2005, in ASP Conf. Ser. 342: 1604–2004: Supernovae as Cosmological Lighthouses, ed. M. e. a. Turatto, 247

Filippenko, A. V. 1997, ARA&A, 35, 309

—. 2001, PASP, 113, 1441

Filippenko, A. V. 2005a, in ASP Conf. Ser. 332: The Fate of the Most Massive Stars, ed. R. Humphreys & K. Stanek, 33–+

Filippenko, A. V. 2005b, in ASSL Vol. 332: White dwarfs: cosmological and galactic probes, ed. E. M. Sion, S. Vennes, & H. L. Shipman, 97–133

Filippenko, A. V., Li, W. D., Treffers, R. R., & Modjaz, M. 2001, in ASP Conf. Ser. 246: IAU Colloq. 183: Small Telescope Astronomy on Global Scales, ed. B. Paczynski, W.-P. Chen, & C. Lemme, 121

Filippenko, A. V., Richmond, M. W., Branch, D., Gaskell, M., Herbst, W., Ford, C. H., Treffers, R. R., Matheson, T., Ho, L. C., Dey, A., Sargent, W. L. W., Small, T. A., & van Breugel, W. J. M. 1992a, AJ, 104, 1543

Filippenko, A. V., Richmond, M. W., Matheson, T., Shields, J. C., Burbidge, E. M., Cohen, R. D., Dickinson, M., Malkan, M. A., Nelson, B., Pietz, J., Schlegel, D., Schmeer, P., Spinrad, H., Steidel, C. C., Tran, H. D., & Wren, W. 1992b, ApJ, 384, L15

Finkbeiner, D. P., Davis, M., & Schlegel, D. J. 1999, ApJ, 524, 867

Foley, R. J., Filippenko, A. V., Leonard, D. C., Riess, A. G., Nugent, P., & Perlmutter, S. 2005, ApJ, 626, L11

Frieman, J., Adelman-McCarthy, J., Barentine, J., Becker, A., Boroski, W., Brewington, H., Connolly, A., DeJongh, F., Dembicky, J., Dilday, B., Doi, M., Gunn, J., Harvanek, M., Hawley, S., Hoeflich, P., Hogan, C., Holtzman, J., Johnston, D., Kaplan, J., Kessler, R., Ketzeback, B., Kilper, G., Kleinman, A., Kleinman, S., Kron, R. G., Krughoff, S., Krzesinski, J., Lamenti, D., Lampeitl, H., Long, D., Marriner, J., McMillan, R., Miknaitis, G., Newman, P. R., Nichol, R., Riess, A., Romani, R., Sako, M., Scranton, R., Snedden, S., Stoughton, C., Subbarao, M., Tucker, D., Wang, L., Yasuda, N., York, D., & SDSS. 2004, in Bulletin of the American Astronomical Society, 1548

Gallagher, J. S., Garnavich, P. M., Berlind, P., Challis, P., Jha, S., & Kirshner, R. P. 2005, ApJ, 634, 210

Garnavich, P. M., Kirshner, R. P., Challis, P., Tonry, J., Gilliland, R. L., Smith, R. C., Clocchiatti, A., Diercks, A., Filippenko, A. V., Hamuy, M., Hogan, C. J., Leibundgut, B., Phillips, M. M., Reiss, D., Riess, A. G., Schmidt, B. P., Schommer, R. A., Spyromilio, J., Stubbs, C., Suntzeff, N. B., & Wells, L. 1998, ApJ, 493, L53+

Goldhaber, G., Groom, D. E., Kim, A., Aldering, G., Astier, P., Conley, A., Deustua, S. E., Ellis, R., Fabbro, S., Fruchter, A. S., Goobar, A., Hook, I., Irwin, M., Kim, M., Knop, R. A., Lidman, C., McMahon, R., Nugent, P. E., Pain, R., Panagia, N., Pennypacker, C. R., Perlmutter, S., Ruiz-Lapuente, P., Schaefer, B., Walton, N. A., & York, T. 2001, ApJ, 558, 359

Goobar, A., Bergström, L., & Mörtsell, E. 2002, A&A, 384, 1

Guy, J., Astier, P., Nobili, S., Regnault, N., & Pain, R. 2005, A&A, 443, 781

Hamuy, M., Folatelli, G., Morrell, N. I., Phillips, M. M., Suntzeff, N. B., Persson, S. E., Roth, M., Gonzalez, S., Krzeminski, W., Contreras, C., Freedman, W. L., Murphy, D. C., Madore, B. F., Wyatt, P., Maza, J., Filippenko, A. V., Li, W., & Pinto, P. A. 2006, PASP, 118, 2

Hamuy, M., Phillips, M. M., Suntzeff, N. B., Schommer, R. A., Maza, J., & Aviles, R. 1996, AJ, 112, 2391

Hamuy, M., Phillips, M. M., Wells, L. A., & Maza, J. . 1993, PASP, 105, 787

Hamuy, M., Trager, S. C., Pinto, P. A., Phillips, M. M., Schommer, R. A., Ivanov, V., & Suntzeff, N. B. 2000, AJ, 120, 1479

Hansen, L., Jorgensen, H. E., & Norgaard-Nielsen, H. U. 1987, The Messenger, 47, 46

Hatano, K., Branch, D., & Deaton, J. 1998, ApJ, 502, 177

Hicken, M., Challis, P., Kirshner, R. P., Modjaz, M., Wood-Vasey, M., Berlind, P., Calkins, M., Stubbs, C., Matheson, T., Rest, A., & Jha, S. 2006, in American Astronomical Society Meeting Abstracts, 72.04

Holz, D. E. & Linder, E. V. 2005, ApJ, 631, 678

Hook, I. M., Howell, D. A., Aldering, G., Amanullah, R., Burns, M. S., Conley, A., Deustua, S. E., Ellis, R., Fabbro, S., Fadeyev, V., Folatelli, G., Garavini, G., Gibbons, R., Goldhaber, G., Goobar, A., Groom, D. E., Kim, A. G., Knop, R. A., Kowalski, M., Lidman, C., Nobili, S., Nugent, P. E., Pain, R., Pennypacker, C. R., Perlmutter, S., Ruiz-Lapuente, P., Sainton, G., Schaefer, B. E., Smith, E., Spadafora, A. L., Stanishev, V., Thomas, R. C., Walton, N. A., Wang, L., & Wood-Vasey, W. M. 2005, AJ, 130, 2788

Howell, D. A., Sullivan, M., Nugent, P. E., Ellis, R. S., Conley, A. J., Le Borgne, D., Carlberg, R. G., Guy, J., Balam, D., Basa, S., Fouchez, D., Hook, I. M., Hsiao, E. Y., Neill, J. D., Pain, R., Perrett, K. M., & Pritchet, C. J. 2006, Nature, 443, 308

Howell, D. A., Sullivan, M., Perrett, K., Bronder, T. J., Hook, I. M., Astier, P., Aubourg, E., Balam, D., Basa, S., Carlberg, R. G., Fabbro, S., Fouchez, D., Guy, J., Lafoux, H., Neill, J. D., Pain, R., Palanque-Delabrouille, N., Pritchet, C. J., Regnault, N., Rich, J., Taillet, R., Knop, R., McMahon, R. G., Perlmutter, S., & Walton, N. A. 2005, ApJ, 634, 1190

Hubble, E. P. 1929, ApJ, 69, 103

Hui, L. & Greene, P. B. 2006, Phys. Rev. D, 73, 123526

Jha, S., Branch, D., Chornock, R., Foley, R. J., Li, W., Swift, B. J., Casebeer, D., & Filippenko, A. V. 2006a, AJ, 132, 189

Jha, S., Kirshner, R. P., Challis, P., Garnavich, P. M., Matheson, T., Soderberg, A. M., Graves, G. J. M., Hicken, M., Alves, J. F., Arce, H. G., Balog, Z., Barmby, P., Barton, E. J., Berlind, P., Bragg, A. E., Briceño, C., Brown, W. R., Buckley, J. H., Caldwell, N., Calkins, M. L., Carter, B. J., Concannon, K. D., Donnelly, R. H., Eriksen, K. A., Fabricant, D. G., Falco, E. E., Fiore, F., Garcia, M. R., Gómez, M., Grogin, N. A., Groner, T., Groot, P. J., Haisch, Jr., K. E., Hartmann, L., Hergenrother, C. W., Holman, M. J., Huchra, J. P., Jayawardhana, R., Jerius, D., Kannappan, S. J., Kim, D.-W., Kleyna, J. T., Kochanek, C. S., Koranyi, D. M., Krockenberger, M., Lada, C. J., Luhman, K. L., Luu, J. X., Macri, L. M., Mader, J. A., Mahdavi, A., Marengo, M., Marsden, B. G., McLeod, B. A., McNamara, B. R., Megeath, S. T., Moraru, D., Mossman, A. E., Muench, A. A., Muñoz, J. A., Muzerolle, J., Naranjo, O., Nelson-Patel, K., Pahre, M. A., Patten, B. M., Peters, J., Peters, W., Raymond, J. C., Rines, K., Schild, R. E., Sobczak, G. J., Spahr, T. B., Stauffer, J. R., Stefanik, R. P., Szentgyorgyi, A. H., Tollestrup, E. V., Väisänen, P., Vikhlinin, A., Wang, Z., Willner, S. P., Wolk, S. J., Zajac, J. M., Zhao, P., & Stanek, K. Z. 2006b, AJ, 131, 527

Jha, S., Riess, A. G., & Kirshner, R. P. 2007, ApJ

Kim, A., Goobar, A., & Perlmutter, S. 1996, PASP, 108, 190

Kim, A. G., Linder, E. V., Miquel, R., & Mostek, N. 2004, MNRAS, 347, 909

Kirshner, R. P. 2002, The extravagant universe : exploding stars, dark energy and the accelerating cosmos (The extravagant universe : exploding stars, dark energy and

the accelerating cosmos / Robert P. Kirshner. Princeton, N.J. : Princeton University Press, c2002.)

Knop, R. A., Aldering, G., Amanullah, R., Astier, P., Blanc, G., Burns, M. S., Conley, A., Deustua, S. E., Doi, M., Ellis, R., Fabbro, S., Folatelli, G., Fruchter, A. S., Garavini, G., Garmond, S., Garton, K., Gibbons, R., Goldhaber, G., Goobar, A., Groom, D. E., Hardin, D., Hook, I., Howell, D. A., Kim, A. G., Lee, B. C., Lidman, C., Mendez, J., Nobili, S., Nugent, P. E., Pain, R., Panagia, N., Pennypacker, C. R., Perlmutter, S., Quimby, R., Raux, J., Regnault, N., Ruiz-Lapuente, P., Sainton, G., Schaefer, B., Schahmaneche, K., Smith, E., Spadafora, A. L., Stanishev, V., Sullivan, M., Walton, N. A., Wang, L., Wood-Vasey, W. M., & Yasuda, N. 2003, ApJ, 598, 102

Kowal, C. T. 1968, AJ, 73, 1021

Krisciunas, K., Garnavich, P. M., Challis, P., Prieto, J. L., Riess, A. G., Barris, B., Aguilera, C., Becker, A. C., Blondin, S., Chornock, R., Clocchiatti, A., Covarrubias, R., Filippenko, A. V., Foley, R. J., Hicken, M., Jha, S., Kirshner, R. P., Leibundgut, B., Li, W., Matheson, T., Miceli, A., Miknaitis, G., Rest, A., Salvo, M. E., Schmidt, B. P., Smith, R. C., Sollerman, J., Spyromilio, J., Stubbs, C. W., Suntzeff, N. B., Tonry, J. L., & Wood-Vasey, W. M. 2005, AJ, 130, 2453

Krisciunas, K., Hastings, N. C., Loomis, K., McMillan, R., Rest, A., Riess, A. G., & Stubbs, C. 2000, ApJ, 539, 658

Leibundgut, B. 1990, A&A, 229, 1

—. 2001, ARA&A, 39, 67

Leibundgut, B., Kirshner, R. P., Phillips, M. M., Wells, L. A., Suntzeff, N. B., Hamuy, M., Schommer, R. A., Walker, A. R., Gonzalez, L., Ugarte, P., Williams, R. E., Williger, G., Gomez, M., Marzke, R., Schmidt, B. P., Whitney, B., Coldwell, N., Peters, J., Chaffee, F. H., Foltz, C. B., Rehner, D., Siciliano, L., Barnes, T. G., Cheng, K.-P., Hintzen, P. M. N., Kim, Y.-C., Maza, J., Parker, J. W., Porter, A. C., Schmidtke, P. C., & Sonneborn, G. 1993, AJ, 105, 301

Leibundgut, B., Schommer, R., Phillips, M., Riess, A., Schmidt, B., Spyromilio, J., Walsh, J., Suntzeff, N., Hamuy, M., Maza, J., Kirshner, R. P., Challis, P., Garnavich, P., Smith, R. C., Dressler, A., & Ciardullo, R. 1996, ApJ, 466, L21+

Li, C., Holz, D. E., & Cooray, A. 2006, ArXiv Astrophysics e-prints

Li, W., Filippenko, A. V., Chornock, R., Berger, E., Berlind, P., Calkins, M. L., Challis, P., Fassnacht, C., Jha, S., Kirshner, R. P., Matheson, T., Sargent, W. L. W., Simcoe, R. A., Smith, G. H., & Squires, G. 2003, PASP, 115, 453

Li, W., Filippenko, A. V., Gates, E., Chornock, R., Gal-Yam, A., Ofek, E. O., Leonard, D. C., Modjaz, M., Rich, R. M., Riess, A. G., & Treffers, R. R. 2001, PASP, 113, 1178

Li, W. D., Filippenko, A. V., Treffers, R. R., Friedman, A., Halderson, E., Johnson, R. A., King, J. Y., Modjaz, M., Papenkova, M., Sato, Y., & Shefler, T. 2000, in American Institute of Physics Conference Series, ed. S. S. Holt & W. W. Zhang, 103–106

Lidman, C. 2004, The Messenger, 118, 24

Lidman, C., Howell, D. A., Folatelli, G., Garavini, G., Nobili, S., Aldering, G., Amanullah, R., Antilogus, P., Astier, P., Blanc, G., Burns, M. S., Conley, A., Deustua, S. E., Doi, M., Ellis, R., Fabbro, S., Fadeyev, V., Gibbons, R., Goldhaber, G., Goobar, A., Groom, D. E., Hook, I., Kashikawa, N., Kim, A. G., Knop, R. A., Lee, B. C., Mendez, J., Morokuma, T., Motohara, K., Nugent, P. E., Pain, R., Perlmutter, S., Prasad, V., Quimby, R., Raux, J., Regnault, N., Ruiz-Lapuente, P., Sainton, G., Schaefer, B. E., Schahmaneche, K., Smith, E., Spadafora, A. L., Stanishev, V., Walton, N. A., Wang, L., Wood-Vasey, W. M., Yasuda, N., & The Supernova Cosmology Project. 2005, A&A, 430, 843

Linder, E. V. 2003, Physical Review Letters, 90, 091301

Lira, P. 1995, Master's thesis, University of Chile

Matheson, T., Blondin, S., Foley, R. J., Chornock, R., Filippenko, A. V., Leibundgut, B., Smith, R. C., Sollerman, J., Spyromilio, J., Kirshner, R. P., Clocchiatti, A., Aguilera, C., Barris, B., Becker, A. C., Challis, P., Covarrubias, R., Garnavich, P., Hicken, M., Jha, S., Krisciunas, K., Li, W., Miceli, A., Miknaitis, G., Prieto, J. L., Rest, A., Riess, A. G., Salvo, M. E., Schmidt, B. P., Stubbs, C. W., Suntzeff, N. B., & Tonry, J. L. 2005, AJ, 129, 2352

Miknaitis, G., Pignata, G., Rest, A., Wood-Vasey, W. M., Blondin, S., Challis, P., Smith, R. C., Stubbs, C. W., Aguilera, C., Blackman, J. W., Becker, A. C., Chornock, R., Clocchiatti, A., Conley, A., Covarrubias, R., Davis, T. M., Filippenko, A. V., Foley, R. J., Garg, A., Garnavich, P. M., Hicken, M., Kirshner, R. P., Jha, S., Krisciunas, K., Leibundgut, B., Li, W., Matheson, T., Miceli, A., Narayan, G., Prieto, J. L., Riess, A. G., Salvo, M. E., Schmidt, B. P., Sollerman, J., Spyromilio, J., Tonry, J. L., Suntzeff, N. B., & Zenteno, A. 2007

Minkowski, R. 1941, PASP, 53, 224

Neill, J. D., Sullivan, M., Balam, D., Pritchet, C. J., Howell, D. A., Perrett, K., Astier, P., Aubourg, E., Basa, S., Carlberg, R. G., Conley, A., Fabbro, S., Fouchez, D., Guy, J., Hook, I., Pain, R., Palanque-Delabrouille, N., Regnault, N., Rich, J., Taillet, R., Aldering, G., Antilogus, P., Arsenijevic, V., Balland, C., Baumont, S., Bronder, J., Ellis, R. S., Filiol, M., Gonçalves, A. C., Hardin, D., Kowalski, M., Lidman, C., Lusset, V., Mouchet, M., Mourao, A., Perlmutter, S., Ripoche, P., Schlegel, D., & Tao, C. 2006, AJ, 132, 1126

Nobili, S., Amanullah, R., Garavini, G., Goobar, A., Lidman, C., Stanishev, V., Aldering, G., Antilogus, P., Astier, P., Burns, M. S., Conley, A., Deustua, S. E., Ellis, R., Fabbro, S., Fadeyev, V., Folatelli, G., Gibbons, R., Goldhaber, G., Groom, D. E., Hook, I., Howell, D. A., Kim, A. G., Knop, R. A., Nugent, P. E., Pain, R., Perlmutter, S., Quimby, R., Raux, J., Regnault, N., Ruiz-Lapuente, P., Sainton, G., Schahmaneche, K., Smith, E., Spadafora, A. L., Thomas, R. C., Wang, L., & The Supernova Cosmology Project. 2005, A&A, 437, 789

Norgaard-Nielsen, H. U., Hansen, L., Jorgensen, H. E., Aragon Salamanca, A., & Ellis, R. S. 1989, Nature, 339, 523

Nugent, P., Kim, A., & Perlmutter, S. 2002, PASP, 114, 803

Östman, L., Goobar, A., & Mörtsell, E. 2006, A&A, 450, 971

Overbye, D. 1999, Lonely Hearts of the Cosmos, paperback edn. (Boston: Little, Brown (Boston)), 426–436

Percival, W. J., Baugh, C. M., Bland-Hawthorn, J., Bridges, T., Cannon, R., Cole, S., Colless, M., Collins, C., Couch, W., Dalton, G., De Propris, R., Driver, S. P., Efstathiou, G., Ellis, R. S., Frenk, C. S., Glazebrook, K., Jackson, C., Lahav, O., Lewis, I., Lumsden, S., Maddox, S., Moody, S., Norberg, P., Peacock, J. A., Peterson, B. A., Sutherland, W., & Taylor, K. 2001, MNRAS, 327, 1297

Percival, W. J., Sutherland, W., Peacock, J. A., Baugh, C. M., Bland-Hawthorn, J., Bridges, T., Cannon, R., Cole, S., Colless, M., Collins, C., Couch, W., Dalton, G., De Propris, R., Driver, S. P., Efstathiou, G., Ellis, R. S., Frenk, C. S., Glazebrook, K., Jackson, C., Lahav, O., Lewis, I., Lumsden, S., Maddox, S., Moody, S., Norberg, P., Peterson, B. A., & Taylor, K. 2002, MNRAS, 337, 1068

Perlmutter, S. 2003, Physics Today, 56, 53

Perlmutter, S., Aldering, G., della Valle, M., Deustua, S., Ellis, R. S., Fabbro, S., Fruchter, A., Goldhaber, G., Groom, D. E., Hook, I. M., Kim, A. G., Kim, M. Y., Knop, R. A., Lidman, C., McMahon, R. G., Nugent, P., Pain, R., Panagia, N., Pennypacker, C. R., Ruiz-Lapuente, P., Schaefer, B., & Walton, N. 1998, Nature, 391, 51

Perlmutter, S., Aldering, G., Goldhaber, G., Knop, R. A., Nugent, P., Castro, P. G., Deustua, S., Fabbro, S., Goobar, A., Groom, D. E., Hook, I. M., Kim, A. G., Kim, M. Y., Lee, J. C., Nunes, N. J., Pain, R., Pennypacker, C. R., Quimby, R., Lidman, C., Ellis, R. S., Irwin, M., McMahon, R. G., Ruiz-Lapuente, P., Walton, N., Schaefer, B., Boyle, B. J., Filippenko, A. V., Matheson, T., Fruchter, A. S., Panagia, N., Newberg, H. J. M., Couch, W. J., & The Supernova Cosmology Project. 1999, ApJ, 517, 565

Perlmutter, S., Gabi, S., Goldhaber, G., Goobar, A., Groom, D. E., Hook, I. M., Kim, A. G., Kim, M. Y., Lee, J. C., Pain, R., Pennypacker, C. R., Small, I. A., Ellis, R. S., McMahon, R. G., Boyle, B. J., Bunclark, P. S., Carter, D., Irwin, M. J., Glazebrook, K., Newberg, H. J. M., Filippenko, A. V., Matheson, T., Dopita, M., Couch, W. J., & The Supernova Cosmology Project. 1997, ApJ, 483, 565

Perlmutter, S., Pennypacker, C. R., Goldhaber, G., Goobar, A., Muller, R. A., Newberg, H. J. M., Desai, J., Kim, A. G., Kim, M. Y., Small, I. A., Boyle, B. J., Crawford, C. S., McMahon, R. G., Bunclark, P. S., Carter, D., Irwin, M. J., Terlevich, R. J., Ellis, R. S., Glazebrook, K., Couch, W. J., Mould, J. R., Small, T. A., & Abraham, R. G. 1995, ApJ, 440, L41

Petric, A. O., Telis, G. A., Paerels, F., & Helfand, D. J. 2006, ApJ, 678

Phillips, M. M. 1993, ApJ, 413, L105

Phillips, M. M., Lira, P., Suntzeff, N. B., Schommer, R. A., Hamuy, M., & Maza, J. 1999, AJ, 118, 1766

Phillips, M. M., Wells, L. A., Suntzeff, N. B., Hamuy, M., Leibundgut, B., Kirshner, R. P., & Foltz, C. B. 1992, AJ, 103, 1632

Pignata, G., Rest, A., Clocchiatti, A., Aguilera, C., Blackman, J. W., Becker, A. C., Blondin, S., Challis, P., Chornock, R., Conley, A., Covarrubias, R., Davis, T. M., Filippenko, A. V., Foley, R. J., Garg, A., Garnavich, P. M., Hicken, M., Jha, S., Kirshner, R. P., Krisciunas, K., Leibundgut, B., Li, W., Matheson, T., Miceli, A., Narayan, G., Prieto, J. L., Riess, A. G., Salvo, M. E., Schmidt, B. P., Smith, R. C., Sollerman, J., Spyromilio, J., Tonry, J. L., Suntzeff, N. B., & Zenteno, A. 2007

Prieto, J. L., Rest, A., & Suntzeff, N. B. 2006, ApJ, 647, 501

Pskovskii, I. P. 1977, Soviet Astronomy, 21, 675

Radburn-Smith, D. J., Lucey, J. R., & Hudson, M. J. 2004, MNRAS, 355, 1378

Rapetti, D., Allen, S. W., Amin, M. A., & Blandford, R. D. 2006, ArXiv Astrophysics
    e-prints

Reindl, B., Tammann, G. A., Sandage, A., & Saha, A. 2005, ApJ, 624, 532

Riello, M. & Patat, F. 2005, MNRAS, 362, 671

Riess, A. G. 2000, PASP, 112, 1284

Riess, A. G., Filippenko, A. V., Challis, P., Clocchiatti, A., Diercks, A., Garnavich, P. M.,
    Gilliland, R. L., Hogan, C. J., Jha, S., Kirshner, R. P., Leibundgut, B., Phillips,
    M. M., Reiss, D., Schmidt, B. P., Schommer, R. A., Smith, R. C., Spyromilio, J.,
    Stubbs, C., Suntzeff, N. B., & Tonry, J. 1998, AJ, 116, 1009

Riess, A. G., Filippenko, A. V., Leonard, D. C., Schmidt, B. P., Suntzeff, N., Phillips,
    M. M., Schommer, R., Clocchiatti, A., Kirshner, R. P., Garnavich, P., Challis, P.,
    Leibundgut, B., Spyromilio, J., & Smith, R. C. 1997, AJ, 114, 722

Riess, A. G., Filippenko, A. V., Liu, M. C., Challis, P., Clocchiatti, A., Diercks, A., Gar-
    navich, P. M., Hogan, C. J., Jha, S., Kirshner, R. P., Leibundgut, B., Phillips, M. M.,
    Reiss, D., Schmidt, B. P., Schommer, R. A., Smith, R. C., Spyromilio, J., Stubbs, C.,
    Suntzeff, N. B., Tonry, J., Woudt, P., Brunner, R. J., Dey, A., Gal, R., Graham, J.,
    Larkin, J., Odewahn, S. C., & Oppenheimer, B. 2000, ApJ, 536, 62

Riess, A. G., Kirshner, R. P., Schmidt, B. P., Jha, S., Challis, P., Garnavich, P. M., Esin,
    A. A., Carpenter, C., Grashius, R., Schild, R. E., Berlind, P. L., Huchra, J. P.,
    Prosser, C. F., Falco, E. E., Benson, P. J., Briceño, C., Brown, W. R., Caldwell,
    N., dell'Antonio, I. P., Filippenko, A. V., Goodman, A. A., Grogin, N. A., Groner,
    T., Hughes, J. P., Green, P. J., Jansen, R. A., Kleyna, J. T., Luu, J. X., Macri,
    L. M., McLeod, B. A., McLeod, K. K., McNamara, B. R., McLean, B., Milone,
    A. A. E., Mohr, J. J., Moraru, D., Peng, C., Peters, J., Prestwich, A. H., Stanek,
    K. Z., Szentgyorgyi, A., & Zhao, P. 1999, AJ, 117, 707

Riess, A. G., Press, W. H., & Kirshner, R. P. 1995, ApJ, 445, L91

—. 1996, ApJ, 473, 88

Riess, A. G., Strolger, L., Tonry, J., Casertano, S., Ferguson, H. C., Mobasher, B., Challis, P., Filippenko, A. V., Jha, S., Li, W., Chornock, R., Kirshner, R. P., Leibundgut, B., Dickinson, M., Livio, M., Giavalisco, M., Steidel, C. C., Benitez, N., & Tsvetanov, Z. 2004, ArXiv Astrophysics e-prints

Rust, B. W. 1974, PhD thesis, University of Texas

Schlegel, D. J., Finkbeiner, D. P., & Davis, M. 1998, ApJ, 500, 525

Schmidt, B. P., Suntzeff, N. B., Phillips, M. M., Schommer, R. A., Clocchiatti, A., Kirshner, R. P., Garnavich, P., Challis, P., Leibundgut, B., Spyromilio, J., Riess, A. G., Filippenko, A. V., Hamuy, M., Smith, R. C., Hogan, C., Stubbs, C., Diercks, A., Reiss, D., Gilliland, R., Tonry, J., Maza, J., Dressler, A., Walsh, J., & Ciardullo, R. 1998, ApJ, 507, 46

Shapley, H. 1919, PASP, 31, 261

Spergel, D. N., Bean, R., Dore', O., Nolta, M. R., Bennett, C. L., Hinshaw, G., Jarosik, N., Komatsu, E., Page, L., Peiris, H. V., Verde, L., Barnes, C., Halpern, M., Hill, R. S., Kogut, A., Limon, M., Meyer, S. S., Odegard, N., Tucker, G. S., Weiland, J. L., Wollack, E., & Wright, E. L. 2006, ArXiv Astrophysics e-prints

Stubbs, C. W. & Tonry, J. L. 2006, ApJ, 646, 1436

Sullivan, M., Ellis, R. S., Aldering, G., Amanullah, R., Astier, P., Blanc, G., Burns, M. S., Conley, A., Deustua, S. E., Doi, M., Fabbro, S., Folatelli, G., Fruchter, A. S., Garavini, G., Gibbons, R., Goldhaber, G., Goobar, A., Groom, D. E., Hardin, D., Hook, I., Howell, D. A., Irwin, M., Kim, A. G., Knop, R. A., Lidman, C., McMahon, R., Mendez, J., Nobili, S., Nugent, P. E., Pain, R., Panagia, N., Pennypacker, C. R., Perlmutter, S., Quimby, R., Raux, J., Regnault, N., Ruiz-Lapuente, P., Schaefer, B., Schahmaneche, K., Spadafora, A. L., Walton, N. A., Wang, L., Wood-Vasey, W. M., & Yasuda, N. 2003, MNRAS, 340, 1057

Sullivan, M., Howell, D. A., Perrett, K., Nugent, P. E., Astier, P., Aubourg, E., Balam, D., Basa, S., Carlberg, R. G., Conley, A., Fabbro, S., Fouchez, D., Guy, J., Hook, I., Lafoux, H., Neill, J. D., Pain, R., Palanque-Delabrouille, N., Pritchet, C. J., Regnault, N., Rich, J., Taillet, R., Aldering, G., Baumont, S., Bronder, J., Filiol, M., Knop, R. A., Perlmutter, S., & Tao, C. 2006a, AJ, 131, 960

Sullivan, M., Le Borgne, D., Pritchet, C. J., Hodsman, A., Neill, J. D., Howell, D. A., Carlberg, R. G., Astier, P., Aubourg, E., Balam, D., Basa, S., Conley, A., Fabbro,

S., Fouchez, D., Guy, J., Hook, I., Pain, R., Palanque-Delabrouille, N., Perrett, K., Regnault, N., Rich, J., Taillet, R., Baumont, S., Bronder, J., Ellis, R. S., Filiol, M., Lusset, V., Perlmutter, S., Ripoche, P., & Tao, C. 2006b, ApJ, 648, 868

Tammann, G. A. 1979, in Scientific Research with the Space Telescope, ed. M. S. Longair & J. W. Warner, 263–293

Tonry, J. L., Schmidt, B. P., Barris, B., Candia, P., Challis, P., Clocchiatti, A., Coil, A. L., Filippenko, A. V., Garnavich, P., Hogan, C., Holland, S. T., Jha, S., Kirshner, R. P., Krisciunas, K., Leibundgut, B., Li, W., Matheson, T., Phillips, M. M., Riess, A. G., Schommer, R., Smith, R. C., Sollerman, J., Spyromilio, J., Stubbs, C. W., & Suntzeff, N. B. 2003, ApJ, 594, 1

Tripp, R. 1998, A&A, 331, 815

Voit, G. M. 2005, Reviews of Modern Physics, 77, 207

Wang, L., Goldhaber, G., Aldering, G., & Perlmutter, S. 2003, ApJ, 590, 944

White, M. 1998, ApJ, 506, 495

Williams, B. F., Hogan, C. J., Barris, B., Candia, P., Challis, P., Clocchiatti, A., Coil, A. L., Filippenko, A. V., Garnavich, P., Kirshner, R. P., Holland, S. T., Jha, S., Krisciunas, K., Leibundgut, B., Li, W., Matheson, T., Maza, J., Phillips, M. M., Riess, A. G., Schmidt, B. P., Schommer, R. A., Smith, R. C., Sollerman, J., Spyromilio, J., Stubbs, C., Suntzeff, N. B., & Tonry, J. L. 2003, AJ, 126, 2608

Wilson, O. C. 1939, ApJ, 90, 634

Wood-Vasey, W. M., Aldering, G., Lee, B. C., Loken, S., Nugent, P., Perlmutter, S., Siegrist, J., Wang, L., Antilogus, P., Astier, P., Hardin, D., Pain, R., Copin, Y., Smadja, G., Gangler, E., Castera, A., Adam, G., Bacon, R., Lemonnier, J.-P., Pécontal, A., Pécontal, E., & Kessler, R. 2004, New Astronomy Review, 48, 637

Zehavi, I., Riess, A. G., Kirshner, R. P., & Dekel, A. 1998, ApJ, 503, 483
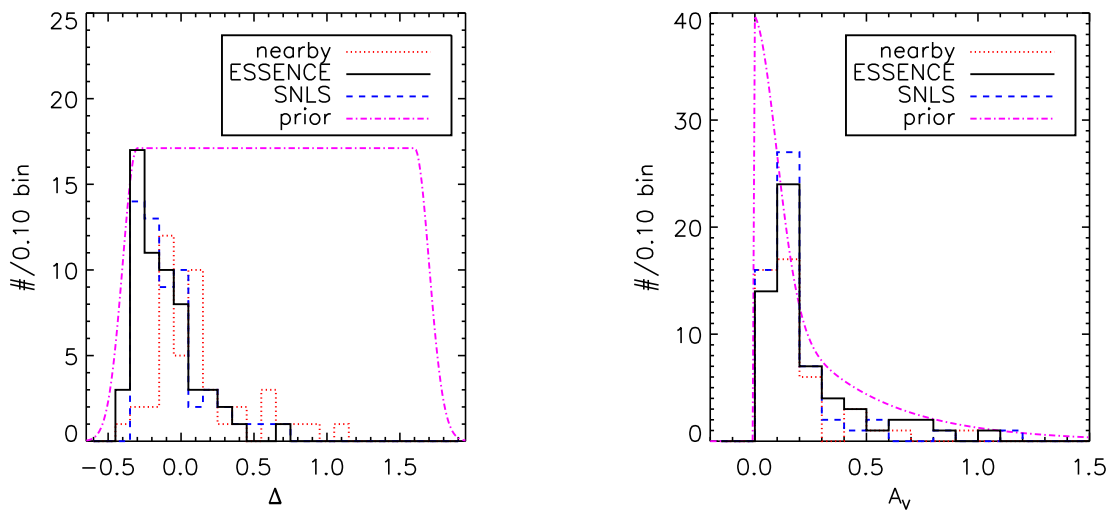
Fig. 1.— The distribution of the MLCS2k2 light-curve width parameter Δ and A_V for the MLCS2k2 fits with the "glosz" prior to the nearby (dotted line), ESSENCE (solid line), and SNLS (dashed line) SNe Ia considered in this paper. The "glosz" prior (dotted-dashed line) is shown here for $z = 0$ where it is equivalent to the "glos" prior. Note that we are mixing two slightly different things in showing the prior with these estimated mean fit parameters. The prior, which directly relates to the mode, is not expected to match the a posteriori mean distribution of the fit parameters. See Fig. 4 for the ESSENCE selection effect as a function of redshift. See Table 9 for the full set of MLCS2k2 light-curve fit results for these SNe Ia.
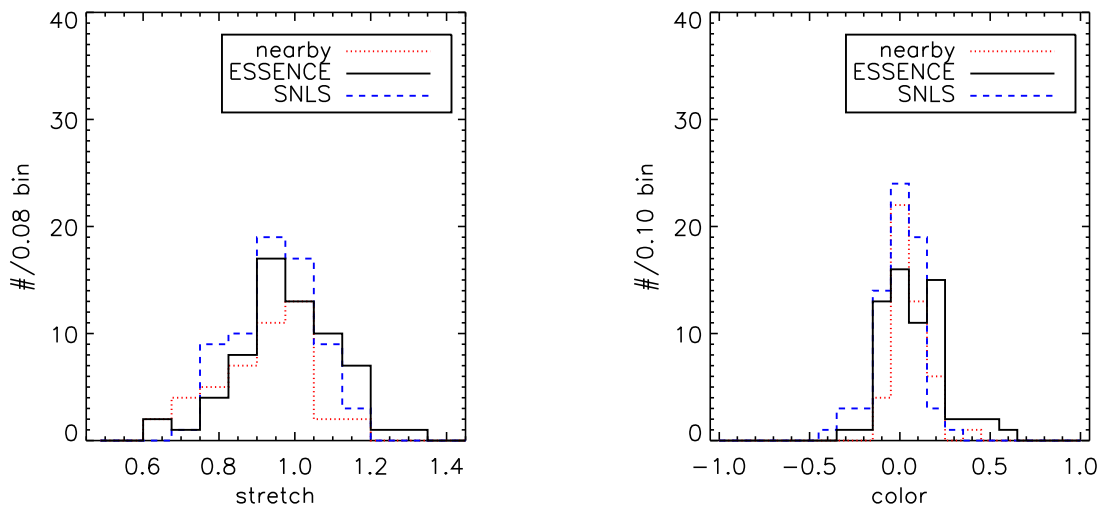
Fig. 2.— The distribution of the SALT light-curve stretch and the estimated color plus extinction for the nearby (dotted line), ESSENCE (solid line), and SNLS (dashed line) SNe Ia considered in this paper. The priors for SALT are effectively flat for stretch and color, and SALT quotes minimum χ^2 values instead of the estimated mean parameter values of MLCS2k2. See Table 10 for the full set of SALT light-curve fit results for these SNe Ia.
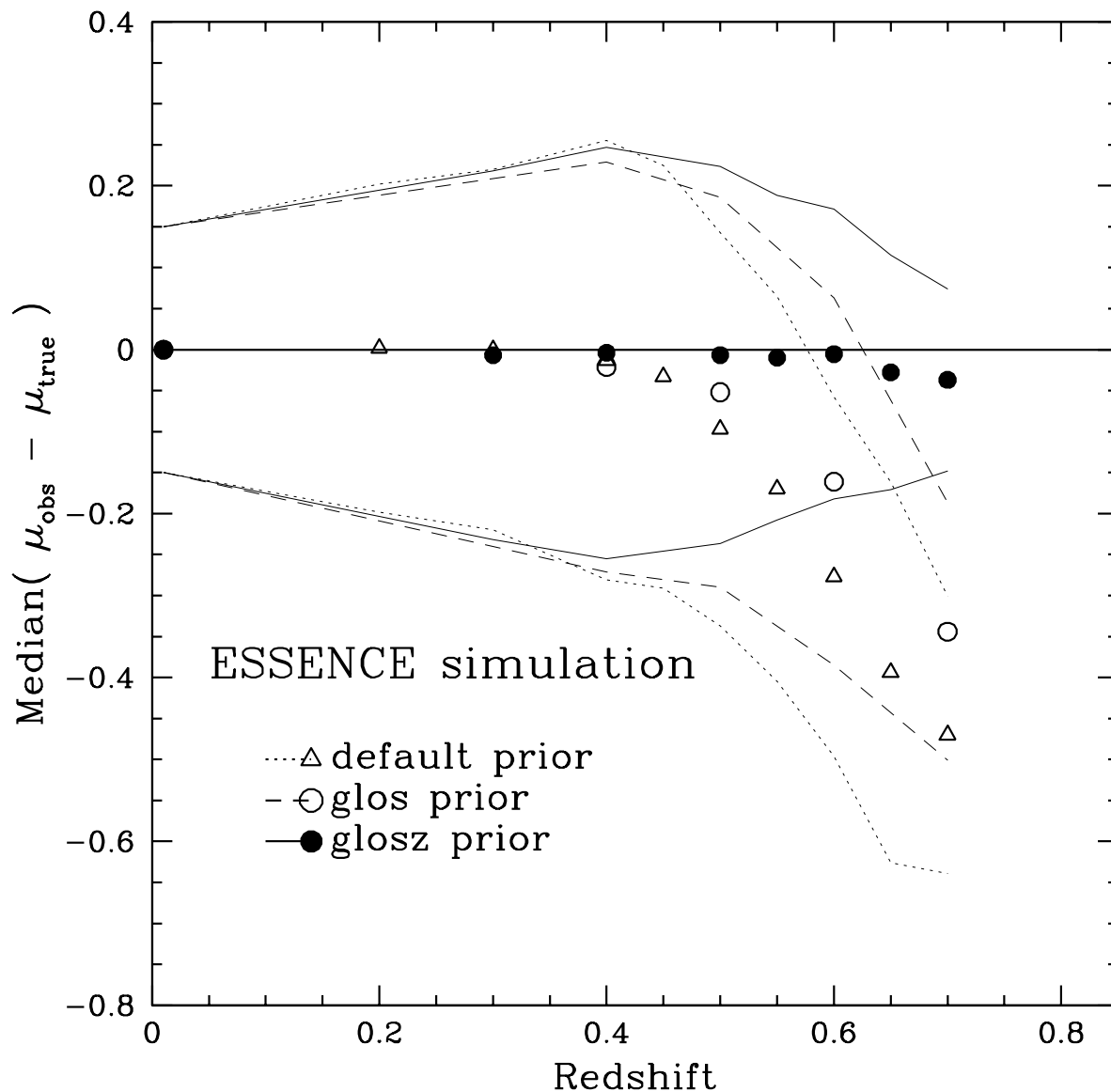
Fig. 3.— The median of the distance modulus error as a function of redshift for the simulated data sets. The points show the median value of the difference between the input μ_{true} and recovered μ_{obs} of about 1000 simulated supernovae at each redshift. The lines indicate the root-mean-square spread of the recovered distance modulus.
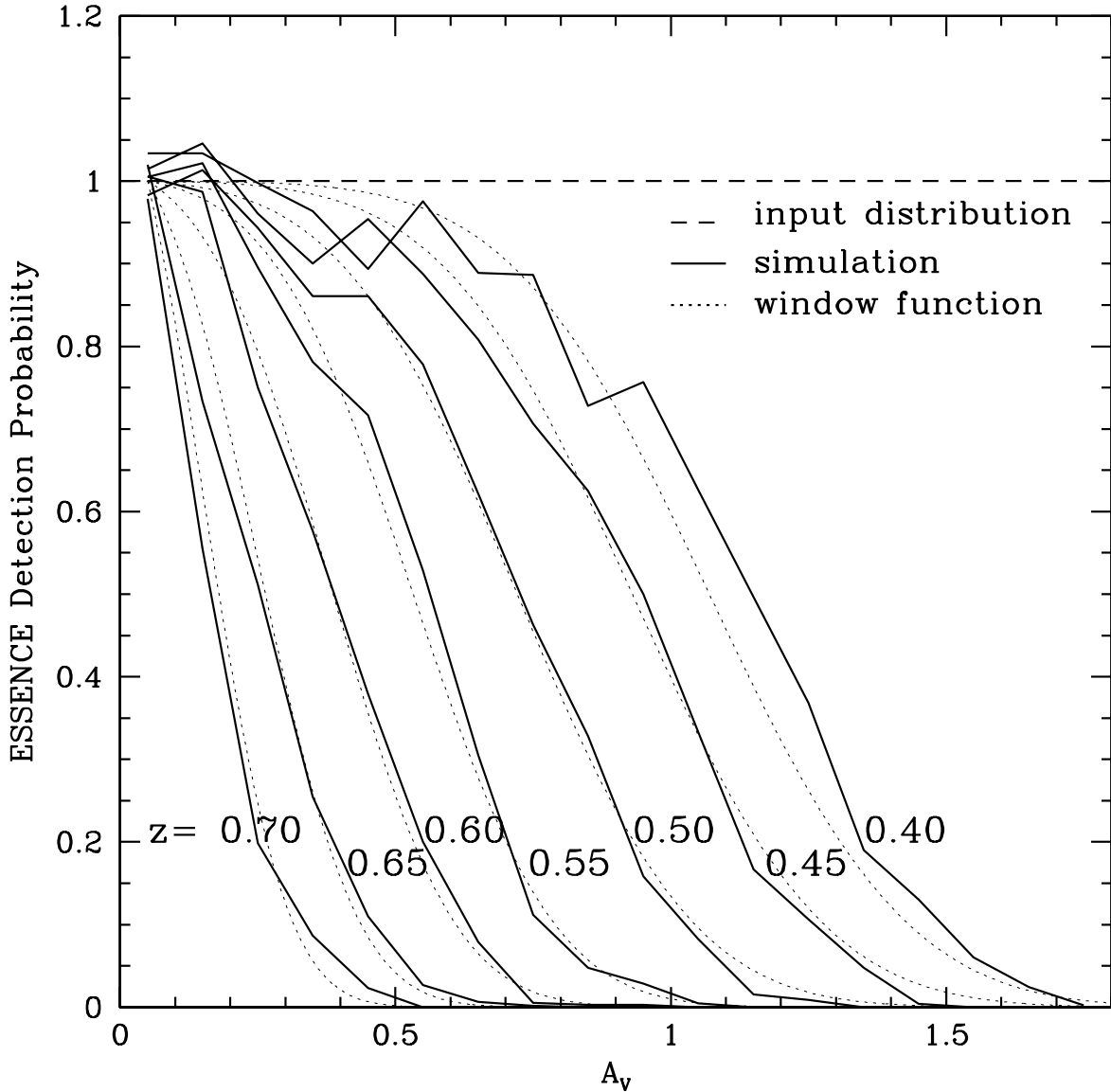
Fig. 4.— The recovered distribution of visual extinctions for simulated supernovae in the ESSENCE sample if the input distribution were uniform in A_V out to large extinctions. The curves are fit to determine the parameters of the window function (see Table 2) which is then used to modify the "glos" prior a function of redshift into the "glosz" prior. We estimate the SNLS selection function as extending +0.2 in redshift deeper than the ESSENCE selection function.
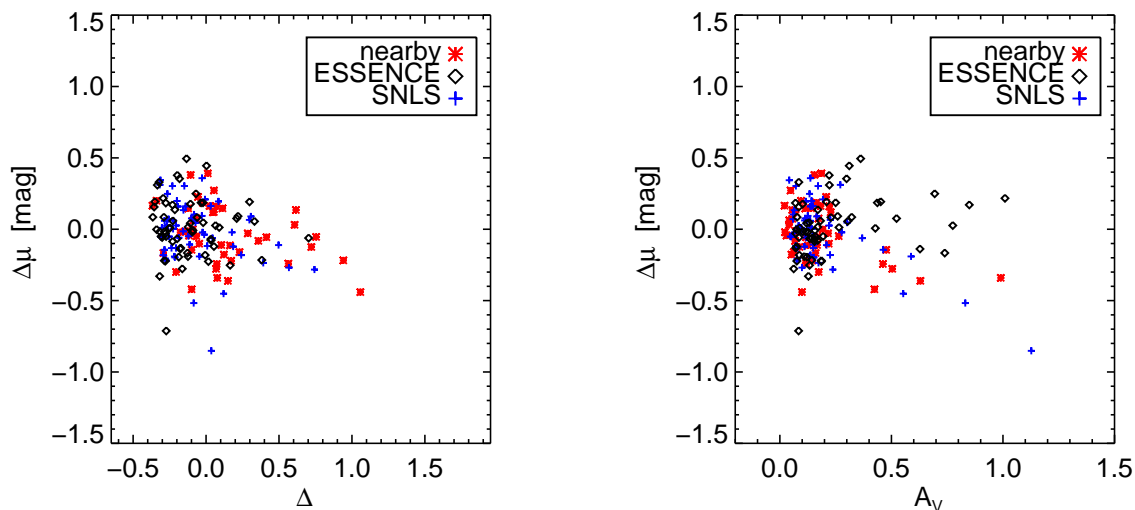
Fig. 5.— Distance modulus, μ, residuals with respect to a ΛCDM cosmology as a function of the MLCS2k2 "glosz" fit parameters: Δ and A_V. See Table 9.
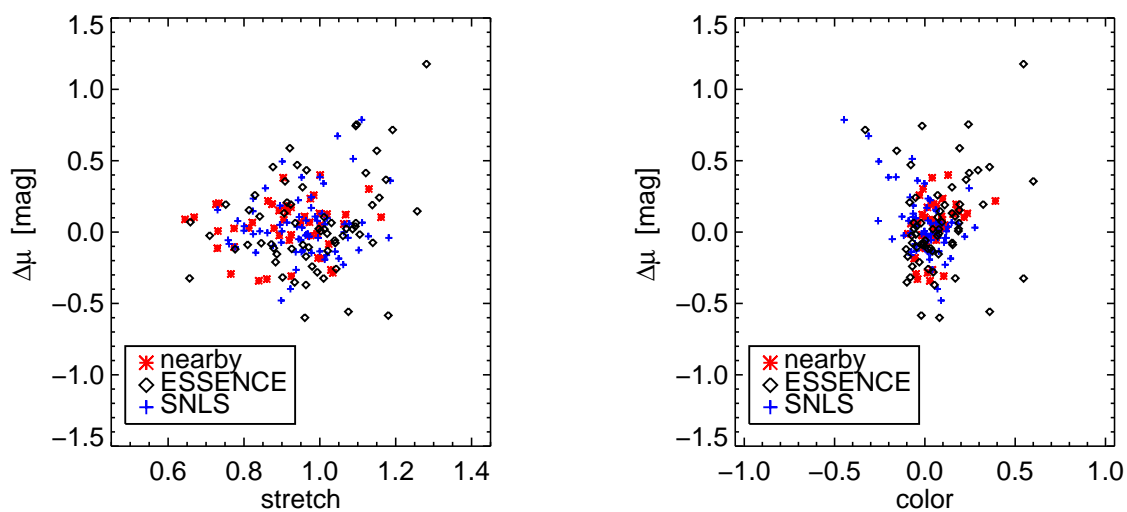
Fig. 6.— Distance modulus, μ, residuals with respect to a ΛCDM cosmology as a function of the SALT fit parameters: stretch and color. See Table 10.
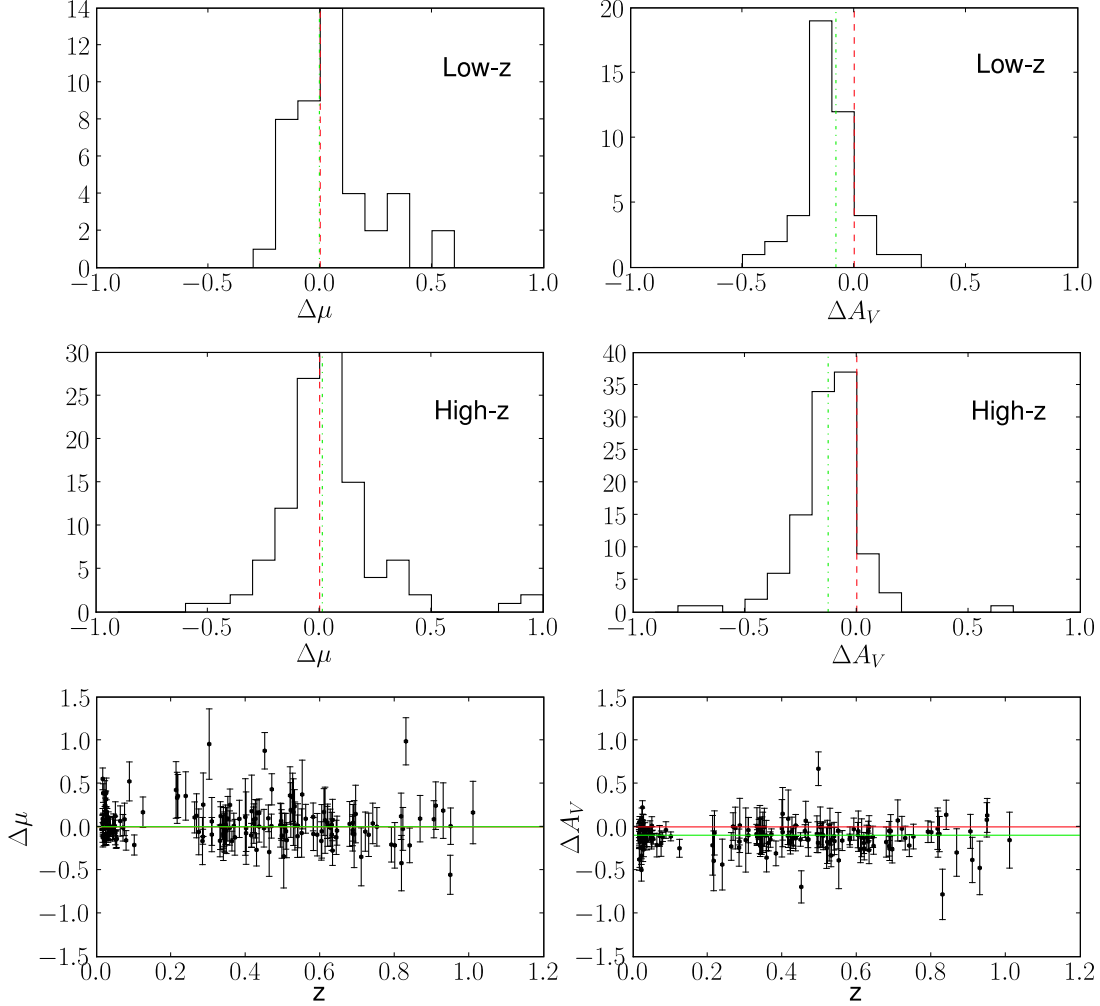
Fig. 7.— The distance modulus and A_V as a function of redshift for MLCS2k2 "glosz" minus the SALT distance modulus and $\beta \times$ color ($\beta = 1.57$) for the ESSENCE, SNLS, and nearby data sets. High-z refers to SNe Ia with $z \geq 0.15$, low-z to $z < 0.15$. The dot-dash line shows the weighted average of the difference for each quantity while the dashed line shows the line of zero difference. While the luminosity distances are offset between the two fitters, this is mainly due to a slightly different definition of the $\mathcal{M}$ parameter that defines the absolute luminosity of a SN Ia and the Hubble constant. The relative average difference between low redshift and high redshift is -0.0023 mag. This agreement translates to a similar agreement in the cosmological parameters obtained with each approach (see Figs. 10 and 11).
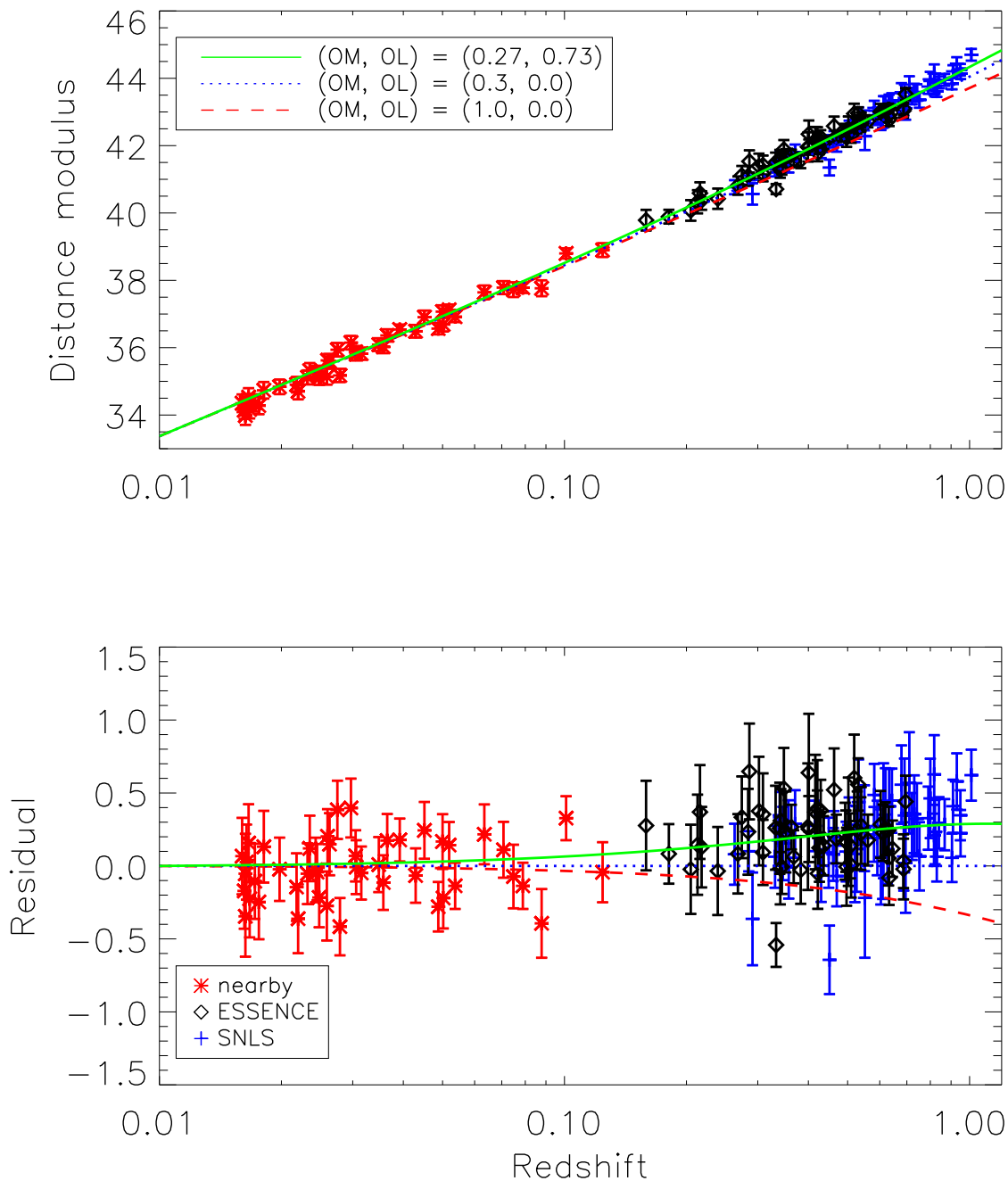
Fig. 8.— Luminosity distance modulus vs. redshift for the ESSENCE, SNLS, and nearby SNe Ia for MLCS2k2 with the "glosz" A_V prior. For comparison the overplotted solid line and residuals are for a ΛCDM $(w, \Omega_M, \Omega_\Lambda) = (-1, 0.27, 0.73)$ Universe.
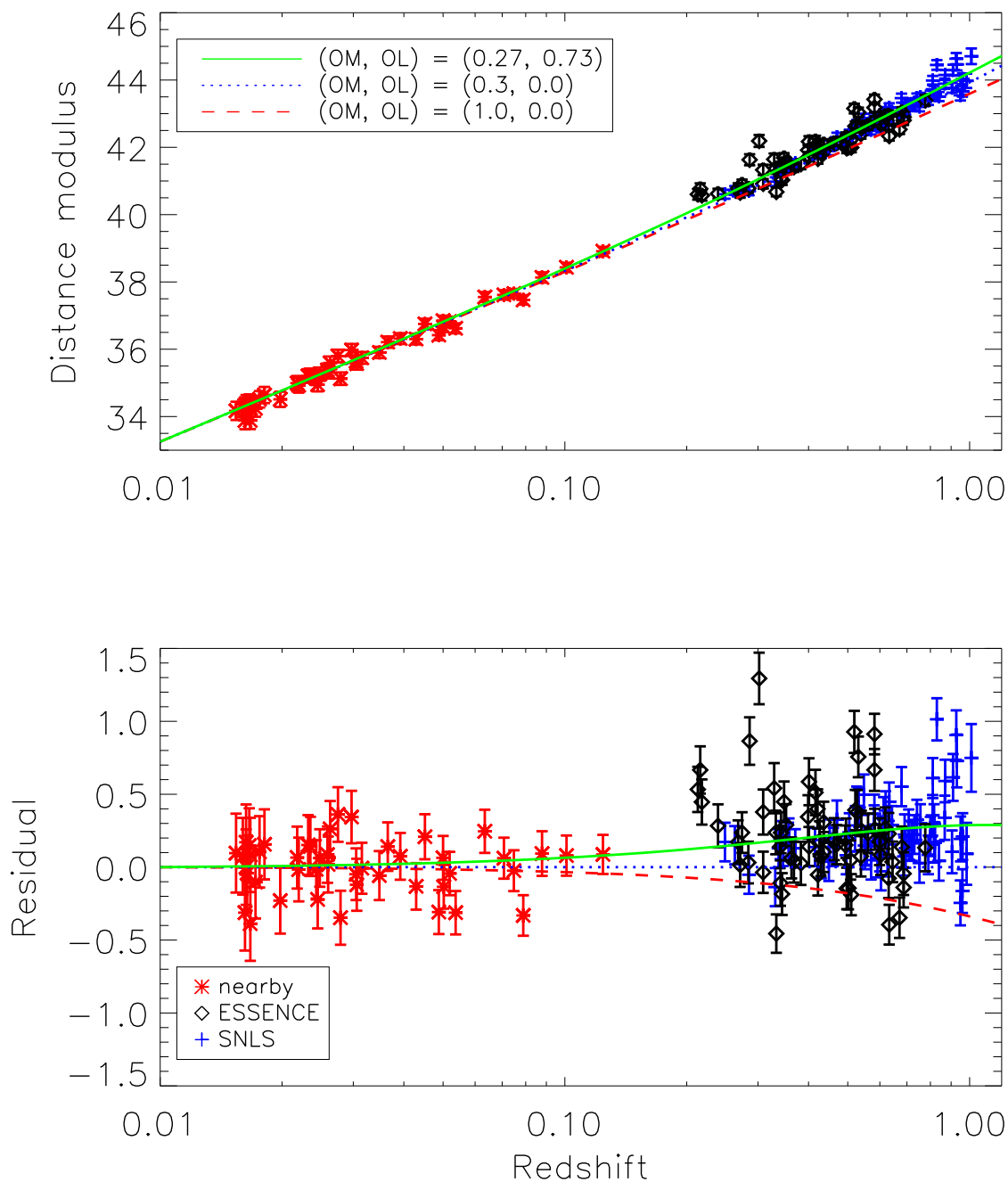
Fig. 9.— Luminosity distance modulus vs. redshift for the ESSENCE, SNLS, and nearby SNe Ia for SALT. For comparison the overplotted solid line and residuals are for a ΛCDM $(w, \Omega_{\mathrm{M}}, \Omega_{\Lambda}) = (-1, 0.27, 0.73)$ Universe.
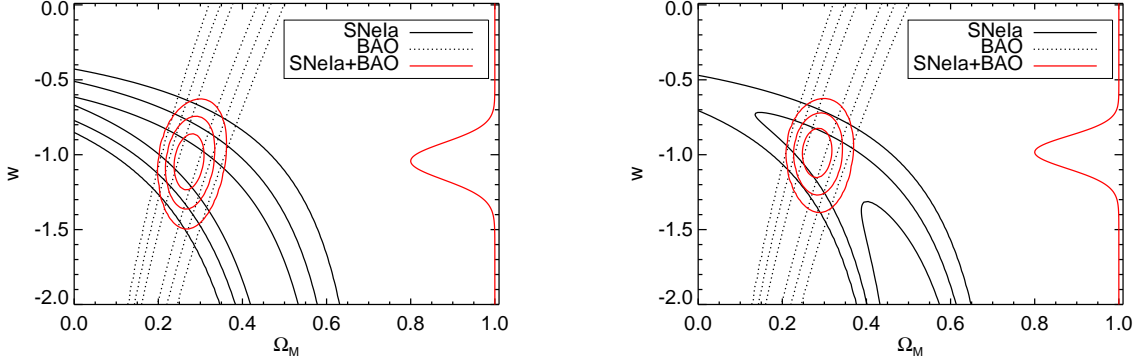
Fig. 10.— The Ω_M-w 1σ, 2σ, and 3σ contours from the ESSENCE + nearby sample for MLCS2k2 with the "glosz" A_V prior and with the SALT fitter. The baryon acoustic oscillation (BAO) constraints are from Eisenstein et al. (2005).
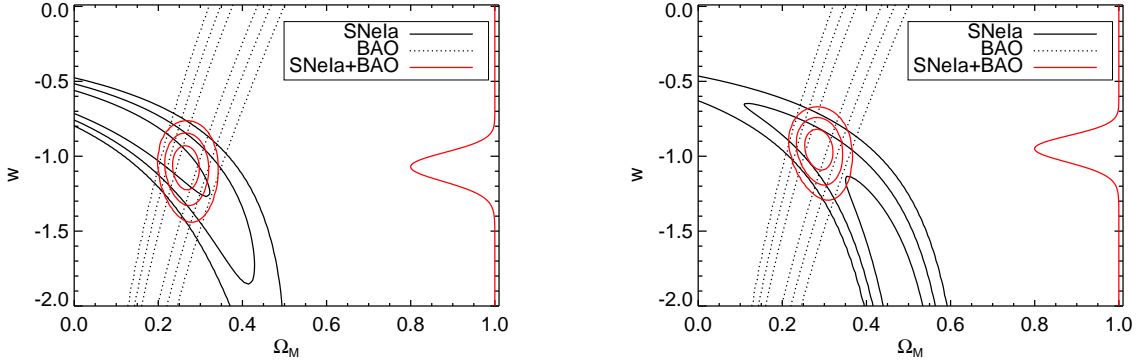
Fig. 11.— The Ω_M-w contours from the SNLS + ESSENCE + nearby sample for MLCS2k2 with "glosz" A_V prior and for the SALT fitter. The baryon acoustic oscillation (BAO) constraints are from Eisenstein et al. (2005).
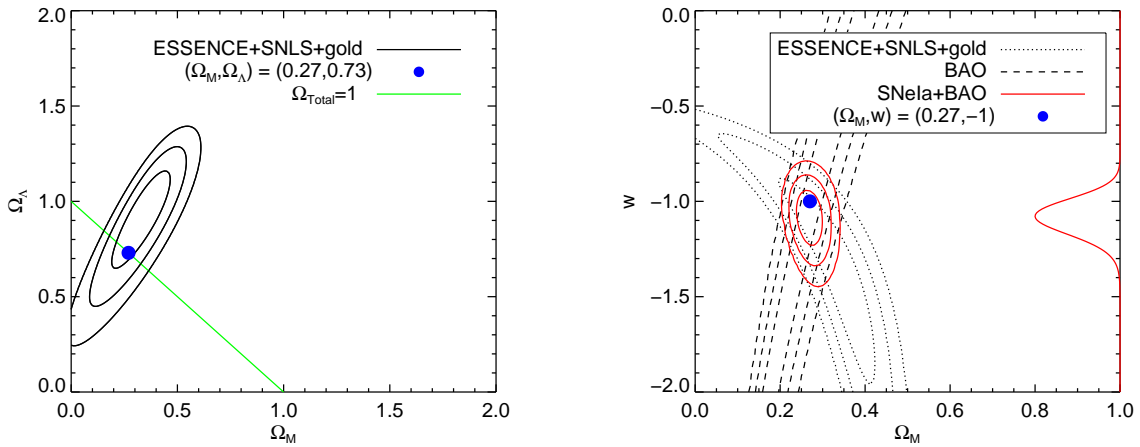
Fig. 12.— The SN Ia $(\Omega_M, \Omega_\Lambda)$ and (Ω_M, w) contours from combining the MLCS2k2 luminosity distances for the ESSENCE SNe Ia analyzed here in combination with the nearby SNe Ia, SNLS SNe Ia, and the Riess "gold" sample. The diagonal line in the $(\Omega_M, \Omega_\Lambda)$ plot represents a flat Universe, $\Omega_{\text{total}} = \Omega_M + \Omega_\Lambda = 1$. From the SNe Ia data alone, an empty Universe is ruled out at 4.5 σ, an $(\Omega_M, \Omega_\Lambda) = (0.3, 0)$ Universe at 10 σ, and an $(\Omega_M, \Omega_\Lambda) = (1, 0)$ σ Universe at > 20 σ. The best combination of data will come after a complete analysis of the calibration and systematic errors of all the data sets. We offer this interim result to indicate the potential of combining low-z, ESSENCE, and supernovae at redshifts beyond 1.
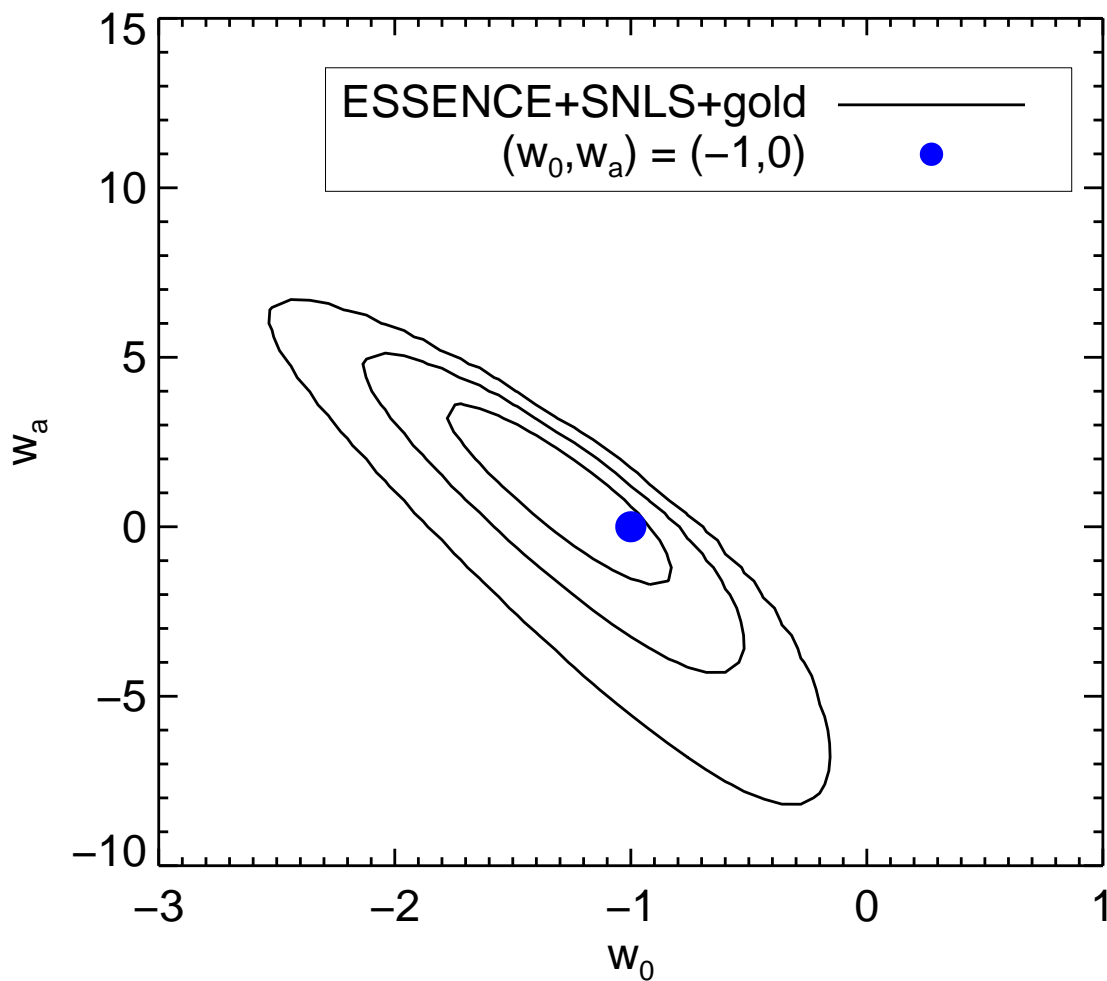
Fig. 13.— Combined constraints on (w_0, w_a) using the MLCS2k2 luminosity distances for the ESSENCE SNe Ia analyzed here in combination with the nearby SNe Ia, SNLS SNe Ia, and the Riess "gold" sample. Here we are considering a two-parameter representation of the dark energy equation-of-state parameter, $w = w_0 + w_a(1-a)$. Instead of the BAO constraints we have simply taken $\Omega_M = 0.27 \pm 0.03$. (See cautionary note from Fig. 12.)

Table 1.   MLCS2k2 Fit Parameter Quality Cuts

Fit Parameter	Requirement
χ^2_ν	$\chi^2_\nu \leq 3$
# Degrees of Freedom	DoF ≥ 4
Δ	$-0.4 \leq \Delta \leq 1.7$
Time of Maximum uncertainty	$\mathrm{Tmax_{err}} \leq 2.0$ rest-frame days
First observation w/ SNR > 5	$\leq +4$ days
Last observation w/ SNR > 5	$\geq +9$ days

Note. — See Tables. 9 for the MLCS2k2 fit parameters used for the cosmological analysis presented in this paper. These selection criteria were derived based on Monte Carlo simulations discussed in §2.5. The number of degrees of freedom is the number of light-curve points with SNR> 5 minus the 4 independent MLCS2k2 fit parameters: m_V, Δ, A_V and $T_{\max}$.

Table 2.   "glosz" Window Function Parameters

z	$A_{1/2}$	σ_A	$\Delta_{1/2}$	σ_Δ
0.35	1.35	2.2	0.93	2.4
0.40	1.05	2.5	0.75	2.4
0.45	0.88	2.6	0.60	2.6
0.50	0.67	2.8	0.43	2.6
0.55	0.48	3.5	0.29	2.7
0.60	0.33	4.0	0.17	2.8
0.65	0.20	5.0	0.05	3.0
0.70	0.10	6.0	-0.09	3.3
0.75	0.05	7.5	-0.25	3.3

Table 3.   SALT Fit Parameter Quality Cuts

Fit Parameter	Requirement
χ^2_ν	$\chi^2_\nu \leq 3$
# Degrees of Freedom	DoF ≥ 5
stretch	$0.5 \leq s < 1.4$
Time of Maximum uncertainty	$\mathrm{Tmax_{err}} \leq 2.0$ rest-frame days
# Observations after B-band maximum	> 1
First observation w/ SNR > 5	$\leq +5$ days

Note. — See Tables. 10 for the SALT fit parameters used for the cosmological analysis presented in this paper. These selection criteria were based on Astier et al. (2006) with additional sanity checks on the stretch parameter and uncertainty in the time of maximum light. The number of degrees of freedom is the number of light-curve points with SNR> 5 minus the 4 independent SALT fit parameters: m_B, strech, color, and $T_{\max}$.

Table 4.   Sources of Increased μ Dispersion

Source	σ_μ
Flatfielding	0.01
Focal-plane PSF	0.02
Field-field zeropoint	0.01
Image subtraction	0.01
Subtotal (quadrature sum)	0.026
Gravitational lensing	0.03
Total (quadrature sum)	0.04

Note. — The photometric and astrophysical uncertainties that add increased scatter, but no bias, to the measured SN Iadistance moduli, μ.

Table 5. Potential Sources of Systematic Error on the Measurement of w

Source	dw/dx	Δx	Δ_w	Notes
Phot. errors from astrometric uncertainties of faint objects	1/mag	0.005 mag	0.005	
Bias in diff im photometry	0.5 / mag	0.002 mag	0.001	
CCD linearity	1 / mag	0.005 mag	0.005	
Photometric zeropoint diff in R,I	2 / mag	0.02 mag	0.04	
Zpt. offset between low and high z	1 / mag	0.02 mag	0.02	
K-corrections	0.5 / mag	0.01 mag	0.005	
Filter passband structure	0 / mag	0.001 mag	0	
Galactic extinction	1 / mag	0.01 mag	0.01	
Host galaxy R_V	0.02 / R_V	0.5	0.01	"glosz"
Host galaxy extinction treatment	0.08	prior choice	0.08	different priors
Intrinsic color of SNe Ia	3 / mag	0.02 mag	0.06	interacts strongly with prior
Malmquist bias/selection effects	0.7 / mag	0.03 mag	0.02	"glosz"
SN Ia evolution	1 / mag	0.02 mag	0.02	
Hubble bubble	$3/\delta H_{\text{effective}}$	0.02	0.06	
Gravitational lensing	$1/\sqrt{N}$ / mag	0.01 mag	< 0.001	Holz & Linder (2005)
Grey dust	1 / mag	0.01 mag	0.01	
Subtotal w/o extinction+color	$\cdots$	$\cdots$	0.082	
Total	$\cdots$	$\cdots$	0.13	
Joint ESSENCE+SNLS comparison	$\cdots$	$\cdots$	0.02	photometric system
Joint ESSENCE + SNLS Total	$\cdots$	$\cdots$	0.13	

Note. — The systematic error table for this first ESSENCE cosmological analysis. The issue of treatment of A_V and color distribution is clearly the dominant systematic effect and will need to be seriously addressed to reduce our systematic errors to our target of 5%.

Table 6.   Effect of different fixed R_V on w for the two different A_V priors considered in our MLCS2k2 analysis of the ESSENCE+nearby sample.

A_V prior	R_V value	w	$w\text{-}w_{R_V=3.1}$ for given prior
glosz	2.1	$-0.986^{+0.116}_{-0.114}$	$+0.061$
glosz	3.1	$-1.047^{+0.125}_{-0.124}$	$\cdots$
glosz	4.1	$-1.073^{+0.121}_{-0.120}$	-0.026
glos	2.1	$-0.932^{+0.116}_{-0.114}$	$+0.025$
glos	3.1	$-0.957^{+0.127}_{-0.124}$	$\cdots$
glos	4.1	$-1.039^{+0.134}_{-0.131}$	-0.082
exponential	2.1	$-0.855^{+0.126}_{-0.122}$	$+0.027$
exponential	3.1	$-0.882^{+0.134}_{-0.130}$	$\cdots$
exponential	4.1	$-0.808^{+0.147}_{-0.141}$	$+0.074$

Note. — Systematic effect of choosing different fixed R_V values for the different A_V priors discussed here for MLCS2k2.

Table 7. Cosmological Parameters from ESSENCE+nearby and BAO Constraints

Sample	#SNe Ia[a]	ΛCDM[b] χ^2/DoF	flat, constant-w (marg. 1D) χ^2/DoF	w_0	Ω_M
MLCS2k2: "glosz"					
All ESSENCE+nearby	102	0.96	0.96	$-1.047^{+0.125}_{-0.124}$	$0.274^{+0.032}_{-0.020}$
ESSENCE only	57	0.88	0.91	$\cdots$	$\cdots$
nearby only	45	1.00	1.01	$\cdots$	$\cdots$
SALT					
All ESSENCE+nearby	106	2.62	2.66	$-0.988^{+0.110}_{-0.109}$	$0.284^{+0.031}_{-0.020}$
ESSENCE only	60	4.64	4.72	$\cdots$	$\cdots$
nearby only	46	1.01	1.04	$\cdots$	$\cdots$

[a]$0.015 < z$.

[b]ΛCDM refers to a universe with $(w, \Omega_M, \Omega_\Lambda) = (-1, 0.27, 0.73)$.

Note. — The ESSENCE cosmological results given here are for our favored MLCS2k2 "glosz" A_V prior and the SALT fitter of Guy et al. (2005). The DoF for the ΛCDM model is the number of SNe Ia in each set minus the one fit parameters, $\mathcal{M}$. The DoF for the best-fit model is the number of SNe Ia minus the three fit parameters $(w, \Omega_M, \mathcal{M})$. For the subsets, the same cosmological fit is used but $\mathcal{M}$ is allowed to float. The χ^2/DoF for ΛCDM for the nearby set is 1 by construction. The appropriate additional σ_μ to add in quadrature to recover the full intrinsic dispersion of SNe Ia is determined by requiring χ^2/DoF of the nearby set to be 1 for ΛCDM with an assumed peculiar velocity of 400 km/s. The value for w_0 is marginalized over Ω_M assuming a flat, $\Omega_M + \Omega_\Lambda = 1$ Universe. Note that the χ^2/DoF values for the marginalized 1D values are higher than the ΛCDM model. This is possible because the mean marginalized 1D values are not the points of lowest χ^2. This indicates that there is no reason to favor the marginalized 1D values over the ΛCDM model.

Table 8.   Joint Cosmological Parameters from ESSENCE+SNLS+nearby and BAO
Constraints

Sample	#SNe Ia[a]	ΛCDM[b] χ^2/DoF	flat, constant-w (marg. 1D)		
			χ^2/DoF	w_0	$\Omega_{\rm M}$
MLCS2k2: "glosz"					
All ESSENCE+SNLS+nearby	162	0.90	0.91	$-1.069^{+0.091}_{-0.093}$	$0.267^{+0.028}_{-0.018}$
ESSENCE only	60	0.91	0.93	$\cdots$	$\cdots$
SNLS only	57	0.82	0.82	$\cdots$	$\cdots$
nearby only	45	0.99	1.01	$\cdots$	$\cdots$
SALT					
All ESSENCE+SNLS+nearby	178	2.76	2.79	$-0.958^{+0.088}_{-0.090}$	$0.288^{+0.029}_{-0.019}$
ESSENCE only	64	4.77	4.78	$\cdots$	$\cdots$
SNLS only	68	2.07	2.12	$\cdots$	$\cdots$
nearby only	46	0.99	1.02	$\cdots$	$\cdots$

[a]$0.015 < z$.

[b]ΛCDM refers to a universe with $(w, \Omega_{\rm M}, \Omega_\Lambda) = (-1, 0.27, 0.73)$.

Note. — See notes for Table 7. We include the full sample here without the redshift cut of the ESSENCE-only analysis to consistently include all of the usable SNe Ia.

Table 9. MLCS2k2 "glosz" Luminosity Distances of all SNe Ia.

Name	z	σ_z[a]	μ [mag]	σ_μ[b] [mag]	A_V [mag]	σ_{A_V} [mag]	Δ	σ_Δ	$T_{\max}$ [MJD]	$\sigma_{T_{\max}}$ [MJD]	χ^2/DoF	DoF	T_{first} [day]	T_{last} [day]	Failed
b010	0.5910	0.007	42.984	0.199	0.104	0.094	−0.166	0.182	52592.80	2.69	1.01	3	0.22	19.70	x
b013	0.4260	0.004	41.976	0.205	0.170	0.149	+0.034	0.141	52586.33	1.51	0.22	12	−2.21	35.64	
b016	0.3290	0.003	41.349	0.411	0.359	0.275	+0.190	0.384	52587.76	2.29	3.31	1	−0.56	16.76	x
b020	0.4250	0.003	41.766	0.371	0.202	0.204	+0.059	0.323	52599.88	0.90	$\cdots$	0	−8.94	7.21	x
d033	0.5310	0.008	42.960	0.138	0.085	0.091	−0.322	0.109	52934.26	1.87	0.98	5	−2.12	23.41	
d058	0.5830	0.009	43.103	0.151	0.119	0.104	−0.470	0.077	52941.76	1.53	1.70	7	−6.11	33.04	x
d083	0.3330	0.002	40.709	0.104	0.084	0.080	−0.273	0.061	52936.71	0.83	0.25	20	−4.17	43.08	
d084	0.5190	0.007	42.948	0.274	0.221	0.188	−0.197	0.207	52937.24	1.81	1.15	4	−4.01	13.77	
d085	0.4010	0.001	41.956	0.199	0.182	0.154	−0.228	0.115	52941.47	0.85	0.98	15	−6.75	33.25	
d086	0.2050	0.003	40.075	0.284	0.628	0.300	−0.177	0.083	52945.40	0.33	0.49	17	−11.11	35.41	
d087	0.3400	0.001	41.320	0.173	0.126	0.119	−0.112	0.094	52925.00	2.22	0.68	15	5.26	53.05	x
d089	0.4360	0.006	42.048	0.168	0.134	0.133	−0.198	0.121	52929.20	2.18	0.44	9	1.36	25.75	
d093	0.3630	0.006	41.726	0.101	0.077	0.076	−0.365	0.054	52946.30	0.47	0.81	26	−11.09	42.46	
d097	0.4360	0.008	42.097	0.143	0.116	0.112	−0.317	0.069	52935.36	1.50	0.70	17	−2.90	42.35	
d099	0.2110	0.003	40.422	0.176	0.118	0.121	−0.110	0.085	52922.12	1.88	0.39	25	8.25	67.71	x
d117	0.3090	0.006	41.424	0.255	0.209	0.182	+0.298	0.197	52948.95	0.49	0.37	12	−6.71	28.44	
d149	0.3420	0.006	41.626	0.182	0.170	0.144	−0.214	0.090	52954.53	0.43	0.41	18	−9.24	33.98	
e020	0.1590	0.007	39.786	0.268	0.437	0.311	−0.034	0.144	52965.34	0.51	0.74	14	−6.32	24.77	
e029	0.3320	0.008	41.505	0.260	0.259	0.206	+0.219	0.232	52964.93	0.98	0.92	8	−3.65	17.39	
e108	0.4690	0.005	42.275	0.125	0.071	0.075	−0.280	0.125	52979.57	0.65	0.87	9	−11.86	9.91	
e132	0.2390	0.006	40.424	0.275	0.739	0.291	−0.128	0.109	52972.59	0.39	0.80	22	−10.07	25.45	
e136	0.3520	0.007	41.618	0.251	0.304	0.212	+0.332	0.170	52967.29	0.72	1.08	19	−5.31	24.28	
e138	0.6120	0.009	42.990	0.155	0.103	0.087	−0.284	0.122	52956.19	0.95	0.79	7	−8.71	24.81	
e140	0.6310	0.007	42.893	0.150	0.121	0.088	−0.187	0.145	52968.09	1.58	1.37	13	−4.85	14.78	
e147	0.6450	0.010	43.015	0.155	0.071	0.062	−0.174	0.150	52963.99	1.95	0.41	10	−2.31	17.14	
e148	0.4290	0.006	42.249	0.178	0.102	0.101	−0.107	0.170	52975.92	0.61	0.69	15	−8.23	19.77	
e149	0.4970	0.006	42.230	0.243	0.186	0.175	+0.016	0.158	52950.81	0.60	1.30	17	−13.11	27.64	
f011	0.5390	0.004	42.661	0.224	0.157	0.133	−0.090	0.237	52982.72	2.70	1.06	9	2.21	13.92	
f041	0.5610	0.006	42.718	0.135	0.086	0.085	−0.301	0.124	52986.22	0.89	1.14	13	−9.06	10.15	
f076	0.4100	0.007	41.473	0.317	0.227	0.199	+0.175	0.301	52990.35	1.08	0.62	2	−12.95	8.30	x
f096	0.4120	0.006	41.613	0.374	0.324	0.261	+0.171	0.370	52989.56	2.89	4.42	1	6.01	10.28	x
f216	0.5990	0.005	43.339	0.232	0.117	0.100	−0.104	0.234	52985.07	1.31	0.41	3	−6.86	6.94	x

Table 9—Continued

Name	z	$\sigma_z{}^{\mathrm{a}}$	μ [mag]	$\sigma_\mu{}^{\mathrm{b}}$ [mag]	A_V [mag]	σ_{A_V} [mag]	Δ	σ_Δ	$T_{\max}$ [MJD]	$\sigma_{T_{\max}}$ [MJD]	χ^2/DoF	DoF	T_{first} [day]	T_{last} [day]	Failed
f231	0.6190	0.008	43.046	0.142	0.089	0.076	−0.247	0.143	52985.60	0.70	1.04	13	−9.61	11.41	
f235	0.4220	0.007	41.777	0.213	0.133	0.106	+0.165	0.217	52988.95	0.67	1.38	8	−11.87	9.22	
f244	0.5400	0.004	42.721	0.240	0.131	0.123	−0.020	0.257	52985.58	2.45	0.70	6	0.37	10.74	
f308	0.3940	0.009	42.429	0.258	0.171	0.156	−0.019	0.267	52992.37	1.16	1.75	6	−4.44	4.14	x
g005	0.2180	0.007	40.371	0.242	0.428	0.252	−0.253	0.060	53294.09	0.52	0.53	21	−7.44	50.87	
g050	0.6330	0.006	42.767	0.150	0.128	0.091	−0.318	0.123	53301.59	0.97	2.57	7	−11.36	18.04	
g052	0.3830	0.008	41.563	0.199	0.143	0.119	+0.382	0.164	53297.52	0.62	1.10	8	−10.46	32.21	
g055	0.3020	0.006	41.391	0.353	1.009	0.345	−0.294	0.095	53289.24	1.45	0.69	9	−4.67	40.60	
g097	0.3400	0.004	41.559	0.292	0.322	0.267	−0.289	0.109	53298.68	0.55	0.83	9	−11.66	32.38	
g120	0.5100	0.009	42.304	0.187	0.186	0.144	−0.286	0.111	53298.36	1.06	1.95	11	−7.50	21.70	
g133	0.4210	0.003	42.216	0.314	0.452	0.298	−0.351	0.080	53291.25	2.64	2.04	8	2.71	44.23	
g142	0.3990	0.003	41.960	0.420	0.523	0.310	+0.210	0.429	53296.27	1.12	2.16	7	−8.04	17.70	
g160	0.4930	0.003	42.385	0.240	0.194	0.189	−0.308	0.086	53283.44	0.93	1.09	8	−10.20	39.35	
g240	0.6870	0.005	43.038	0.177	0.062	0.054	−0.163	0.172	53307.71	1.21	0.65	4	−7.53	10.27	
h283	0.5020	0.008	42.495	0.353	0.265	0.206	+0.090	0.350	53321.80	1.58	1.32	4	−4.45	13.55	
h300	0.6870	0.012	43.092	0.142	0.076	0.059	−0.279	0.135	53309.63	1.15	1.46	4	−7.40	11.57	
h311	0.7500	0.010	43.445	0.111	0.065	0.048	−0.491	0.084	53313.39	1.25	4.81	4	−10.49	23.22	x
h319	0.4950	0.004	42.395	0.180	0.159	0.135	−0.274	0.116	53336.46	0.69	0.72	10	−8.93	31.17	
h323	0.6030	0.006	43.009	0.201	0.120	0.099	−0.108	0.186	53328.22	0.93	0.48	7	−8.15	13.68	
h342	0.4210	0.002	42.179	0.120	0.085	0.089	−0.356	0.075	53326.33	1.46	0.32	18	−3.65	38.53	
h359	0.3480	0.004	41.888	0.255	0.299	0.224	−0.182	0.099	53341.72	0.52	0.53	12	−9.38	29.19	
h363	0.2130	0.006	40.333	0.319	0.775	0.339	+0.065	0.114	53338.43	0.31	0.49	15	−12.61	38.47	
h364	0.3440	0.007	41.323	0.143	0.087	0.089	−0.006	0.109	53333.45	0.50	0.46	15	−13.61	38.45	
k396	0.2710	0.006	40.289	0.345	0.175	0.151	+0.843	0.354	53355.99	0.50	0.94	6	−9.40	3.19	x
k425	0.2740	0.003	41.116	0.257	0.250	0.234	−0.021	0.196	53334.89	0.41	1.15	10	−9.27	19.79	
k429	0.1810	0.008	39.891	0.138	0.126	0.127	−0.094	0.093	53350.23	0.44	0.19	10	−6.83	31.21	
k430	0.5820	0.010	43.311	0.204	0.113	0.100	−0.112	0.220	53350.64	1.82	0.64	6	−4.15	4.68	x
k441	0.6800	0.010	43.243	0.163	0.091	0.065	−0.203	0.181	53351.99	2.19	0.57	7	−4.65	3.67	x
k448	0.4010	0.005	42.342	0.388	0.311	0.258	+0.003	0.328	53355.53	1.67	0.51	6	−6.74	19.64	
k485	0.4160	0.005	42.163	0.376	0.849	0.303	−0.230	0.252	53349.83	1.59	2.00	7	−4.02	20.66	
m022	0.2400	0.003	41.634	0.336	0.698	0.352	−0.727	0.057	53638.18	2.25	2.41	17	0.66	74.90	x
m026	0.6530	0.008	43.023	0.223	0.102	0.081	−0.201	0.176	53628.96	3.05	0.39	2	6.11	15.16	x
m027	0.2860	0.006	41.532	0.306	0.362	0.294	−0.134	0.143	53639.18	1.36	1.33	6	−0.08	44.25	

Table 9—Continued

Name	z	$\sigma_z{}^{\rm a}$	μ [mag]	$\sigma_\mu{}^{\rm b}$ [mag]	A_V [mag]	σ_{A_V} [mag]	Δ	σ_Δ	$T_{\rm max}$ [MJD]	$\sigma_{T_{\rm max}}$ [MJD]	χ^2/DoF	DoF	$T_{\rm first}$ [day]	$T_{\rm last}$ [day]	Failed
m032	0.1550	0.004	39.954	0.154	0.092	0.101	−0.158	0.083	53631.73	2.09	0.30	18	6.30	89.46	x
m034	0.5620	0.006	42.799	0.228	0.130	0.120	−0.087	0.215	53633.45	3.02	0.22	1	3.65	13.27	x
m039	0.2490	0.003	40.799	0.347	0.507	0.330	−0.223	0.136	53627.73	2.36	1.33	10	9.15	88.36	x
m043	0.2660	0.003	40.819	0.337	1.033	0.358	−0.466	0.067	53634.13	2.50	1.06	14	3.89	58.38	x
m057	0.1840	0.003	41.327	0.200	0.218	0.191	−0.601	0.069	53632.99	2.45	2.49	17	6.87	88.76	x
m062	0.3170	0.005	41.279	0.252	0.135	0.112	+0.149	0.303	53645.07	1.50	1.29	3	−3.02	6.84	x
m075	0.1020	0.001	40.785	0.218	0.233	0.270	−0.387	0.100	53645.58	2.12	4.25	1	−4.12	56.69	x
m138	0.5820	0.004	42.815	0.192	0.073	0.074	−0.306	0.120	53660.34	2.03	3.19	3	−7.13	27.66	x
m158	0.4630	0.007	42.580	0.260	0.222	0.199	−0.334	0.113	53656.47	1.75	0.62	7	−5.08	31.14	
m193	0.3410	0.009	41.291	0.212	0.109	0.109	−0.124	0.131	53662.82	0.63	0.31	17	−10.19	56.13	
m226	0.6710	0.004	43.129	0.200	0.113	0.090	−0.227	0.215	53651.47	2.02	11.26	1	−7.38	1.59	x
n256	0.6310	0.012	43.086	0.108	0.075	0.068	−0.339	0.089	53696.76	1.43	0.78	12	−8.96	25.34	
n258	0.5220	0.007	42.740	0.212	0.110	0.106	+0.032	0.216	53697.67	1.86	3.26	8	−1.02	19.98	x
n263	0.3680	0.007	41.556	0.139	0.075	0.076	+0.054	0.119	53702.98	0.67	0.27	12	−5.00	25.67	
n278	0.3090	0.006	41.163	0.190	0.156	0.139	+0.033	0.191	53700.16	1.21	0.74	7	−1.61	26.65	
n285	0.5280	0.006	42.631	0.243	0.170	0.141	−0.122	0.214	53687.99	1.91	0.90	7	−3.89	13.13	
n326	0.2680	0.006	40.813	0.244	0.144	0.146	+0.703	0.210	53710.01	0.52	0.91	9	−9.45	22.11	
n404	0.2160	0.008	40.590	0.290	0.694	0.342	−0.069	0.192	53713.02	0.46	0.86	11	−13.86	20.62	
p425	0.4530	0.006	42.267	0.405	0.224	0.220	+0.183	0.349	52952.54	2.93	$\cdots$	0	7.92	12.05	x
p454	0.6950	0.010	43.530	0.137	0.070	0.055	−0.276	0.134	53704.17	2.25	1.74	8	−3.58	15.90	
p455	0.2840	0.006	41.102	0.269	0.229	0.211	−0.061	0.287	53721.31	0.57	1.37	13	−13.38	13.06	
p524	0.5080	0.001	42.428	0.195	0.155	0.131	−0.229	0.146	53718.84	0.62	0.20	10	−11.04	12.77	
p528	0.7770	0.005	43.762	0.115	0.041	0.039	−0.310	0.121	53726.35	1.57	0.61	6	−7.99	6.58	x
p534	0.6150	0.008	42.841	0.209	0.107	0.090	−0.096	0.235	53742.26	1.57	2.27	4	−8.78	−2.59	x
sn1990O	0.0306	0.001	35.805	0.095	0.073	0.058	−0.144	0.067	48076.01	1.04	0.31	26	0.67	84.90	
sn1990af	0.0502	0.001	36.691	0.165	0.119	0.116	+0.564	0.116	48195.95	0.45	0.13	43	−3.19	21.59	
sn1992P	0.0263	0.001	35.597	0.123	0.114	0.089	−0.122	0.084	48719.24	0.87	0.32	23	−0.56	72.43	
sn1992ae	0.0748	0.001	37.723	0.185	0.167	0.143	+0.105	0.111	48804.16	1.29	0.30	25	1.55	37.90	
sn1992ag	0.0259	0.001	35.138	0.159	0.504	0.141	+0.069	0.080	48807.05	0.79	1.07	42	−0.51	63.85	
sn1992aq	0.1009	0.001	38.799	0.103	0.048	0.040	+0.054	0.088	48832.27	1.06	0.52	33	3.27	53.93	
sn1992bc	0.0198	0.001	34.838	0.047	0.023	0.018	−0.177	0.036	48911.98	0.16	0.36	135	−10.07	98.66	
sn1992bh	0.0451	0.001	36.906	0.143	0.208	0.122	−0.055	0.085	48920.18	1.05	0.11	35	−0.34	41.73	
sn1992bl	0.0429	0.001	36.487	0.129	0.068	0.049	+0.359	0.124	48946.32	1.18	0.37	31	3.10	63.47	

Table 9—Continued

Name	z	σ_z[a]	μ [mag]	σ_μ[b] [mag]	A_V [mag]	σ_{A_V} [mag]	Δ	σ_Δ	$T_{\max}$ [MJD]	$\sigma_{T_{\max}}$ [MJD]	χ^2/DoF	DoF	T_{first} [day]	T_{last} [day]	Failed
sn1992bo	0.0181	0.001	34.734	0.095	0.056	0.048	+0.616	0.075	48986.24	0.16	0.31	73	−7.48	53.31	
sn1992bp	0.0789	0.001	37.782	0.110	0.052	0.049	+0.122	0.096	48980.44	0.75	0.35	53	−1.62	55.72	
sn1992br	0.0878	0.001	37.764	0.207	0.099	0.077	+1.058	0.165	48985.15	1.22	0.74	15	1.42	50.92	
sn1992bs	0.0634	0.001	37.642	0.167	0.164	0.133	−0.022	0.088	48984.99	1.32	0.14	31	2.58	49.51	
sn1993B	0.0707	0.001	37.783	0.152	0.173	0.118	−0.067	0.077	49004.05	1.18	0.41	36	3.52	69.91	
sn1993H	0.0248	0.001	35.098	0.095	0.116	0.076	+0.941	0.077	49068.90	0.44	0.28	96	−1.09	91.54	
sn1993O	0.0519	0.001	37.123	0.096	0.071	0.053	+0.054	0.071	49134.34	0.43	0.20	78	−6.29	50.62	
sn1993ag	0.0500	0.001	37.070	0.138	0.140	0.102	+0.113	0.093	49316.51	0.74	0.28	45	−1.58	69.78	
sn1994M	0.0243	0.001	35.242	0.124	0.216	0.116	+0.286	0.084	49473.83	0.96	0.31	55	2.86	71.16	
sn1994S	0.0160	0.001	34.350	0.077	0.056	0.041	−0.077	0.075	49518.29	0.50	0.41	33	−4.52	34.88	
sn1994T	0.0357	0.001	36.024	0.117	0.088	0.071	+0.722	0.108	49514.36	0.54	1.40	31	0.42	31.25	
sn1995ac	0.0488	0.001	36.566	0.111	0.174	0.104	−0.205	0.049	49992.91	0.41	0.26	91	−5.02	53.14	
sn1995ak	0.0220	0.001	34.702	0.131	0.630	0.122	+0.150	0.067	50021.22	0.86	0.63	57	3.49	68.93	
sn1996C	0.0275	0.001	35.940	0.106	0.155	0.092	−0.106	0.055	50128.40	0.93	0.20	60	2.47	86.03	
sn1996ab	0.1242	0.001	38.899	0.175	0.126	0.101	+0.164	0.138	50225.12	1.11	0.41	23	0.61	52.13	
sn1996bl	0.0348	0.001	36.090	0.117	0.192	0.114	−0.091	0.066	50376.29	0.59	0.20	40	−2.41	46.63	
sn1996bo	0.0163	0.001	33.983	0.125	0.990	0.125	+0.077	0.072	50386.95	0.30	0.75	51	−6.20	44.97	
sn1996bv	0.0167	0.001	34.171	0.158	0.587	0.162	−0.200	0.065	50403.61	1.26	0.27	26	5.20	81.63	x
sn1997Y	0.0166	0.001	34.530	0.111	0.222	0.095	+0.071	0.080	50486.79	1.38	0.15	30	2.14	58.15	
sn1997dg	0.0297	0.001	36.149	0.121	0.186	0.109	+0.012	0.079	50720.04	0.84	0.24	30	0.83	87.85	
sn1998V	0.0172	0.001	34.360	0.103	0.219	0.123	−0.047	0.064	50891.21	0.81	0.16	49	2.74	94.95	
sn1998ab	0.0279	0.001	35.175	0.103	0.424	0.083	−0.099	0.052	50914.38	0.25	0.39	63	−7.36	71.41	
sn1998dx	0.0537	0.001	36.917	0.098	0.062	0.054	+0.229	0.098	51071.57	0.76	0.45	25	1.00	61.70	
sn1998ef	0.0167	0.001	34.164	0.107	0.145	0.094	+0.172	0.101	51113.88	0.25	0.50	26	−7.14	80.39	
sn1998eg	0.0235	0.001	35.318	0.124	0.228	0.130	+0.047	0.128	51110.69	1.21	0.15	19	−0.02	82.87	
sn1999aw	0.0392	0.001	36.539	0.045	0.021	0.020	−0.367	0.032	51253.89	0.30	0.67	89	−8.18	57.53	
sn1999cc	0.0315	0.001	35.822	0.093	0.118	0.086	+0.414	0.096	51315.68	0.44	0.21	70	−2.75	27.26	
sn1999ek	0.0176	0.001	34.279	0.107	0.462	0.294	+0.073	0.064	51481.80	0.40	0.21	145	−2.91	62.94	
sn1999gp	0.0260	0.001	35.624	0.065	0.095	0.055	−0.339	0.028	51550.06	0.14	0.31	186	−12.91	78.45	
sn2000ca	0.0245	0.001	35.245	0.063	0.030	0.027	−0.117	0.049	51666.22	0.45	0.27	74	−2.41	89.18	
sn2000cf	0.0365	0.001	36.363	0.111	0.183	0.105	+0.024	0.068	51672.17	0.86	0.18	69	3.40	83.48	
sn2000cn	0.0232	0.001	35.118	0.088	0.166	0.113	+0.755	0.072	51707.81	0.16	0.38	65	−7.78	93.61	
sn2000dk	0.0164	0.001	34.370	0.077	0.041	0.033	+0.607	0.066	51812.44	0.28	0.38	54	−4.49	92.61	

Table 9—Continued

Name	z	σ_z[a]	μ [mag]	σ_μ[b] [mag]	A_V [mag]	σ_{A_V} [mag]	Δ	σ_Δ	$T_{\max}$ [MJD]	$\sigma_{T_{\max}}$ [MJD]	χ^2/DoF	DoF	T_{first} [day]	T_{last} [day]	Failed
sn2000fa	0.0218	0.001	34.901	0.122	0.477	0.100	−0.099	0.063	51891.98	0.19	0.44	43	−9.86	70.29	
sn2001V	0.0162	0.001	34.142	0.076	0.160	0.064	−0.292	0.031	51973.25	0.13	0.36	186	−13.01	86.14	
sn2001ba	0.0305	0.001	35.876	0.075	0.042	0.034	−0.087	0.056	52034.22	0.54	0.24	93	−3.52	55.63	
sn2001cn	0.0154	0.001	34.058	0.107	0.515	0.101	+0.017	0.052	52071.04	0.74	0.12	99	4.73	84.37	x
sn2001cz	0.0163	0.001	34.275	0.119	0.264	0.127	−0.066	0.054	52103.89	0.30	0.13	48	−6.29	50.84	
03D1au	0.5043	0.001	42.553	0.155	0.136	0.121	−0.285	0.067	52907.72	0.72	0.24	21	−14.04	54.87	
03D1aw	0.5817	0.001	43.119	0.184	0.133	0.107	−0.265	0.138	52900.42	0.99	0.34	7	−8.73	10.14	
03D1ax	0.4960	0.001	42.329	0.174	0.110	0.109	+0.186	0.119	52915.56	0.44	0.30	17	−10.04	19.30	
03D1bp	0.3460	0.001	41.497	0.227	0.277	0.204	+0.177	0.121	52920.14	0.36	0.29	25	−11.60	58.76	
03D1cm	0.8700	0.001	43.997	0.124	0.082	0.065	−0.431	0.074	52948.21	1.05	0.46	10	−10.04	22.49	x
03D1co	0.6790	0.001	43.586	0.247	0.171	0.158	−0.231	0.116	52952.98	0.71	0.34	10	−11.62	25.24	
03D1ew	0.8680	0.001	43.954	0.139	0.096	0.071	−0.303	0.100	52989.98	1.41	0.36	7	−9.48	19.43	
03D1fc	0.3310	0.001	41.299	0.184	0.149	0.112	−0.113	0.154	53001.49	0.48	0.17	13	−8.44	18.67	
03D1fl	0.6880	0.001	43.128	0.208	0.132	0.134	−0.217	0.122	52990.08	2.38	0.51	9	0.11	21.44	
03D1fq	0.8000	0.001	43.919	0.250	0.116	0.098	+0.085	0.200	52997.37	1.60	0.84	7	−3.95	16.05	
03D1gt	0.5480	0.001	42.417	0.411	0.697	0.383	+0.383	0.289	53013.72	0.61	1.10	5	−9.35	8.15	x
03D3af	0.5320	0.001	42.844	0.272	0.193	0.177	−0.007	0.175	52731.82	0.86	0.83	5	−6.71	18.05	
03D3aw	0.4490	0.001	42.073	0.215	0.071	0.072	+0.008	0.147	52766.92	0.70	0.57	10	−9.23	39.60	
03D3ay	0.3709	0.001	41.800	0.205	0.060	0.061	−0.082	0.141	52766.85	0.64	0.71	13	−9.70	41.91	
03D3ba	0.2912	0.001	40.565	0.299	0.831	0.283	−0.085	0.089	52749.20	0.44	0.63	14	−14.53	58.16	
03D3bh	0.2486	0.001	42.175	0.060	0.053	0.044	−1.170	0.035	52750.72	0.28	19.21	11	−16.24	58.93	x
03D3cc	0.4627	0.001	42.254	0.143	0.092	0.084	−0.157	0.089	52780.65	0.43	0.33	11	−17.21	29.84	
03D3cd	0.4607	0.001	42.125	0.146	0.079	0.071	−0.206	0.153	52800.81	0.78	0.17	9	−6.43	16.08	
03D4ag	0.2850	0.001	40.977	0.086	0.047	0.039	−0.254	0.059	52829.47	0.31	0.56	34	−13.15	67.54	
03D4at	0.6330	0.001	43.257	0.233	0.139	0.149	−0.140	0.136	52815.54	1.07	0.45	6	−10.99	22.01	
03D4cn	0.8180	0.001	44.142	0.247	0.137	0.101	−0.028	0.234	52875.69	2.52	2.26	5	−1.78	15.76	
03D4cx	0.9490	0.001	44.256	0.134	0.059	0.047	−0.257	0.144	52881.56	2.45	0.69	6	−4.67	11.69	
03D4cy	0.9271	0.001	44.153	0.139	0.061	0.051	−0.251	0.149	52898.28	1.10	0.55	5	−11.31	7.80	x
03D4cz	0.6950	0.001	43.110	0.325	0.173	0.143	+0.392	0.199	52894.38	0.60	0.64	10	−10.58	11.17	
03D4dh	0.6268	0.001	42.938	0.212	0.150	0.145	−0.237	0.088	52905.27	0.58	0.34	18	−15.26	22.75	
03D4di	0.9050	0.001	43.838	0.127	0.076	0.057	−0.274	0.099	52899.90	0.83	0.62	12	−12.29	18.06	
03D4dy	0.6040	0.001	42.790	0.308	0.225	0.232	−0.294	0.076	52903.06	0.57	0.67	18	−14.09	24.45	
03D4fd	0.7910	0.001	43.754	0.188	0.122	0.105	−0.225	0.154	52936.20	1.67	0.26	6	−3.83	14.55	

Table 9—Continued

Name	z	$\sigma_z{}^{\mathrm{a}}$	μ [mag]	$\sigma_\mu{}^{\mathrm{b}}$ [mag]	A_V [mag]	σ_{A_V} [mag]	Δ	σ_Δ	$T_{\max}$ [MJD]	$\sigma_{T_{\max}}$ [MJD]	χ^2/DoF	DoF	T_{first} [day]	T_{last} [day]	Failed
03D4gf	0.5810	0.001	42.846	0.154	0.065	0.048	−0.024	0.136	52935.91	0.73	0.92	9	−14.30	16.67	
03D4gg	0.5920	0.001	42.869	0.232	0.147	0.115	−0.121	0.183	52941.19	1.09	0.56	7	−7.45	13.23	
03D4gl	0.5710	0.001	42.445	0.345	0.165	0.139	+0.149	0.321	52953.29	0.67	1.07	5	−12.08	5.71	x
04D1ag	0.5570	0.001	42.598	0.184	0.107	0.084	−0.112	0.202	53016.73	0.63	1.11	7	−13.73	6.17	x
04D1aj	0.7210	0.001	43.455	0.203	0.134	0.129	−0.279	0.114	52997.66	1.35	0.66	10	−4.32	16.66	
04D1ak	0.5260	0.001	42.494	0.273	0.209	0.206	+0.497	0.182	53010.73	0.41	0.46	8	−12.08	10.23	
04D2cf	0.3690	0.001	41.807	0.142	0.109	0.098	+0.094	0.118	53074.68	2.04	0.48	13	4.21	53.07	x
04D2fp	0.4150	0.001	42.062	0.136	0.113	0.098	−0.100	0.089	53106.36	0.48	0.21	14	−9.18	29.61	
04D2fs	0.3570	0.001	41.645	0.197	0.301	0.175	−0.073	0.098	53106.77	0.45	0.35	14	−9.88	30.57	
04D2gb	0.4300	0.001	41.809	0.145	0.099	0.104	+0.568	0.105	53108.56	0.43	0.22	11	−10.62	27.11	
04D2gc	0.5210	0.001	42.436	0.313	0.463	0.247	−0.285	0.084	53115.04	0.70	1.10	13	−14.25	21.84	
04D2gp	0.7070	0.001	43.438	0.309	0.135	0.141	+0.181	0.233	53109.96	1.69	0.77	3	−2.72	15.41	x
04D2iu	0.6910	0.001	43.420	0.375	0.165	0.169	+0.307	0.243	53120.36	1.08	0.27	5	−8.90	15.95	
04D2ja	0.7410	0.001	43.579	0.219	0.111	0.108	−0.089	0.167	53121.81	0.89	0.35	6	−9.47	14.65	
04D3co	0.6200	0.001	43.203	0.239	0.148	0.123	+0.032	0.153	53101.92	0.71	0.55	15	−12.54	29.23	
04D3cp	0.8300	0.001	43.617	0.133	0.077	0.071	−0.280	0.075	53108.79	0.92	0.44	14	−7.79	22.12	
04D3cy	0.6430	0.001	43.336	0.192	0.142	0.114	−0.200	0.110	53100.96	0.68	1.11	16	−12.40	29.43	
04D3dd	1.0100	0.001	44.698	0.138	0.042	0.032	−0.313	0.118	53113.63	1.97	1.10	4	−9.50	10.28	
04D3df	0.4700	0.001	42.027	0.178	0.237	0.194	+0.743	0.123	53119.94	0.48	1.09	22	−7.11	49.93	
04D3do	0.6100	0.001	42.816	0.268	0.137	0.149	+0.241	0.153	53113.59	0.71	0.53	16	−11.83	22.19	
04D3ez	0.2630	0.001	40.765	0.179	0.369	0.160	+0.044	0.073	53114.52	0.60	0.44	40	−3.98	71.13	
04D3fk	0.3578	0.001	41.414	0.184	0.588	0.165	−0.046	0.078	53126.45	0.36	0.39	35	−12.49	57.37	
04D3fq	0.7300	0.001	43.571	0.244	0.125	0.124	−0.029	0.187	53118.79	1.10	0.63	10	−5.38	17.62	
04D3gt	0.4510	0.001	41.350	0.209	1.127	0.184	+0.036	0.088	53137.47	0.38	0.74	26	−13.79	44.67	
04D3gx	0.9100	0.001	44.206	0.147	0.065	0.054	−0.155	0.137	53125.29	1.19	0.50	11	−8.27	12.55	
04D3hn	0.5516	0.001	42.279	0.396	0.553	0.326	+0.120	0.131	53136.87	0.43	1.12	17	−12.51	42.16	
04D3is	0.7100	0.001	43.714	0.330	0.271	0.230	−0.317	0.119	53142.78	1.33	0.81	9	−4.97	19.03	
04D3ki	0.9300	0.001	44.434	0.160	0.072	0.053	−0.149	0.162	53141.50	1.37	1.45	5	−9.37	12.35	
04D3kr	0.3373	0.001	41.456	0.136	0.143	0.117	−0.226	0.067	53164.36	0.30	0.31	24	−13.40	29.91	
04D3ks	0.7520	0.001	43.360	0.208	0.152	0.126	−0.214	0.119	53161.72	0.80	0.61	12	−8.73	20.30	
04D3lp	0.9830	0.001	44.702	0.161	0.042	0.039	−0.246	0.144	53150.84	2.22	2.57	2	−8.34	9.34	x
04D3lu	0.8218	0.001	43.759	0.193	0.113	0.090	−0.013	0.135	53167.90	0.77	0.93	9	−10.23	16.13	
04D3ml	0.9500	0.001	44.136	0.118	0.051	0.045	−0.312	0.111	53178.79	1.47	0.57	8	−6.90	12.05	

Table 9—Continued

Name	z	σ_z[a]	μ [mag]	σ_μ[b] [mag]	A_V [mag]	σ_{A_V} [mag]	Δ	σ_Δ	$T_{\max}$ [MJD]	$\sigma_{T_{\max}}$ [MJD]	χ^2/DoF	DoF	T_{first} [day]	T_{last} [day]	Failed
04D3nc	0.8170	0.001	43.721	0.180	0.118	0.094	−0.187	0.142	53186.44	0.77	1.06	11	−11.61	9.85	
04D3nh	0.3402	0.001	41.635	0.137	0.137	0.110	−0.193	0.092	53173.34	0.62	0.24	18	−5.97	23.14	
04D3nr	0.9600	0.001	44.292	0.130	0.049	0.044	−0.277	0.133	53183.23	1.23	0.59	3	−9.12	9.72	x
04D3ny	0.8100	0.001	43.637	0.250	0.124	0.118	+0.054	0.195	53193.46	0.91	1.13	6	−10.02	6.01	x
04D3oe	0.7560	0.001	43.538	0.217	0.098	0.095	−0.041	0.207	53196.35	1.00	1.02	6	−11.97	4.56	x
04D4an	0.6130	0.001	43.076	0.379	0.226	0.215	+0.297	0.245	53183.09	0.95	0.42	10	−5.93	16.42	
04D4bk	0.8400	0.001	43.880	0.140	0.084	0.070	−0.270	0.117	53190.57	0.86	0.49	10	−9.26	10.33	
04D4bq	0.5500	0.001	42.749	0.274	0.220	0.206	−0.206	0.156	53192.64	0.57	0.46	9	−12.30	10.92	
04D4dm	0.8110	0.001	43.917	0.219	0.123	0.115	−0.171	0.190	53197.46	1.17	1.03	5	−9.34	6.69	x
04D4dw	0.9610	0.001	44.158	0.132	0.049	0.043	−0.261	0.138	53198.00	1.07	1.56	3	−12.48	5.88	x

[a]We add a 400 km/s peculiar velocity dispersion in quadrature to these redshift uncertainties for our cosmological fits.

[b]An "intrinsic" dispersion of 0.10 should be added in quadrature to these values output by MLCS2k2 (Jha et al. 2006a) to fully account for the intrinsic dispersion of SNe Ia.

Note. — The luminosity distances and extinctions as determined by MLCS2k2 of the full ESSENCE SNe Ia and nearby sample using the "glosz" prior Hatano et al. (1998); Commins (2004); Riello & Patat (2005) described in 2. SN Ia fit marked as "Failed" did not pass the MLCS2k2 quality cuts given Table 1. See Table. 1 and §2 for further discussion of the quality cuts applied here. Redshifts of SNe Ia come from SNID fits (Miknaitis et al. 2007; Blondin 2007).

Table 10. SALT Luminosity Distances of all SNe Ia.

Name	z	σ_z[a]	μ [mag]	σ_μ[b] [mag]	color	σ_{color}	stretch	$\sigma_{\mathrm{stretch}}$	T_{max} [MJD]	$\sigma_{T_{\mathrm{max}}}$ [MJD]	χ^2/DoF	DoF	Rise	Tail	Failed
b010	0.5910	0.007	43.524	0.241	−0.127	0.086	1.232	0.141	52589.42	4.98	0.99	15	0	19	x
b013	0.4260	0.004	42.144	0.085	+0.077	0.039	1.012	0.050	52586.02	0.94	0.71	13	2	15	
b016	0.3290	0.003	41.876	0.169	+0.246	0.102	1.121	0.002	52579.73	0.05	0.73	6	0	10	
b020	0.4250	0.003	41.696	0.315	+0.068	0.176	0.840	0.111	52599.81	1.07	$\cdots$	0	1	3	x
d033	0.5310	0.008	43.271	0.136	−0.156	0.059	1.150	0.088	52932.50	1.70	1.74	17	2	19	
d058	0.5830	0.009	43.011	0.092	+0.188	0.068	1.095	0.006	52938.34	0.09	4.24	16	3	17	
d083	0.3330	0.002	40.908	0.028	−0.020	0.014	1.180	0.015	52936.99	0.18	5.44	15	4	15	
d084	0.5190	0.007	43.385	0.187	−0.015	0.090	1.095	0.114	52935.42	2.17	2.30	17	4	17	
d085	0.4010	0.001	41.957	0.071	+0.077	0.042	1.019	0.028	52942.32	0.34	4.02	15	6	13	
d086	0.2050	0.003	40.417	0.019	+0.000	0.000	0.940	0.012	52947.06	0.11	0.43	8	4	7	x
d087	0.3400	0.001	39.870	0.056	+0.000	0.000	0.733	0.043	52919.20	0.99	0.13	2	0	5	x
d089	0.4360	0.006	42.126	0.065	+0.002	0.037	1.039	0.030	52930.43	0.58	1.99	12	1	15	
d093	0.3630	0.006	41.636	0.054	−0.070	0.032	1.041	0.014	52948.28	0.16	3.24	20	7	17	
d097	0.4360	0.008	42.331	0.079	+0.084	0.038	1.257	0.047	52934.37	0.94	1.47	14	1	17	
d099	0.2110	0.003	40.436	0.073	−0.062	0.042	0.925	0.002	52925.29	0.03	1.86	8	0	12	x
d117	0.3090	0.006	41.561	0.107	+0.071	0.063	0.829	0.021	52949.07	0.27	0.87	20	8	16	
d149	0.3420	0.006	41.664	0.047	+0.071	0.030	1.011	0.003	52956.45	0.04	1.89	21	3	22	
e020	0.1590	0.007	40.273	0.028	+0.000	0.000	1.031	0.022	52966.81	0.15	6.01	6	3	6	x
e029	0.3320	0.008	41.594	0.094	+0.167	0.045	0.842	0.050	52965.22	0.46	1.85	8	4	8	
e108	0.4690	0.005	42.358	0.060	−0.050	0.031	1.105	0.034	52981.71	0.36	2.10	11	9	6	
e132	0.2390	0.006	40.855	0.049	+0.194	0.026	0.923	0.016	52973.26	0.17	2.38	22	11	15	
e136	0.3520	0.007	41.787	0.056	+0.191	0.037	0.813	0.002	52967.24	0.04	2.61	22	4	22	
e138	0.6120	0.009	43.239	0.094	+0.656	0.068	1.400	0.014	52961.44	1.33	24.09	18	4	18	x
e140	0.6310	0.007	42.877	0.102	+0.047	0.045	0.993	0.066	52969.61	1.16	2.36	21	6	19	
e147	0.6450	0.010	43.045	0.064	−0.095	0.047	0.964	0.007	52962.52	0.21	1.09	24	5	23	
e148	0.4290	0.006	42.057	0.054	−0.021	0.033	0.872	0.022	52976.40	0.27	2.18	21	14	11	
e149	0.4970	0.006	42.202	0.093	+0.546	0.054	1.010	0.034	52949.97	0.43	26.94	26	7	23	
f011	0.5390	0.004	42.627	0.099	+0.032	0.057	0.878	0.043	52985.39	0.68	1.38	12	2	14	
f041	0.5610	0.006	42.886	0.098	−0.046	0.050	1.093	0.057	52989.10	0.75	1.96	16	8	12	
f076	0.4100	0.007	41.652	0.092	+0.085	0.059	0.897	0.030	52990.07	0.01	0.88	3	5	2	x
f096	0.4120	0.006	42.372	0.162	+0.368	0.104	1.212	0.004	52994.91	0.02	2.54	2	0	6	x
f216	0.5990	0.005	42.995	0.193	−0.073	0.114	0.710	0.075	52984.30	0.75	0.63	15	10	9	
f231	0.6190	0.008	43.172	0.119	−0.062	0.060	1.030	0.066	52987.62	0.91	1.20	19	12	11	

Table 10—Continued

Name	z	$\sigma_z{}^{\mathrm{a}}$	μ [mag]	$\sigma_\mu{}^{\mathrm{b}}$ [mag]	color	σ_{color}	stretch	$\sigma_{\mathrm{stretch}}$	$T_{\max}$ [MJD]	$\sigma_{T_{\max}}$ [MJD]	χ^2/DoF	DoF	Rise	Tail	Failed
f235	0.4220	0.007	41.889	0.081	−0.031	0.050	0.883	0.030	52988.84	0.49	2.43	11	8	7	
f244	0.5400	0.004	42.808	0.084	−0.021	0.061	0.935	0.002	52985.81	0.01	1.00	11	2	13	
f308	0.394	0.009	42.394	0.080	0.043	0.055	0.889	0.004	52993.671	0.013	3.41	8	6	6	x
g005	0.2180	0.007	40.802	0.055	+0.228	0.025	1.175	0.027	53295.26	0.21	4.78	12	6	10	
g050	0.6330	0.006	42.567	0.082	+0.081	0.060	0.960	0.010	53302.64	0.22	2.26	13	9	8	
g052	0.3830	0.008	41.729	0.082	−0.104	0.050	0.777	0.021	53296.92	0.27	2.38	12	5	11	
g055	0.3020	0.006	42.422	0.202	+0.546	0.086	1.281	0.107	53290.60	1.32	0.78	9	3	10	
g097	0.3400	0.004	41.552	0.097	+0.185	0.051	1.003	0.037	53300.83	0.38	0.64	12	7	9	
g120	0.5100	0.009	42.224	0.078	+0.053	0.045	0.963	0.036	53299.45	0.61	2.80	17	7	14	
g133	0.4210	0.003	42.467	0.094	+0.283	0.062	1.113	0.001	53291.07	0.04	1.21	4	0	8	x
g142	0.3990	0.003	42.148	0.139	+0.323	0.075	0.752	0.061	53295.80	0.66	2.26	14	6	12	
g160	0.4930	0.003	42.479	0.082	+0.070	0.061	1.061	0.006	53285.08	0.14	1.56	8	2	10	
g240	0.6870	0.005	43.033	0.094	−0.100	0.067	0.933	0.010	53307.84	0.55	1.22	16	11	9	
h283	0.5020	0.008	42.229	0.096	+0.168	0.066	0.656	0.008	53321.47	0.24	4.63	14	3	15	
h300	0.6870	0.012	43.127	0.109	+0.019	0.059	1.043	0.054	53310.89	0.60	0.99	16	7	13	
h311	0.7410	0.011	43.634	0.165	+0.326	0.078	1.400	0.101	53317.81	1.16	2.01	15	4	15	x
h319	0.4950	0.004	42.537	0.090	+0.044	0.041	1.086	0.054	53338.52	0.53	1.99	13	5	12	
h323	0.6030	0.006	42.920	0.094	+0.016	0.069	0.926	0.015	53329.10	0.08	1.21	15	4	15	
h342	0.4210	0.002	42.335	0.085	−0.051	0.039	1.157	0.051	53327.67	0.84	5.42	17	4	17	
h359	0.3480	0.004	41.919	0.071	+0.150	0.041	0.954	0.025	53343.09	0.36	1.19	18	6	16	
h363	0.2130	0.006	40.834	0.072	+0.358	0.039	0.876	0.016	53339.05	0.17	3.26	15	6	13	
h364	0.3440	0.007	41.257	0.057	−0.081	0.034	0.902	0.016	53333.60	0.19	1.48	13	5	12	
k396	0.2710	0.006	40.884	0.084	+0.154	0.045	0.810	0.028	53357.09	0.32	1.67	6	8	2	
k425	0.2740	0.003	41.133	0.063	+0.151	0.038	0.906	0.001	53336.11	0.02	3.36	10	4	10	
k429	0.1810	0.008	39.836	0.017	+0.000	0.000	0.946	0.013	53351.31	0.11	7.75	4	3	4	x
k430	0.5820	0.010	43.414	0.131	−0.078	0.078	0.940	0.063	53348.70	1.09	1.03	16	8	12	
k441	0.6800	0.010	43.283	0.139	+0.151	0.068	1.140	0.084	53353.90	0.48	0.69	16	7	13	
k448	0.4010	0.005	42.402	0.156	+0.294	0.102	0.965	0.011	53358.16	0.10	0.46	11	9	6	
k485	0.4160	0.005	42.419	0.180	+0.601	0.087	0.908	0.097	53350.51	1.09	1.63	13	6	11	
m022	0.2400	0.003	42.430	0.131	+0.519	0.073	1.400	0.029	53639.86	0.54	3.96	9	2	11	x
m026	0.6530	0.008	43.178	0.166	−0.083	0.103	1.381	0.056	53609.05	52.47	1.45	4	0	8	x
m027	0.2860	0.006	41.862	0.202	+0.241	0.069	1.097	0.132	53639.51	1.13	2.08	5	2	7	
m032	0.1550	0.004	39.722	0.161	+0.000	0.000	0.958	0.064	53629.15	3.60	0.11	1	0	4	x

Table 10—Continued

Name	z	σ_z[a]	μ [mag]	σ_μ[b] [mag]	color	σ_{color}	stretch	$\sigma_{\mathrm{stretch}}$	$T_{\max}$ [MJD]	$\sigma_{T_{\max}}$ [MJD]	χ^2/DoF	DoF	Rise	Tail	Failed
m034	0.5620	0.006	43.342	0.134	−0.316	0.096	1.308	0.018	53616.46	0.46	1.61	4	0	8	x
m039	0.2490	0.003	41.124	0.173	+0.250	0.066	0.944	0.081	53632.85	2.55	14.58	6	0	10	x
m043	0.2660	0.003	41.868	0.958	+0.758	0.064	1.291	0.771	53637.87	2.78	1.18	6	0	10	x
m057	0.1840	0.003	42.108	0.784	+0.000	0.000	1.400	0.635	53639.47	1.30	6.41	9	0	4	x
m062	0.3170	0.005	41.274	0.165	+0.021	0.061	0.834	0.100	53645.33	0.96	1.75	4	1	7	x
m075	0.1020	0.001	40.365	1.185	+0.000	0.000	0.400	0.649	52985.99	0.33	1.75	4	0	3	x
m138	0.5820	0.004	43.659	0.152	−0.331	0.091	1.192	0.073	53657.82	0.24	0.86	9	7	6	
m158	0.4630	0.007	42.364	0.107	+0.186	0.068	0.997	0.036	53659.67	0.58	1.56	14	10	8	
m193	0.3410	0.009	41.312	0.078	−0.070	0.038	0.980	0.026	53664.32	0.17	1.82	13	6	11	
m226	0.6710	0.004	42.764	0.175	+0.359	0.091	1.075	0.102	53652.30	0.07	1.97	7	3	8	
n256	0.6310	0.012	43.182	0.098	−0.060	0.043	1.070	0.063	53697.62	0.84	1.42	13	4	13	
n258	0.5220	0.007	42.863	0.086	−0.085	0.055	0.914	0.032	53698.31	0.70	3.75	15	3	16	
n263	0.3680	0.007	41.641	0.049	−0.045	0.029	0.970	0.019	53702.50	0.23	2.04	14	5	13	
n278	0.3090	0.006	41.148	0.055	+0.075	0.028	0.886	0.026	53701.31	0.31	2.63	9	3	10	
n285	0.5280	0.006	42.876	0.298	+0.110	0.102	1.138	0.210	53687.33	2.46	1.05	9	1	12	
n326	0.2680	0.006	41.015	0.071	+0.094	0.041	0.659	0.017	53708.99	0.24	1.37	11	9	6	
n404	0.2160	0.008	41.000	0.055	+0.192	0.031	0.921	0.011	53713.99	0.14	3.31	12	10	6	
p425	0.4530	0.006	41.219	4.557	+4.000	3.635	0.400	0.019	52963.46	0.02	9.20	22	4	22	x
p454	0.6950	0.010	44.994	2.529	+1.278	1.675	1.400	0.977	52938.07	38.03	1.34	14	4	14	x
p455	0.2840	0.006	41.013	0.043	−0.007	0.025	0.846	0.010	53721.16	0.12	3.38	13	10	7	
p524	0.5080	0.001	42.452	0.071	+0.041	0.041	1.020	0.031	53720.41	0.33	1.03	10	10	4	
p528	0.7770	0.005	43.626	0.337	−0.010	0.084	0.955	0.248	53729.58	2.44	1.29	12	10	6	
p534	0.6150	0.008	42.529	0.172	−0.109	0.079	0.587	0.110	53737.33	1.75	3.95	4	6	2	x
sn1990O	0.0306	0.001	35.806	0.045	+0.007	0.016	1.024	0.028	48076.64	0.50	1.06	9	0	13	
sn1990af	0.0502	0.001	36.889	0.018	+0.004	0.009	0.730	0.009	48196.11	0.12	0.88	43	9	38	
sn1992P	0.0263	0.001	35.823	0.103	−0.011	0.017	1.129	0.081	48718.27	0.88	0.95	10	0	14	
sn1992ae	0.0748	0.001	37.884	0.030	−0.017	0.020	0.924	0.004	48803.98	0.12	0.88	24	0	28	
sn1992ag	0.0259	0.001	35.611	0.044	+0.158	0.018	1.019	0.026	48805.87	0.53	1.99	15	0	19	
sn1992aq	0.1009	0.001	38.664	0.053	−0.039	0.021	0.822	0.031	48834.48	0.60	0.63	25	0	29	
sn1992bc	0.0198	0.001	34.744	0.012	−0.059	0.005	1.005	0.006	48913.30	0.05	4.13	77	38	43	
sn1992bh	0.0451	0.001	36.984	0.031	+0.098	0.015	0.975	0.015	48920.62	0.39	0.64	22	2	24	
sn1992bl	0.0429	0.001	36.534	0.045	−0.007	0.020	0.774	0.015	48947.71	0.48	1.25	20	0	24	
sn1992bo	0.0181	0.001	34.871	0.015	+0.033	0.008	0.734	0.005	48986.28	0.04	1.44	47	13	38	

Table 10—Continued

Name	z	σ_z[a]	μ [mag]	σ_μ[b] [mag]	color	σ_{color}	stretch	$\sigma_{stretch}$	T_{max} [MJD]	$\sigma_{T_{max}}$ [MJD]	χ^2/DoF	DoF	Rise	Tail	Failed
sn1992bp	0.0789	0.001	37.700	0.026	−0.041	0.013	0.860	0.014	48980.90	0.21	1.60	37	6	35	
sn1992br	0.0878	0.001	38.364	0.089	+0.040	0.036	0.645	0.027	48984.27	1.00	2.04	15	0	19	
sn1992bs	0.0634	0.001	37.784	0.051	−0.030	0.019	0.984	0.018	48984.18	0.68	0.74	29	0	33	
sn1993B	0.0707	0.001	37.847	0.022	+0.044	0.015	0.973	0.001	49004.23	0.01	2.19	16	0	20	
sn1993H	0.0248	0.001	35.490	0.020	+0.217	0.009	0.668	0.009	49069.62	0.16	1.78	39	4	39	
sn1993O	0.0519	0.001	37.050	0.021	−0.015	0.011	0.893	0.010	49134.53	0.11	1.94	37	7	34	
sn1993ag	0.0500	0.001	37.080	0.035	+0.097	0.018	0.904	0.018	49316.95	0.26	1.04	16	4	16	
sn1994M	0.0243	0.001	35.367	0.028	+0.117	0.011	0.774	0.011	49476.68	0.30	3.94	30	0	34	
sn1994S	0.0160	0.001	34.470	0.040	−0.014	0.012	1.068	0.027	49517.69	0.31	3.01	23	9	18	
sn1994T	0.0357	0.001	36.300	0.018	+0.030	0.011	0.874	0.000	49508.19	0.00	20.35	20	0	24	x
sn1995ac	0.0488	0.001	36.650	0.016	+0.015	0.006	1.034	0.010	49993.31	0.11	2.39	58	15	47	
sn1995ak	0.0220	0.001	35.161	0.070	+0.084	0.026	0.879	0.020	50020.75	0.75	3.64	28	0	32	
sn1996C	0.0275	0.001	36.029	0.034	+0.129	0.012	1.001	0.018	50130.33	0.46	1.67	33	0	37	
sn1996ab	0.1242	0.001	39.142	0.021	−0.077	0.014	0.949	0.004	50223.62	0.02	1.11	25	0	29	
sn1996bl	0.0348	0.001	36.136	0.022	+0.050	0.009	0.976	0.013	50376.62	0.15	2.02	24	6	22	
sn1996bo	0.0163	0.001	34.612	0.012	+0.391	0.005	0.863	0.007	50387.50	0.04	7.35	31	10	25	
sn1996bv	0.0167	0.001	34.586	0.029	+0.235	0.006	0.999	0.020	50405.92	0.32	3.95	13	0	17	
sn1997Y	0.0166	0.001	34.635	0.026	+0.047	0.009	0.874	0.018	50488.55	0.50	1.07	15	0	19	
sn1997dg	0.0297	0.001	36.209	0.028	+0.040	0.008	0.903	0.019	50721.03	0.22	3.87	15	4	15	
sn1998V	0.0172	0.001	34.475	0.018	+0.064	0.005	0.920	0.012	50892.83	0.21	7.60	28	0	32	
sn1998ab	0.0279	0.001	35.357	0.016	+0.104	0.006	0.925	0.007	50914.89	0.04	9.95	28	4	28	
sn1998dx	0.0537	0.001	36.854	0.035	−0.049	0.013	0.765	0.020	51073.03	0.30	4.81	11	3	12	
sn1998ef	0.0167	0.001	34.114	0.016	+0.028	0.005	0.839	0.009	51114.37	0.09	9.49	16	16	4	
sn1998eg	0.0235	0.001	35.453	0.034	+0.063	0.009	0.912	0.025	51111.15	0.27	1.55	12	4	12	
sn1999aw	0.0392	0.001	36.548	0.011	−0.001	0.004	1.162	0.007	51254.92	0.06	8.26	53	7	50	
sn1999cc	0.0315	0.001	35.976	0.010	+0.051	0.004	0.813	0.006	51315.57	0.08	2.00	52	12	44	
sn1999ek	0.0176	0.001	34.744	0.009	+0.183	0.003	0.893	0.006	51482.49	0.06	3.40	103	24	83	
sn1999gp	0.0260	0.001	35.552	0.006	+0.072	0.003	1.063	0.004	51551.37	0.03	6.68	121	54	71	
sn2000ca	0.0245	0.001	35.178	0.016	−0.055	0.005	0.995	0.011	51666.35	0.11	7.85	35	8	31	
sn2000cf	0.0365	0.001	36.443	0.029	+0.015	0.009	0.924	0.011	51672.39	0.39	3.99	45	0	49	
sn2000cn	0.0232	0.001	35.437	0.011	+0.173	0.005	0.726	0.005	51707.68	0.04	3.41	42	19	27	
sn2000dk	0.0164	0.001	34.416	0.010	+0.060	0.004	0.731	0.006	51812.74	0.04	5.12	32	16	20	
sn2000fa	0.0218	0.001	35.225	0.015	+0.091	0.005	0.960	0.010	51893.09	0.14	12.97	16	4	16	

Table 10—Continued

Name	z	σ_z[a]	μ [mag]	σ_μ[b] [mag]	color	$\sigma_{\rm color}$	stretch	$\sigma_{\rm stretch}$	$T_{\rm max}$ [MJD]	$\sigma_{T_{\rm max}}$ [MJD]	χ^2/DoF	DoF	Rise	Tail	Failed
sn2001V	0.0162	0.001	34.114	0.007	+0.041	0.003	1.029	0.004	51974.64	0.03	5.06	96	32	68	
sn2001ba	0.0305	0.001	35.871	0.018	−0.093	0.008	0.993	0.011	52034.20	0.15	1.42	49	8	45	
sn2001cn	0.0154	0.001	34.400	0.018	+0.184	0.005	0.914	0.008	52072.75	0.23	2.38	50	0	54	
sn2001cz	0.0163	0.001	34.441	0.016	+0.110	0.005	1.001	0.011	52104.03	0.09	2.19	28	6	26	
03D1au	0.5043	0.001	42.624	0.031	+0.033	0.018	1.078	0.015	52909.05	0.17	2.55	25	8	21	
03D1aw	0.5817	0.001	43.111	0.052	+0.010	0.030	0.977	0.024	52902.40	0.31	3.54	19	7	16	
03D1ax	0.4960	0.001	42.425	0.031	−0.047	0.021	0.877	0.010	52916.02	0.10	3.83	22	11	15	
03D1bp	0.3460	0.001	41.595	0.027	+0.119	0.017	0.842	0.007	52920.03	0.07	3.33	28	12	20	
03D1cm	0.8700	0.001	44.381	0.201	−0.041	0.145	1.186	0.045	52950.78	0.52	1.49	14	8	10	
03D1co	0.6790	0.001	43.694	0.077	−0.003	0.046	1.010	0.032	52954.31	0.40	0.97	26	14	16	
03D1ew	0.8680	0.001	44.123	0.229	−0.128	0.169	0.987	0.034	52991.99	0.71	1.97	8	4	8	
03D1fc	0.3310	0.001	41.212	0.009	+0.042	0.004	0.937	0.005	53002.44	0.05	6.02	13	10	7	
03D1fl	0.6880	0.001	43.249	0.038	−0.076	0.020	0.952	0.020	52993.03	0.40	4.10	15	6	13	
03D1fq	0.8000	0.001	43.780	0.082	+0.035	0.042	0.824	0.044	52998.32	0.72	1.61	14	7	11	
03D1gt	0.5480	0.001	43.091	0.094	+0.244	0.050	0.856	0.042	53013.91	0.61	1.34	11	8	7	
03D3af	0.5320	0.001	42.928	0.054	+0.028	0.032	0.943	0.023	52732.83	0.32	2.62	5	5	4	
03D3aw	0.4490	0.001	42.132	0.033	−0.048	0.019	0.955	0.013	52767.88	0.13	2.65	7	4	7	
03D3ay	0.3709	0.001	41.754	0.027	−0.018	0.014	0.968	0.011	52768.01	0.09	2.19	8	4	8	
03D3ba	0.2912	0.001	41.264	0.047	+0.264	0.015	1.036	0.021	52750.16	0.90	1.90	4	0	8	x
03D3bh	0.2486	0.001	40.837	0.026	−0.090	0.013	0.993	0.007	52770.70	0.06	18.05	5	4	5	
03D3cc	0.4627	0.001	42.345	0.154	−0.045	0.060	1.052	0.037	52780.48	3.02	2.22	5	0	9	x
03D3cd	0.4607	0.001	42.298	0.050	+0.020	0.012	1.128	0.036	52801.52	0.14	24.17	5	3	6	
03D4ag	0.2850	0.001	40.937	0.009	−0.078	0.004	1.018	0.005	52830.99	0.06	10.83	13	8	9	
03D4at	0.6330	0.001	43.410	0.054	−0.083	0.029	0.977	0.028	52816.42	0.48	4.36	15	6	13	
03D4cn	0.8180	0.001	43.797	0.203	+0.034	0.157	0.758	0.005	52878.62	0.02	1.72	16	5	15	
03D4cx	0.9490	0.001	43.777	0.182	+0.089	0.123	0.898	0.041	52883.48	0.32	1.55	16	6	14	
03D4cy	0.9271	0.001	44.865	0.243	−0.312	0.173	1.047	0.009	52900.31	0.04	1.40	17	8	13	
03D4cz	0.6950	0.001	43.333	0.071	−0.054	0.043	0.760	0.025	52893.97	0.31	1.10	30	13	21	
03D4dh	0.6268	0.001	43.003	0.028	+0.014	0.016	1.040	0.013	52906.16	0.21	2.18	23	9	18	
03D4di	0.9050	0.001	44.000	0.173	+0.015	0.120	1.103	0.043	52902.06	0.60	1.41	15	8	11	
03D4dy	0.6040	0.001	42.813	0.026	+0.112	0.016	1.062	0.012	52904.28	0.18	2.02	22	8	18	
03D4fd	0.7910	0.001	43.623	0.073	+0.042	0.043	0.936	0.034	52937.87	0.65	1.64	12	6	10	
03D4gf	0.5810	0.001	43.035	0.046	−0.051	0.024	1.019	0.026	52936.80	0.42	1.66	11	6	9	

Table 10—Continued

Name	z	$\sigma_z{}^{\rm a}$	μ [mag]	$\sigma_\mu{}^{\rm b}$ [mag]	color	$\sigma_{\rm color}$	stretch	$\sigma_{\rm stretch}$	$T_{\rm max}$ [MJD]	$\sigma_{T_{\rm max}}$ [MJD]	χ^2/DoF	DoF	Rise	Tail	Failed
03D4gg	0.5920	0.001	42.853	0.080	+0.077	0.035	1.000	0.050	52942.66	0.60	2.32	8	10	2	
03D4gl	0.5710	0.001	42.746	0.061	+0.031	0.028	0.978	0.034	52954.63	0.41	3.28	7	9	2	
04D1ag	0.5570	0.001	42.777	0.029	−0.182	0.017	0.944	0.013	53016.86	0.20	3.85	9	6	7	
04D1aj	0.7210	0.001	43.474	0.100	+0.072	0.038	1.074	0.067	52998.86	0.97	1.65	13	6	11	
04D1ak	0.5260	0.001	42.910	0.057	+0.018	0.033	0.824	0.021	53010.68	0.22	1.50	13	10	7	
04D2cf	0.3690	0.001	41.753	0.015	−0.001	0.010	0.894	0.003	53073.45	0.03	1.97	14	0	18	x
04D2fp	0.4150	0.001	42.038	0.025	+0.006	0.015	0.964	0.010	53107.55	0.12	1.16	11	5	10	
04D2fs	0.3570	0.001	41.706	0.016	+0.128	0.007	0.940	0.008	53107.74	0.10	5.56	17	6	15	
04D2gb	0.4300	0.001	42.043	0.040	−0.008	0.025	0.777	0.013	53108.08	0.18	1.47	11	5	10	
04D2gc	0.5210	0.001	42.705	0.043	+0.185	0.022	1.065	0.024	53118.26	0.28	3.71	8	4	8	
04D2gp	0.7070	0.001	43.503	0.088	−0.052	0.059	0.800	0.002	53110.35	0.06	1.52	9	4	9	
04D2iu	0.6910	0.001	43.411	0.095	+0.074	0.056	0.799	0.035	53120.65	0.52	0.41	8	6	6	
04D2ja	0.7410	0.001	43.693	0.083	−0.067	0.043	0.945	0.036	53122.62	0.45	0.41	8	6	6	
04D3co	0.6200	0.001	43.297	0.049	−0.064	0.030	0.895	0.017	53101.61	0.23	0.96	27	8	23	
04D3cp	0.8300	0.001	44.680	0.238	−0.448	0.180	1.110	0.035	53111.05	0.45	0.85	15	3	16	
04D3cy	0.6430	0.001	43.289	0.046	+0.017	0.029	0.963	0.016	53101.34	0.23	1.52	27	8	23	
04D3dd	1.0100	0.001	44.938	0.333	−0.071	0.205	1.088	0.074	53116.10	1.13	1.81	18	4	18	
04D3df	0.4700	0.001	42.535	0.026	+0.060	0.017	0.730	0.010	53119.13	0.14	4.06	23	6	21	
04D3do	0.6100	0.001	43.062	0.032	−0.079	0.019	0.862	0.013	53113.18	0.21	1.85	26	6	24	
04D3ez	0.2630	0.001	40.949	0.009	+0.091	0.003	0.895	0.006	53115.16	0.07	7.04	22	4	22	
04D3fk	0.3578	0.001	41.741	0.008	+0.148	0.005	0.913	0.000	53126.99	0.01	5.02	30	14	20	
04D3fq	0.7300	0.001	43.553	0.056	−0.003	0.037	0.900	0.014	53119.76	0.27	0.93	32	9	27	
04D3gt	0.4510	0.001	42.303	0.026	+0.276	0.016	0.953	0.010	53138.10	0.13	2.10	27	11	20	
04D3gx	0.9100	0.001	44.525	0.232	−0.202	0.163	0.952	0.047	53126.50	0.63	0.64	16	7	13	
04D3hn	0.5516	0.001	42.727	0.028	+0.106	0.017	0.898	0.011	53137.38	0.15	2.71	27	11	20	
04D3is	0.7100	0.001	43.441	0.054	+0.220	0.037	0.972	0.002	53144.15	0.06	1.40	30	10	24	
04D3ki	0.9300	0.001	44.696	0.278	−0.256	0.194	0.901	0.039	53142.77	0.66	1.41	19	8	15	
04D3kr	0.3373	0.001	41.524	0.007	+0.072	0.003	1.063	0.004	53166.30	0.05	9.83	26	11	19	
04D3ks	0.7520	0.001	43.435	0.079	+0.026	0.043	1.013	0.037	53163.12	0.41	1.01	19	8	15	
04D3lp	0.9830	0.001	44.207	0.319	+0.022	0.211	0.831	0.049	53150.18	0.86	1.80	17	8	13	
04D3lu	0.8218	0.001	43.810	0.155	+0.019	0.116	0.950	0.028	53168.15	0.48	1.16	12	5	11	
04D3ml	0.9500	0.001	44.218	0.174	+0.117	0.121	1.182	0.015	53181.26	0.27	1.12	7	5	6	
04D3nc	0.8170	0.001	43.917	0.199	+0.062	0.140	1.111	0.064	53188.24	0.90	0.63	8	7	5	

Table 10—Continued

Name	z	σ_z[a]	μ [mag]	σ_μ[b] [mag]	color	$\sigma_{\rm color}$	stretch	$\sigma_{\rm stretch}$	$T_{\rm max}$ [MJD]	$\sigma_{T_{\rm max}}$ [MJD]	χ^2/DoF	DoF	Rise	Tail	Failed
04D3nh	0.3402	0.001	41.600	0.009	+0.085	0.004	1.013	0.006	53174.11	0.05	6.21	22	6	20	
04D3nr	0.9600	0.001	43.889	0.166	+0.070	0.110	0.922	0.045	53184.35	0.61	1.72	8	7	5	
04D3ny	0.8100	0.001	43.957	0.223	−0.065	0.152	1.005	0.084	53195.02	1.40	1.45	7	7	4	
04D3oe	0.7560	0.001	43.720	0.060	−0.259	0.033	0.783	0.028	53194.50	0.48	3.22	13	10	7	
04D4an	0.6130	0.001	43.227	0.050	+0.064	0.025	0.823	0.025	53183.63	0.24	1.02	15	6	13	
04D4bk	0.8400	0.001	43.740	0.143	+0.142	0.098	1.050	0.051	53192.39	0.58	1.45	8	3	9	
04D4bq	0.5500	0.001	42.752	0.053	+0.112	0.027	0.995	0.029	53193.84	0.37	2.39	14	6	12	
04D4dm	0.8110	0.001	44.216	0.206	−0.161	0.150	1.000	0.057	53199.61	1.07	0.81	9	8	5	
04D4dw	0.9610	0.001	44.266	0.209	−0.117	0.138	0.962	0.058	53199.47	1.09	1.85	8	8	4	

[a]We add a 400 km/s peculiar velocity dispersion in quadrature to these redshift uncertainties for our cosmological fits.

[b]An "intrinsic" dispersion of $\sigma_\mu = 0.13$ should be added in quadrature to these values output by SALT (Guy et al. 2005) to fully account for the intrinsic dispersion of SNe Ia.

Note. — The luminosity distances and extinctions as determined by SALT of the full SNLS, ESSENCE, and nearby SN Iasample. SN Iafit marked as "Failed" did not pass the SALT quality cuts given Table 3. The SALT fitter quotes minimum chi-sq values for the lightcurve fit parameters rather than estimated mean estimated parameters. See Table. 3 and for the quality cuts applied here.